Aus dem Pharmakologischen Institut

Direktor: Prof. Dr. Robert Grosse

des Fachbereichs Medizin der Philipps-Universität Marburg

Regulation of nuclear INF2 promotes actin polymerization and modulates MRTF-A subcellular localization and activity

Inaugural-Dissertation

zur Erlangung des Doktorgrades der Naturwissenschaften

dem Fachbereich Medizin der Philipps-Universität Marburg vorgelegt von

Michael Melak

aus Mistelbach, Österreich

Marburg, 2017

Aus dem Pharmakologischen Institut

Direktor: Prof. Dr. Robert Grosse

des Fachbereichs Medizin der Philipps-Universität Marburg

Regulation of nuclear INF2 promotes actin polymerization and modulates MRTF-A subcellular localization and activity

Inaugural-Dissertation

zur Erlangung des Doktorgrades der Naturwissenschaften

dem Fachbereich Medizin der Philipps-Universität Marburg vorgelegt von

Michael Melak

aus Mistelbach, Österreich

Marburg, 2017

Angenommen vom Fachbereich Medizin der Philipps-Universität Marburg

am 5. April 2017

Gedruckt mit Genehmigung des Fachbereichs.

Dekan: Herr Prof. Dr. Helmut Schäfer

Referent: Herr Prof. Dr. Robert Grosse

1. Korreferent: Herr PD Dr. Ulrich Mühlenhoff

dedicated to my wife Thea and my children

Table of Contents

List of Figures

List of Tables

Abbreviations

AB	Antibody
ADF	Actin depolymerizing factor
Arp2/3	Actin-related protein 2/3
ARR	Armadillo Repeat Region
CaAR	Calcium-mediated Actin Reset
CC	Coiled coil
CK2	Casein kinase 2
CMT	Charcot–Marie–Tooth
Cobl	Cordon-bleu
Daam	Dishevelled-associated activator of morphogenesis
DAD	Diaphanous autoregulatory domain
DD	Dimerization domain
Dia	Diaphanous
DID	Diaphanous inhibitory domain
DIP	Dia-interacting protein
DRFs	Diaphanous-related formins
ER	Endoplasmic reticulum
F-actin	Filamentous actin
FCS	Fetal bovine serum
FH1	Formin homology 1
FH2	Formin homology 2
FHOD	Formin homology domain-containing protein
FMN	Formin
FMNL	Formin-like protein
FRL	Formin-related gene in leukocytes
FSGS	Focal and segmental glomerulosclerosis
FSI	Formin–Spire interaction domain
G-actin	Globular actin

GAPs	GTPase-activating proteins
GBD	GTPase-binding domain
GEFs	Guanine nucleotide exchange factors
GFP	Green fluorescent protein
GPCR	G-protein-coupled receptors
INF	Inverted formin
Lck	Lymphocyte-specific protein tyrosine kinase
LMB	Leptomycin B
Lmod	Leiomodin
LOV	Light, oxygen, voltage
LPA	Lysophosphatidic acid
MAPK	Mitogen-activated protein kinase
MRTF	Myocardin and myocardin-related transcription factor
nAC	Nuclear-Actin-Chromobody
NES	Nuclear export signals
NLS	Nuclear localization sequence
NM1	Nuclear myosin I
NPFs	Nucleation-promoting factors
o/n	Over night
PDZ	Postsynaptic density protein, Discs large, Zona occludens 1
PIP2	Phosphatidylinositol-4,5-bisphosphate
PKCα	Protein kinase Cα
ROCK	Rho associated coiled coil containing protein kinase
RT	Room temperature
SD	Standard deviation
SDS-PAGE	SDS- polyacrylamide gel electrophoresis
SRF	Serum response factor
TCFs	Ternary complex factors
VCA	Verprolin-homology domain, Connector region, Acidic motif
WH2 domain	WASP-homology 2 domain

Summary

Actin filaments are a fundamental component of the cytoskeleton. In eukaryotes, dynamic actin rearrangement plays a crucial part in cellular processes such as morphogenesis, adhesion, cell motility, cytokinesis and intracellular vesicle transport. Numerous aspects of actin dynamics in the cytoplasm of eukaryotic cells have been studied intensely over the past decades. Those studies revealed a very detailed knowledge about the structure and function of actin filaments as well as about the underlying mechanisms of F-actin formation.

Though actin and proteins involved in actin assembly or disassembly have also been detected in the nuclei of many different eukaryotic cells lines, the detailed regulation and function of actin in the nuclear compartment is poorly defined. Monomeric nuclear actin was identified to participate in specific events such as transcriptional regulation or chromatin remodeling. Nevertheless, the existence and role of filamentous actin inside the nucleus has been controversially debated for years.

Quite recently, specific actin probes have been described which enabled credible visualization of nuclear F-actin structures and provided a first insight into the regulation and function of actin polymerization in the nucleus. For example, a role for nuclear F-actin in response to DNA damage and efficient DNA repair as well as in the regulation of the SRF coactivator MRTF-A has been reported. Both events were shown to involve the assembly of nuclear actin filaments mediated by members of the formin family of actin nucleators.

In this work, we provide evidence of a nuclear function of the disease associated formin INF2. We identified that activation of endogenous INF2 in the nucleus by means of INF2-DID-NLS or INF2-DAD-NLS expression mediated release of autoinhibition promotes the assembly of a nuclear F-actin network. We further observed that INF2 mediated nuclear actin rearrangement efficiently regulates the translocation and activity of MRTF-A. Moreover, by deletion of INF2 using the CRISPR/Cas9 system as well as by siRNA mediated INF2 knockdown we could show that INF2-DAD-NLS driven

nuclear F-actin formation is primarily dependent on the presence of endogenous INF2. However, our data suggest concomitant modulation of nuclear mDia activity upon the release of INF2 autoinhibition in the nucleus.

This study provides evidence for a role of the formin INF2 in the promotion and the formation of a nuclear actin network and thereby regulating the subcellular localization of MRTF-A and subsequent alteration of MRTF/SRF transcriptional activity.

Zusammenfassung

Aktinfilamente sind ein wesentlicher Bestandteil des eukaryotischen Zellskeletts. Durch einen dynamischen Auf- und Abbau dieser Filamente werden zelluläre Vorgänge, wie etwa Morphogenese, Mobilität, Zellteilung oder der intrazelluläre Vesikeltransport, beeinflusst. Verschiedenste Faktoren, die bei dem dynamischen Umbau von Aktinfilamenten im Zytoplasma eine Rolle spielen, wurden in den letzten Jahren und Jahrzehnten ausgiebig studiert. Dank dieser Studien haben wir heute ein durchaus detailliertes, aber bei weitem nicht vollständiges Bild der genauen Struktur und Funktion von Aktinfilamenten, sowie der zugrundeliegenden Mechanismen, welche bei der Ausbildung eben dieser Filamente eine Rolle spielen.

Interessanterweise wurden sowohl Aktin als auch einige weitere Proteine, welche üblicherweise am Auf- und Abbau von zytoplasmatischen Aktinfilamenten beteiligt sind, auch im Zellkern verschiedenster eukaryotischer Zelltypen nachgewiesen. Über die Regulierung und die Funktion von Aktin im Nukleus ist momentan allerdings nur sehr wenig bekannt. Beispielsweise wurde gezeigt, dass monomeres Aktin im Zellkern an der Umgestaltung von Chromatin beteiligt ist und die Gen-Transkription beeinflusst. Die Existenz und die Funktion von kernständigen Aktinfilamenten wurden jedoch von zahlreichen Forschergruppen über viele Jahre hinweg kontrovers diskutiert.

Erst kürzlich konnten mithilfe spezifischer Aktin-bindender Sonden Aktinfilamente im Zellkern zuverlässig und überzeugend visualisiert werden. Dadurch wurden erstmals auch Details über ihre Regulierung und ihre Funktion im Nukleus bekannt. Zum Beispiel wurde gezeigt, dass kernständige Aktinfilamente eine wichtige Rolle bei der zellulären Antwort auf DNA-Schäden und der darauffolgenden DNA-Reparatur spielen. Zusätzlich sind sie in die Regulierung des MRTF/SRF-Signaltransduktionsweges involviert. Bei beiden genannten Prozessen wird die Bildung von kernständigen Aktinfilamenten durch Proteine aus der Familie der Formine begünstigt.

Die vorliegende Doktorarbeit zeigt, dass auch das Formin INF2 zu Aktin-bezogenen Effekten im Nukleus führt. Beispielsweise löst die Expression einer isolierten,

kernständigen INF2-DID oder einer isolierten, kernständigen INF2-DAD eine spezifische Aktivierung von endogenem INF2 im Zellkern aus. Dadurch kommt es dort zur Aufhebung der Autoinhibierung von INF2, was wiederum zur Bildung von Aktinfilamenten im Nukleus führt. Außerdem haben wir beobachtet, dass der INF2-gesteuerte Aufbau von kernständigen Aktinfilamenten eine Anreicherung des SRF-Kofaktors MRTF-A im Zellkern bewirkt. Nach einer Reduktion oder einer vollständigen Deletion von INF2 in der Zelle kamen wir zu der Erkenntnis, dass die kernständigen Filamente, welche nach der Expression der INF2-DAD im Zellkern gebildet werden, primär vom Vorhandensein von endogenem INF2 abhängig sind. Unsere Daten weisen allerdings auch darauf hin, dass mittels dieser Methode zur INF2-Aktivierung neben kernständigem INF2 zusätzlich mDia-Formine im Nukleus koreguliert werden.

Zusammengefasst beschreibt diese Arbeit, dass das Formin INF2 auch im Zellkern an der Bildung von Aktinfilamenten beteiligt ist und dass die Lokalisierung von MRTF-A sowie, in weiterer Folge, die transkriptionelle Aktivität des MRTF/SRF Signalwegs dadurch beeinflusst werden können.

1. Introduction

The existence of a cytoskeleton was revealed in all three domains of life (prokaryotic, eukaryotic and archaea) where it forms an intracellular filamentous scaffold (Wickstead and Gull, 2011). It is in charge of a wide variety of fundamental features such as providing mechanical resistance to deformation, defining the cellular shape and mechanics during processes like migration and cytokinesis, linking the cell physically and biochemically to the extracellular matrix, organizing the contents of the cells or intracellular cargo transport. Three main classes of cytoskeletal structures have been described in eukaryotes: actin filaments, microtubules and the heterogeneous group of intermediate filaments. In general, cytoskeletal structures are dynamically and adaptively modulated by the assembly or disassembly of monomeric subunits into polymers and vice versa, mediated by numerous regulatory and structural proteins (Fletcher and Mullins, 2010).

In the last decades, studies addressing components of the cytoskeleton revealed numerous details and information concerning their structures, functions as well as their mechanisms of formation. In contrast, there is only a minor knowledge about the rather vaguely defined 'nucleoskeleton' (Simon and Wilson, 2011). The general concept of the term nucleoskeleton includes the composition and function of the nuclear architecture involved in processes such as maintaining the nuclear shape, gene expression, chromatin remodeling, DNA processing, cell signaling and of course the dynamic reorganization, for instance during mitosis. The nucleoskeleton is mainly composed of lamin filaments, actin, multisubunit proteins and the genome (Dahl and Kalinowski, 2011). It is connected to the cytoskeleton through the LINC complex which transmits mechanical stimuli and signaling cues from the cytoplasm to the nucleus and vice versa (Ostlund et al., 2009).

Actin was shown to be a key component in both nucleo- and cytoskeleton, although it might be differentially organized and regulated and might fulfill differing functions in the nucleus and the cytoplasm. Many previous studies proposed the existence of actin

in the nucleus solely in a monomeric or short oligomeric state, rather executing regulatory or accessory functions than structural or mechanical tasks (Pederson, 2008; Pederson and Aebi, 2002). However, quite recently, long nuclear actin filaments could be visualized within somatic cell nuclei, together with first insights into nuclear F-actin regulation and function (Baarlink et al., 2013; Belin et al., 2013; Plessner et al., 2015). Nevertheless, further exploration of nuclear actin and nuclear actin binding proteins is needed to fill the gaps in our current understanding of the regulatory mechanistic and functions of F-actin in the nucleus.

1.1 The actin cytoskeleton

Among the three types of cytoskeletal filamentous structures, actin filaments form the thinnest with a diameter of 5 – 9 nm (Holmes et al., 1990). Multiple F-actin cross-linking proteins can organize actin filaments into bundles or network like structures (Dubreuil, 1991; Tseng et al., 2005; Tseng et al., 2002). These higher-order actin structures can shape into multiple varying intracellular structures such as stress fibers or cortical actin, as well as into cellular extensions as microvilli (DeRosier and Tilney, 2000), podosomes (Gimona et al., 2008), filopodia (Mattila and Lappalainen, 2008), lamellipodia (Small et al., 2002) or membrane blebs (Fackler and Grosse, 2008). Due to their diversity, various actin structures can fulfill a wide variety of cellular functions, such as cytokinesis, cell adhesion, cell contraction, cell migration, intracellular transport as well as the regulation of cell-cell contacts, cell polarity and cell shape (Dominguez and Holmes, 2011; Glotzer, 2001; Olson and Sahai, 2009; Pollard and Cooper, 2009). Furthermore, a function of actin in the regulation of gene transcription has been described (Bunnell et al., 2011; Louvet and Percipalle, 2009; Olson and Nordheim, 2010).

1.1.1 Actin assembly and disassembly

The highly conserved cytoskeletal component actin is one of the most abundant proteins in eukaryotic cells (Dominguez and Holmes, 2011). Mammalians express six different actin isoforms. Each isoform is encoded by a separate gene and carries out unique cellular functions. Two of those six isoforms, namely β-cyto-actin and γ-cyto-actin, are ubiquitously expressed, whereas the remaining four isoforms, α-skeletal-actin, α-cardiac-actin, α-smooth-actin and γ-smooth-actin, are expressed primarily in skeletal, cardiac or smooth muscle cells (Perrin and Ervasti, 2010).

Actin exists in two different forms inside cells, either as globular monomer (G-actin) or as polymerized filamentous structure (F-actin), forming a twisted double helix (Holmes et al., 1990). The 42 kDa large actin monomers are composed of four subdomains with an ATP/ADP binding cleft (Otterbein et al., 2001). During F-actin assembly, ATP-bound G-actin gets incorporated into the polymeric F-actin structure at the so called barbed end (plus end), with its ATP/ADP binding cleft directed to the pointed end (minus end), thus leading to structural polarity of F-actin (Begg et al., 1978; Dominguez and Holmes, 2011; Wegner and Isenberg, 1983). As actin also possesses an ATPase function, ATP gets hydrolyzed upon incorporation of the actin monomer into the growing filament. Thus, the actin filament contains just ADP after some time at the pointed end. As F-actin which binds ADP is less stable than that binding ATP, the filament gets depolymerized at the pointed end (Dominguez and Holmes, 2011). This constant process of dissociation of actin monomers from the pointed end and simultaneous incorporation of G-actin at the barbed end is called actin treadmilling (Bugyi and Carlier, 2010).

To maintain an equilibrium between assembly and disassembly of actin filaments at steady state conditions or to modulate F-actin formation or depolymerization upon diverse cell signaling events multiple additional proteins were described to interact with actin structures (Figure 1). For example, several capping proteins, such as F-actin capping protein or gelsolin, were discovered that bind to the barbed end of F-actin and thus prevent elongation of the filament (Kim et al., 2010; Sun et al., 1999). To

modulate disassembly of actin filaments, capping proteins such as tropomodulin can also bind to the filament's pointed end (Pollard et al., 2000; Weber et al., 1994). Proteins as profilin for instance were shown to form a complex with ATP bound G-actin and bind to the barbed end, thereby enhancing the elongation of F-actin (Pollard et al., 2000; Pring et al., 1992). Contrariwise, severing proteins, such as members of the actin depolymerizing factor (ADF)/cofilin family, promote depolymerization of actin filaments at the pointed end (Theriot, 1997).

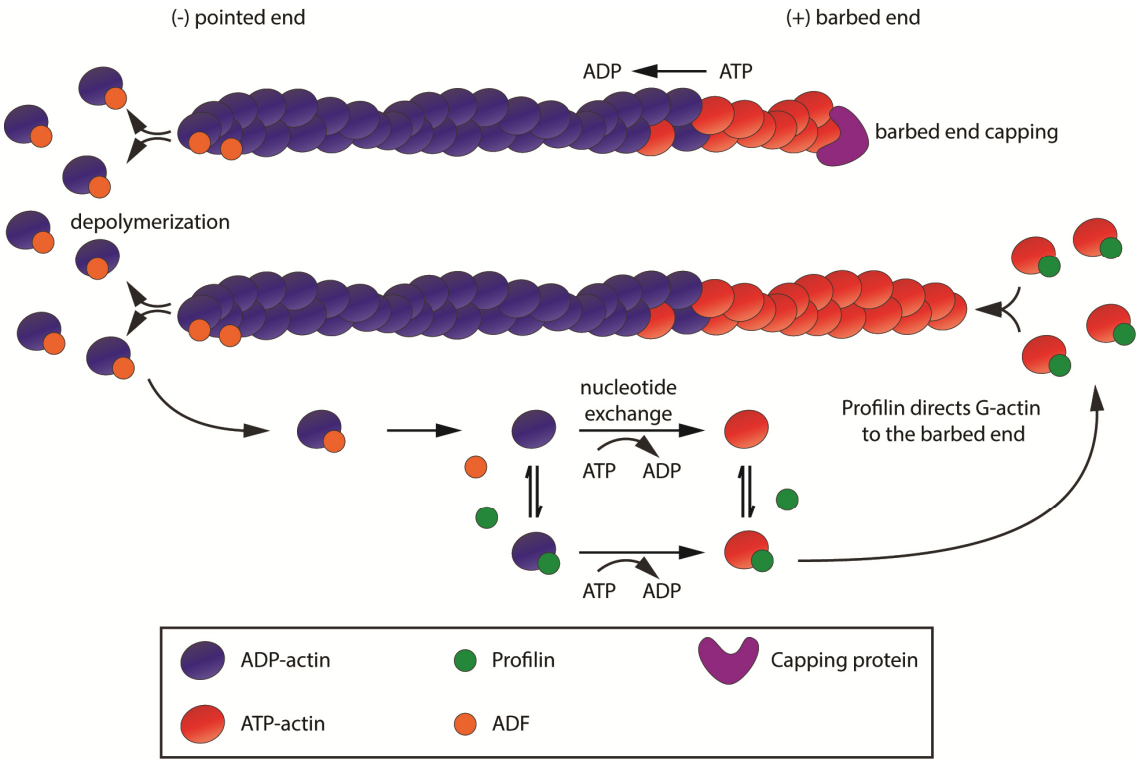

Figure 1: Regulation of actin turnover

The twisted double-helical actin filament is assembled by adding ATP-bound G-actin to the barbed end. Upon hydrolysis of ATP to ADP the filament is destabilized and facilitates the binding of severing proteins such as ADF. This results in depolymerization of F-actin at the pointed end and free ADP-bound G-actin. ADP-actin monomers can then be recycled through nucleotide exchange. Profilin then either binds directly to ATP-actin monomers or, with a lesser affinity, to ADP-G-actin, thereby promoting nucleotide exchange. Subsequently, profilin directs ATP-bound actin monomers to free barbed ends. Capping proteins prevent binding of G-actin to the barbed end and thus inhibit the filament from being elongated. The image was adapted from (Le Clainche and Carlier, 2008).

1.2 Regulation of actin nucleation and elongation

The initial assembly of actin filaments from G-actin requires the formation of a trimeric actin complex. This process is called actin nucleation. Although it was shown *in vitro* that purified G-actin can self-assemble into F-actin, spontaneous nucleation is kinetically unfavorable and is the rate-limiting step in actin polymerization (Campellone and Welch, 2010; Sept and McCammon, 2001).

Until now, three main classes of proteins, so called actin nucleating factors, have been identified that overcome the need for spontaneous actin nucleation and drive the rapid initiation of *de novo* actin filament assembly: (1) the Arp2/3 (actin-related protein 2/3) complex together with nucleation-promoting factors (NPFs) (Goley and Welch, 2006; Stradal and Scita, 2006), (2) tandem-monomer-binding nucleators (Ahuja et al., 2007; Quinlan et al., 2005) and (3) formins (Pruyne et al., 2002) (Figure 2). The multiple classes of actin nucleators give the cell the flexibility to assemble distinct populations of actin filaments in response to specific signals in different cellular locations.

The highly conserved nucleating factor Arp2/3 is a complex composed of seven subunits, namely Arp2, Arp3 and ARPC1 – ARPC5 (Machesky et al., 1994; Robinson et al., 2001). Arp2/3 binds laterally of an already existing actin filament and initiates the formation of a new branched filament at a 70° angle (Blanchoin et al., 2000; Mullins et al., 1998). Thereby, Arp2 and Arp3 act as the first two subunits of the newly formed filament (Volkmann et al., 2001). However, the Arp2/3 complex itself is not able to nucleate actin efficiently. Thus, the Arp2/3 complex requires additional regulatory proteins, NPFs, to initiate formation of a branched actin filament. At the C-terminus, NPFs usually contain three motifs: a verprolin-homology domain, also known as WASP-homology 2 (WH2) domain, a connector region and an acidic motif. This region is therefore termed VCA-domain and binds to actin via its V motif, as well as to the Arp2/3 complex via C and A (Welch and Mullins, 2002). NPFs also contain an N-terminal GTPase-binding domain (GBD) which interact with the C motif and thus autoinhibits the protein. Upon activation by Rho-GTPases, for example CDC42 and

Rac1, together with phosphatidylinositol-4,5-bisphosphate (PIP2), autoinhibition is released, the free VCA domain can bind to Arp2/3 and actin and start actin polymerization subsequently (Bi and Zigmond, 1999; Prehoda et al., 2000). The family of NPFs include proteins such as WASP, N-WASP (a neuronally expressed form of WASP), WAVE/SCAR, WASH or WHAMM (Rotty et al., 2013).

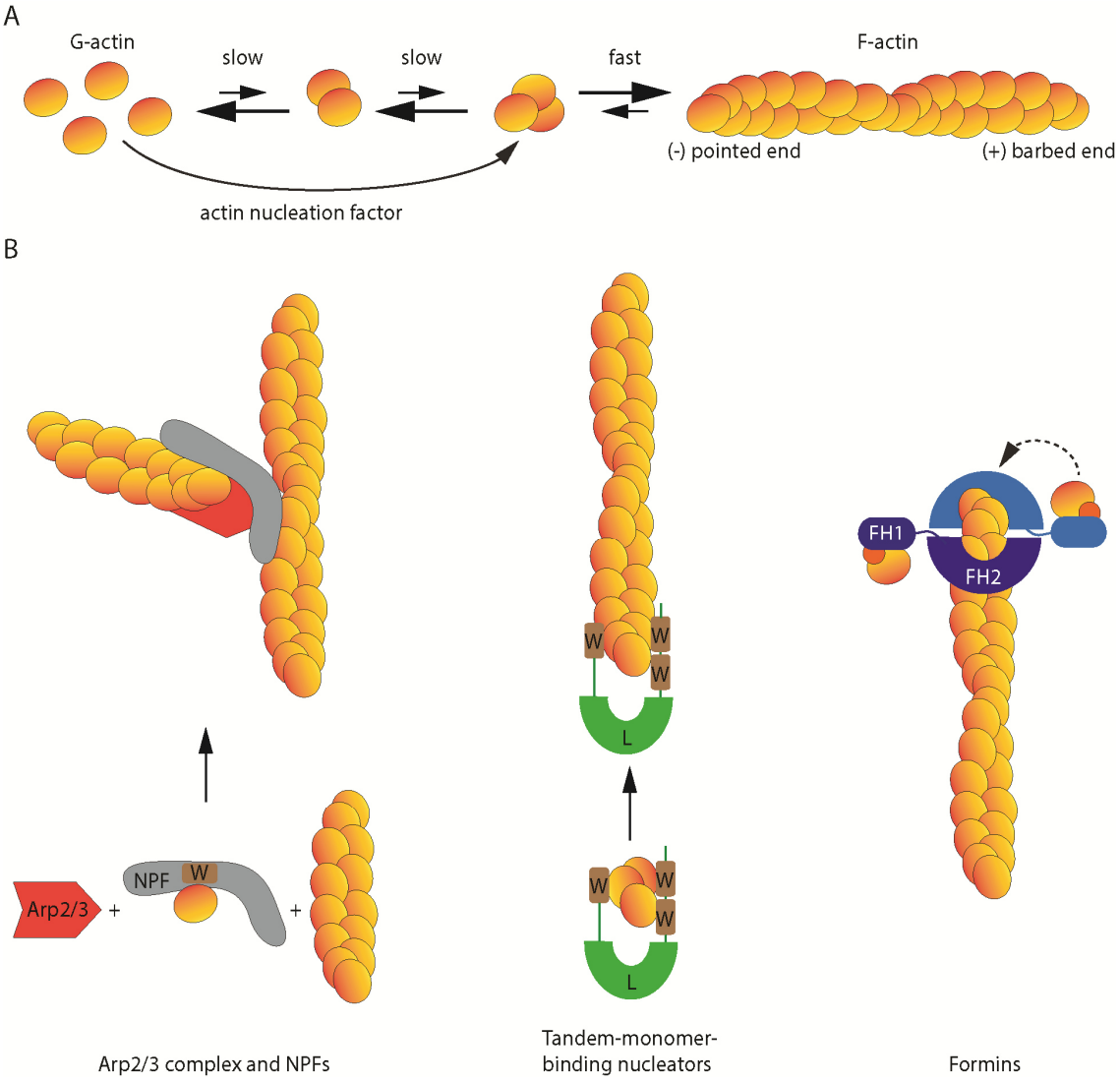

Figure 2: Three classes of actin nucleating factors promote F-actin assembly

A) The initiation of F-actin assembly requires the formation of a trimeric actin nucleus. The actin dimer and trimer intermediate is very unstable, therefore spontaneous nucleation is kinetically unfavorable and requires actin nucleating factors. **B)** The ARP2/3 complex, in the presence of NPFs, promotes actin nucleation after binding to a pre-existing actin filament and generates branched actin filaments at a 70° angle. Members of the family of tandem-monomer-binding nucleators recruit actin monomers and

assemble and stabilize actin nucleation seeds. This cartoon illustrates cordon bleu which nucleates a filament by assembling and stabilizing an actin trimer. It might remain associated with the pointed end of F-actin during elongation. W: WH2 domain, L: linker region. Formins drive the nucleation of long, unbranched filaments. During elongation, they remain associated and move along the barbed end and deliver profilin-bound G-actin. The image was adapted from (Weston et al., 2012).

The second class of actin nucleating factors termed tandem-monomer-binding nucleators was recently identified and includes for example the proteins spire, cordon-bleu (cobl) and leiomodin (lmod) (Ahuja et al., 2007; Chereau et al., 2008; Quinlan et al., 2005). These proteins possess one (lmod) or more (cobl: 3, Spire: 4) WH2 domains separated by short linker sequences or, as lmod, additional actin binding domains, thereby recruiting actin monomers and forming actin polymerization seeds (Chesarone and Goode, 2009).

1.3 Formins

The multidomain protein family of formins, which are present in almost all eukaryotes, represents the third class of actin nucleating factors. They promote the nucleation and elongation of unbranched actin filaments (Pruyne et al., 2002). Phylogenetic analysis of the highly conserved formin homology 2 (FH2) domain revealed that Metazoan formins can be segregated into seven groups: Dia (diaphanous), Daam (dishevelled-associated activator of morphogenesis), FMNL (formin-like protein) or FRL (formin-related gene in leukocytes), FHOD (formin homology domain-containing protein), INF (inverted formin), FMN (formin) and Delphilin. Most groups contain multiple members, for example mammals have 15 identified formin genes in total (Table 1) and therefore formins represent the largest group of actin nucleators (Breitsprecher and Goode, 2013; Higgs, 2005).

Table 1: Mammalian formin members

Subfamily	Members	
Dia	mDia1	(DIAPH1)
	mDia2	(DIAPH3)
	mDia3	(DIAPH2)
Daam	Daam1	
	Daam2	
FMNL	FMNL1	(FRL1)
	FMNL2	(FRL3, FHOD2)
	FMNL3	(FRL2)
FHOD	FHOD1	
	FHOD2	(FMNL2)
	FHOD3	
INF	INF1	
	INF2	
FMN	FMN1	
	FMN2	
Delphilin	Delphilin	

Formins are mainly defined by two regions: the formin homology 2 (FH2) domain and the formin homology 1 (FH1) domain. The catalytic FH2 domain is required for association with the barbed end of growing actin filaments and promotes processive actin assembly (Higashida et al., 2004; Pring et al., 2003; Pruyne et al., 2002) . The proline-rich FH1 domain precedes the FH2 domain and binds profilin-actin to accelerate actin filament elongation (Kovar and Pollard, 2004; Paul et al., 2008).

The most intensely investigated formins belong to the domain-based classification group of Diaphanous-related formins (DRFs), which share a highly conserved domain architecture among diverse model organisms (Breitsprecher and Goode, 2013). Briefly, prototypic DRFs (including Dia, Daam and FMNL) feature an N-terminal regulatory region and a C-terminal activity region. The N-terminal FH3 subdomain diaphanous inhibitory domain (DID), consisting of five armadillo repeats, and the C-terminal diaphanous autoregulatory domain (DAD) interact in an autoinhibitory manner (Figure 4A). Activated Rho-GTPases can relieve this intramolecular inhibition by interacting with the N-terminal GBD (Li and Higgs, 2005; Otomo et al., 2005a; Rose et al., 2005). Upon activation, the FH2 domain forms an antiparallel dimer and subsequently

promotes incorporation of monomeric actin into the growing barbed end of filament (Xu et al., 2004).

Besides DRFs, formins differ strikingly in their domain organization (Figure 3) (Campellone and Welch, 2010). For example, FMN1 and FMN2 possess a formin-spire interaction domain (FSI) (Vizcarra et al., 2011) and delphilin contains a PDZ domain (Miyagi et al., 2002).

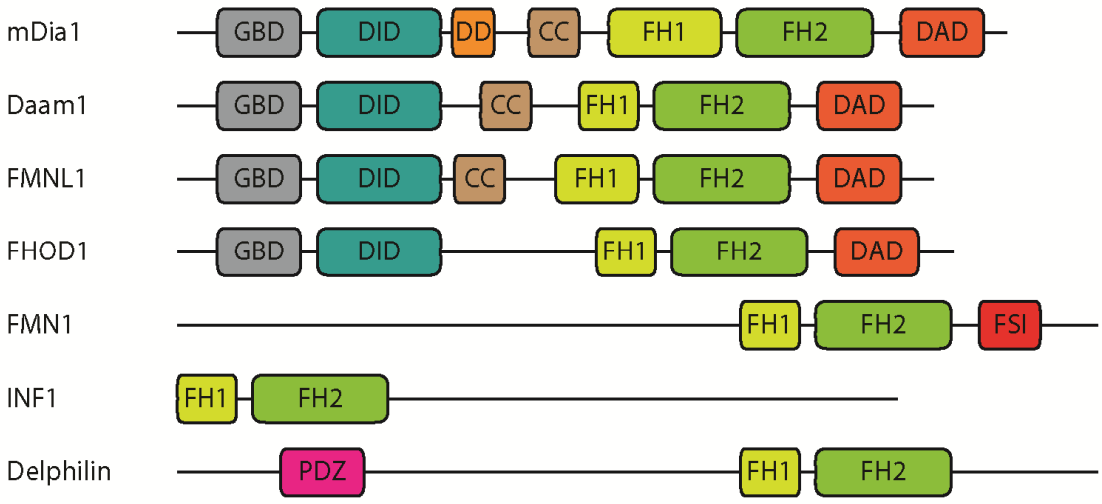

Figure 3: Representative formins of each metazoan subgroup show distinct domain organization
The cartoon illustrates similarities and differences in the domain organization of representative members from each metazoan formin group. All formins share a conserved FH1 and FH2 domain. CC: coiled coil; DAD: diaphanous-autoinhibitory-domain; DD: dimerization domain; FSI: formin–Spire interaction domain; PDZ: Postsynaptic density protein, Discs large, Zona occludens 1 domain. The image was adapted from (Campellone and Welch, 2010; Goode and Eck, 2007).

1.3.1 Formin induced actin assembly

Although detailed information about mechanism, regulation and function of diverse formins became available within the last decade, the precise actin nucleation procedure still has to be determined. It was initially suggested that spontaneously formed actin dimers and trimers are captured and stabilized by the FH2 domain and filaments are assembled subsequently (Pring et al., 2003). However, *in vivo*, the pool

of G-actin is predominantly bound to profilin, which inhibits spontaneous formation of an actin nucleus and thus would make formin-mediated F-actin formation a rather rare event (Chesarone and Goode, 2009). More recently, studies suggested that C-terminal of the FH2 domain located sequences play a role in – either direct or indirect – recruiting actin monomers and promoting actin nucleation (Chhabra and Higgs, 2006; Gould et al., 2011; Heimsath and Higgs, 2012; Thompson et al., 2013).

Upon actin nucleation, the dimeric FH2 domain processively associates with the barbed end of F-actin and permanently incorporates new actin subunits before it dissociates (Otomo et al., 2005b). Additionally, it prevents termination of F-actin elongation by inhibiting the binding of other capping proteins to the barbed end (Zigmond et al., 2003). The processive movement along the barbed end of F-actin was suggested to involve transient, alternating interaction of the two dimerized FH2 domains with the two terminal F-actin subunits. Thereby, the FH2 dimer was suggested to switch between a closed conformation where both FH2 domains are bound to actin subunits, preventing addition of new actin monomers and an open conformation allowing filament elongation (Otomo et al., 2005b; Paul and Pollard, 2009).

In contrast to the slow elongation rate at free barbed ends, the rate at the FH2 bound barbed end is enhanced massively due to the interaction of the FH2 adjacent FH1 domain with profilin bound G-actin (Kovar, 2006; Paul et al., 2008; Romero et al., 2004). The proline rich FH1 domain is thought to recruit multiple profilin-actin complexes, thereby increasing the local concentration of G-actin at the barbed end with subsequent incorporation into the growing filament (Vavylonis et al., 2006). However, the exact mechanism how actin subunits are delivered from the FH1 to the FH2 domain still has to be elucidated. It might be dependent on direct interactions between profilin-actin as well as the FH1 and FH2 domain (Neidt et al., 2009).

In vitro, formins remain attached to the barbed end for minutes without dissociating, thereby assembling actin filaments much longer than they could ever be detected in living cells (Kovar et al., 2006; Neidt et al., 2008). Thus, in vivo regulatory mechanisms

are needed to displace formins from the barbed end and stop formin mediated filament elongation. Such mechanisms have been identified for S. cerevisiae. For example, Bud14 catalyzes the rapid displacement of the yeast formin Bnr1 (Chesarone et al., 2009) and Smy1 interferes with elongation of F-actin by binding to the FH2 domain of Bnr1 (Chesarone-Cataldo et al., 2011). Additionally, it has been shown that the Arp2/3 complex and WAVE can directly inhibit mDia2 mediated filopodia formation (Beli et al., 2008).

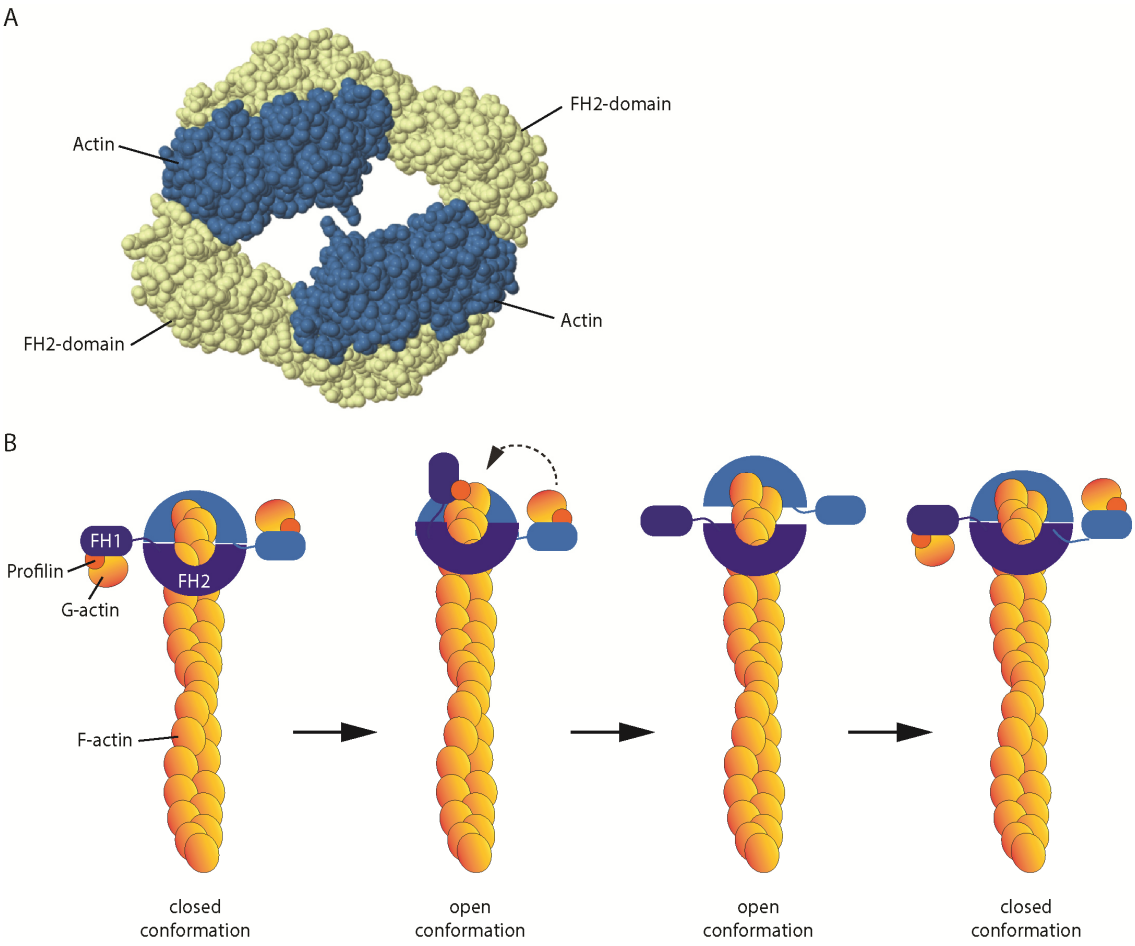

Figure 4: A model of formin-mediated actin polymerization

A) Crystal structure of the dimeric FH2 domain of FMNL3 bound to two subunits of actin. The image was taken and adapted from the RSCB Protein Data Bank (PDB ID: 4EAH), originally published by (Thompson et al., 2013). **B)** A model for formin-mediated actin assembly. (1) The FH2 dimer processively associates with the barbed end of F-actin. In an initial closed conformation, both FH1 domains recruit profilin bound G-actin. (2) Upon delivery of profilin-actin to the barbed end by FH1, the adjacent FH2 domain moves along the barbed end. (3) The process is repeated by the second FH2 domain. (4) Back in a closed

conformation, the filament is prevented by binding of other factors. The image was adapted from (Campellone and Welch, 2010).

1.3.2 Regulation of formin proteins

Autoinhibition of DRFs is mediated by binding of the N-terminal DID with the C-terminal DAD (Alberts, 2001; Li and Higgs, 2005). Two main motifs in the DAD play an important role in the autoinhibition mechanism: an amphipathic helix followed by a sequence rich in basic residues. Co-crystallization of mDia1-DID together with mDia1-DAD revealed binding of the entire DAD polypeptide to the DID, more precisely to the central B helices of the five armadillo repeats at the concave surface, through numerous mainly hydrophobic contacts (Alberts, 2001; Nezami et al., 2006) (Figure 5A). Interaction of the DID and DAD was shown to prevent F-actin elongation mediated by the activity of the FH2 domain through a proposed steric contact inhibition of FH2 and actin (Nezami et al., 2010; Otomo et al., 2010). Noteworthy, it has also been hypothesized for DRFs that autoinhibition does not occur intramolecular but rather in dimeric or higher order configurations (Copeland et al., 2007).

Beside the modulation of DRFs by its DID/DAD mediated autoinhibition, other regulatory mechanisms have been described which interfere with the catalytic activity of the FH2 domain. One example is dia-interacting protein (DIP) which was shown to interact with the FH1 and FH2 domains of mDia2 and modulates cortical actin assembly (Eisenmann et al., 2007).

In general, Rho-GTPases, which belong to the Ras family of small GTPases, have been shown to play crucial roles in the regulation of actin remodeling. For example, they are involved in actin stress fiber formation (Rho) as well as in the formation of lamellipodia (Rac) or filopodia (Cdc42) (Jaffe and Hall, 2005). Briefly, Rho-GTPases function as molecular switches. They cycle between a GTP-bound active and a GDP-bound inactive state. This cycling activity is modulated by guanine nucleotide exchange factors (GEFs), which promote Rho activation through the exchange of GDP to GTP, as well as by

GTPase-activating proteins (GAPs), which mediate inactivation of Rho by stimulating its intrinsic GTPase activity. In an active state, Rho-GTPases fulfill their regulatory functions through interaction with effector proteins (Jaffe and Hall, 2005).

The impact of Rho-GTPases on actin rearrangement is partially mediated through formins, which constitute the largest protein family of Rho effectors. Upon stimulation by extracellular signals, for example serum or lysophosphatidic acid (LPA), G-protein-coupled receptors (GPCRs) get activated (Young and Copeland, 2010). Subsequently, they stimulate RhoGEFs, such as LARG for example which in turn promotes RhoA activation to release autoinhibition of mDia1 (Fukuhara et al., 2000; Goulimari et al., 2008).

Binding of activated members from the Rho-GTPase family to the GBD releases the autoinhibition of DRFs (Figure 5B) (Lammers et al., 2005). In the case of mDia1, activated RhoA binds to the GBD-DID fragment. A model suggests that RhoA sterically interferes via Arg68 with the DAD binding to the DID. Additionally, RhoA binding also stabilizes the position of the GBD relative to the DID and thus a six residue segment of the GBD directly occludes the DAD binding site (Nezami et al., 2006) (Figure 5C).

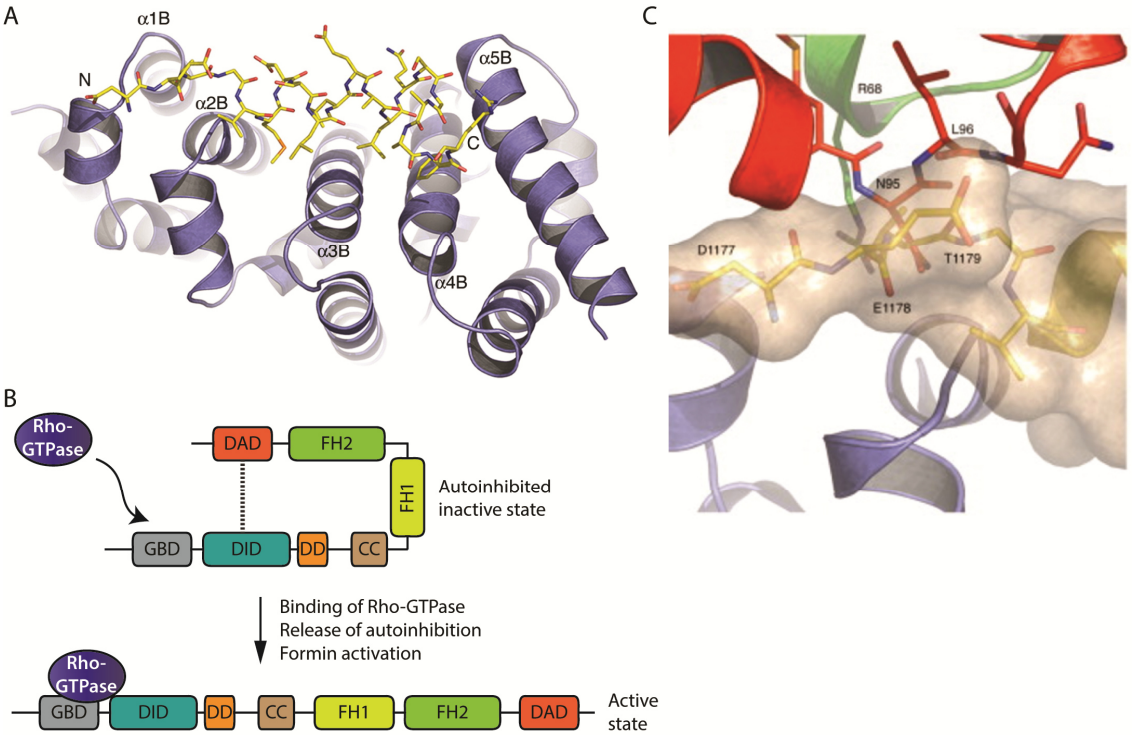

Figure 5: Regulation of DRF autoinhibition

A) This ribbon model illustrates the overall structure of the mDia1-DID/DAD complex in an mDia1-autoinhibited state. The DID is shown in blue, the DAD is shown in yellow. The N and C termini of the DAD domain are indicated and the B helices of the armadillo repeats are labeled from left to right. The image was taken from (Nezami et al., 2006). **B)** DRFs (here: mDia1) are autoinhibited by an intramolecular interaction between DID and DAD. Upon stimulation by binding of Rho-GTPases, the autoinhibition is released and formins get activated. The image was adapted from (Goode and Eck, 2007) **C)** This close-up ribbon model demonstrates the steric masking of the mDia1 DAD binding site by the Rho complex (shown in green). GBD (red) residues 92-97 and Rho residue R68 impact binding of the N-terminus of the DAD (superimposed in yellow) to the DID (purple). Thus, binding of Rho, together with the restructured GBD excludes simultaneous binding of the DAD and drives activation of the formin. The image was taken from (Nezami et al., 2006).

The activation of formins to mediate diverse biological functions requires distinct Rho-GTPases. For example, mDia2 is activated by the Rho-GTPase Rif to induce filopodia (Pellegrin and Mellor, 2005), whereas during endosomal trafficking it is activated by RhoB (Wallar et al., 2007). Moreover, Rac1 has also be reported to be able to regulate mDia2 (Ji et al., 2008). In turn, each Rho-GTPase can act on different formins to carry out diverse biological functions. This is also dependent on the cellular context as well as on the intracellular localization. As an example, Cdc42 activates mDia2 at the leading edge of the cell (Peng et al., 2003), whereas it modulates FMNL1 (also referred to as Frlα) during formation of phagocytic cups (Seth et al., 2006).

However, the process of formin activation is a quite complex interplay between different proteins and therefore is yet not fully understood. For example it was shown that the FH2 domain of mDia1 binds to LARG and thus is able to activate RhoA in a positive feedback loop (Kitzing et al., 2007). It was also shown that other factors than Rho-GTPases are involved in the activation of formins. Autoinhibition of Daam1 for instance was shown to be regulated by interaction with a PDZ domain of Dishevelled, a member of the noncanonical Wnt signaling pathway. This interaction for full activation of Daam1 either occurs independently or together with Rho (Liu et al., 2008).

Additionally, the release of formin autoinhibition as well as their intracellular localization can be mediated by post-translational modifications such as

phosphorylation. For example, Protein kinase Cα (PKCα) phosphorylates FMNL2 within the DAD domain, thereby regulating its localization and activity (Wang et al., 2015). Furthermore, the autoinhibition of FHOD1 can be disrupted by Rho associated coiled coil containing protein kinase (ROCK) mediated phosphorylation at three conserved residues in the polybasic region C-terminal of the DAD, resulting in the formation of stress fibers (Takeya et al., 2008). ROCK was additionally shown to phosphorylate residues in the C-terminus of a muscle specific FHOD3 isoform, leading to activation and subsequent increased F-actin assembly in cardiomyocytes (Iskratsch et al., 2013). In turn, casein kinase 2 (CK2) phosphorylates a site in the FH2 domain of this muscle specific FHOD3 splice variant which targets the formin to the myofibrils in cardiomyocytes (Iskratsch et al., 2010). Moreover, Aurora B kinase phosphorylates residues in FHOD1, thereby regulating actin cables after cell division (Floyd et al., 2013). Aurora B kinase also phosphorylates the FH2-domain of mDia3, which inhibits its ability to stabilize microtubules (Cheng et al., 2011). Furthermore, formins were shown to be post-translationally modified through the attachment of lipid molecules. For example, the formin subfamily of FMNL proteins is N-terminally myristoylated, which regulates its membrane trafficking (Han et al., 2009). Moreover, binding of phospholipids to the N-terminus of mDia1 was suggested to anchor formins at the plasma membrane whereas an interaction with phospholipids in the mDia1 C-terminus might provide a switch for transient inactivation (Ramalingam et al., 2010).

1.3.3 Cellular function of formins

Formins have been described intensely over the last decade (Baarlink et al., 2010; Goode and Eck, 2007; Wallar and Alberts, 2003). They play an essential role in diverse cellular processes such as cell and tissue morphogenesis. For example Daam1 was shown to be essential for Wnt/Frizzled mediated RhoA activation during Xenopus gastrulation (Habas et al., 2001). Furthermore, formins can drive cell motility as it was shown during amoeboid cell migration, where FMNL2 modulates invasiveness of cells (Kitzing et al., 2010). FMNL2 is also involved in the trafficking of β1-integrin, thus

modulating invasion (Wang et al., 2015). Formins additionally participate in the formation of cell-to-cell contacts. For instance, FMNL2 was shown to modulate junctional actin assembly and turnover (Grikscheit et al., 2015). Additionally, formins were shown to be essential during cytokinesis, where mDia2 drives F-actin formation to assemble a scaffold for the contractile ring and stabilizes its position during cytokinesis (Watanabe et al., 2008). Moreover, it was described in Drosophila that mutations in the formin diaphanous lead to a failure in cell division during spermatogenesis and multinucleated spermatids (Castrillon and Wasserman, 1994). Studies in Drosophila revealed further critical functions of formins, such as the maintenance of cell polarity and regulation of embryonic development. For example, the Drosophila formin cappuccino is required for the polarity of fly eggs and embryos (Emmons et al., 1995). Furthermore, in the Drosophila respiratory system, Daam regulates the tracheal cuticle pattern through arranging the actin cytoskeleton (Matusek et al., 2006). Moreover, vesicular transport was also shown to be dependent on the function of formins, such as the human isoform hDia2C, which regulate endosomal dynamics (Gasman et al., 2003).

Besides their role in rearrangement of actin structures, formins possess also an impact on microtubule networks. For example it was described that loss of FMN2 in mouse oocytes results in failed meiotic spindle alignment and fertility (Leader et al., 2002). Furthermore, mDia3 is s required for microtubule attachment to the kinetochore and proper chromosome segregation (Yasuda et al., 2004), whereas mDia1 plays a role in the orientation and coordination of microtubules (Goulimari et al., 2008; Ishizaki et al., 2001).

Another relevant function of formins is their impact on serum response factor (SRF) dependent transcriptional regulation, modulated through formin mediated actin rearrangement (Copeland and Treisman, 2002; Copeland et al., 2007; Grosse et al., 2003).

1.4 Regulation of the MRTF/SRF transcriptional pathway

The transcription factor SRF is abundantly expressed in many different cell types among diverse species, from yeast to human (Norman et al., 1988; Olson and Nordheim, 2010; Shore and Sharrocks, 1995). SRF binds as a homodimer with high affinity to a palindromic CArG-box DNA sequence, also named serum response element (SRE) and promotes transcription of numerous target genes (Treisman, 1986). SRF activity is competitively modulated through binding of two different types of cofactors, the ternary complex factors (TCFs) (Buchwalter et al., 2004) as well as the MRTF family of co-activators (myocardin and myocardin-related transcription factors - MRTFs) (Pipes et al., 2006; Wang et al., 2001; Wang et al., 2002). Both cofactors are differentially signal regulated and enable SRF to drive transcription of different sets of target genes in a competitive manner (Gualdrini et al., 2016). While TCFs respond to signals of the mitogen-activated protein kinase (MAPK) pathway, MRTF mediated transcription is dependent on the rearrangement of the actin cytoskeleton (Gineitis and Treisman, 2001; Zaromytidou et al., 2006). SRF was shown to be essential for numerous biological processes including development of the heart and the cardiovascular system, liver development, activity of T-cells and B-cells, gastrulation, brain development and many more (Olson and Nordheim, 2010). Most of those developmental defects can be explained at least in part by functional defects of actin cytoskeleton dynamics (Schratt et al., 2002).

The MRTF family includes the transcriptional co-activators myocardin which is expressed specifically in the cardiovascular system, as well as the more widely expressed MRTF-A (also known as MAL, MKL1 and BSAC) and MRTF-B (also known as MKL2 and MAL16) (Wang et al., 2001; Wang et al., 2002). MRTFs interact with SRF through a basic region and an adjacent localized Glutamic-acid-rich domain (Olson and Nordheim, 2010). At the N-terminus, MRTF-A and MRTF-B possess three so called RPEL domains (Arg-Pro-X-X-X-Glu-Leu), which form a stable complex with G-actin. In contrast, the RPEL of myocardin differs from that of MRTF-A and MRTF-B and does not

bind monomeric actin efficiently (Guettler et al., 2008; Miralles et al., 2003; Pipes et al., 2006).

In cells featuring low actin polymerization states the pool of G-actin is relatively high compared to F-actin. Thus, MRTF proteins form a reversible complex with G-actin and therefore exist in an inactive state sequestered in the cytoplasm (Posern et al., 2002). However, initiation of F-actin assembly, for example by formins (Copeland and Treisman, 2002), reduces the availability of G-actin through its incorporation into newly formed filaments. G-actin then dissociates from MRTFs, which promotes release of an nuclear localization sequence (NLS) within the RPEL motif (Pawłowski et al., 2010) and allows subsequent nuclear import of MRTFs followed by activation of SRF dependent gene transcription (Miralles et al., 2003). Additionally, MRTF activity is also regulated by G-actin inside the nucleus. It was shown that nuclear export of MRTF is driven by nuclear actin monomers. Furthermore, the nuclear G-actin pool prevents MRTF to activate SRF (Vartiainen et al., 2007).

Studies have revealed more than 200 target genes which are directly regulated by SRF (Cooper et al., 2007). Thereby, TCF and MRTF mediated co-activation differs in terms of SRF target gene expression. TCF modulated target genes encoding proteins with so called immediate-early functions, for example proteins involved in cell cycle progression. MRTF-regulated target genes for instance play a role in muscle-specific contractile functions or actin rearrangement and therefore in processes such as proliferation and cell motility (Buchwalter et al., 2004; Medjkane et al., 2009; Olson and Nordheim, 2010). Interestingly, actin itself was also shown to be a target gene of MRTF/SRF regulated gene expression (Olson and Nordheim, 2010). Thus, nucleocytoplasmic shuttling of MRTF is additionally regulated by a negative feedback loop, as ongoing synthesis of actin results in increased levels of cytoplasmic and nuclear G-actin and subsequent impairment of SRF activity.

1.5 Actin and actin binding proteins in the nucleus

The localization of actin in the nuclear compartment as well as its underlying nucleocytoplasmic shuttling mechanism was previously reported. G-actin is imported as a complex with cofilin in an importin 9-dependent manner (Dopie et al., 2012) and gets exported together with profilin by the export receptor exportin 6 (Stüven et al., 2003; Wada et al., 1998).

The appearance and diverse functions of monomeric and short oligomeric actin in the nucleus was already widely accepted and described. For example, as already mentioned, actin in the nucleus is implicated in specific regulation of the MRTF/SRF transcriptional pathway (Vartiainen et al., 2007). Moreover, multiple studies revealed a role for actin in the regulation of general eukaryotic gene transcription as well as chromatin remodeling (de Lanerolle and Serebryannyy, 2011). For instance, nuclear actin was reported to interact with all three RNA polymerases, Pol I (Philimonenko et al., 2004), Pol II (Hofmann et al., 2004) and Pol III (Hu et al., 2004), and thus may affect their transcriptional function. Actin was also shown to interact in the nucleus with the BAF chromatin-remodeling complex (Zhao et al., 1998). Moreover, it regulates the remodeling activity of the yeast INO80 chromatin remodeling complex in its monomeric form (Kapoor et al., 2013).

Furthermore, actin-binding proteins were reported to play a role in general regulation of gene transcription. For example, the Arp2/3 complex in association with N-WASP has been implicated in transcriptional regulation of RNA polymerase II (Wu et al., 2006; Yoo et al., 2007). Moreover, nuclear myosin I (NM1) has been described to affect transcription mediated by RNA polymerase I and II (Hofmann et al., 2006; Philimonenko et al., 2004; Ye et al., 2008). Also several actin-related proteins, sharing the basal actin-structure but possess functions different from actin, were detected to be functional components of the transcription complex as well as chromatin remodeling complexes (Fenn et al., 2011; Harata et al., 2002; Lee et al., 2007; Szerlong et al., 2008; Zhao et al., 1998).

Interestingly, actin was mostly shown to act in a monomeric or short oligomeric state on nuclear complexes (Grosse and Vartiainen, 2013; Percipalle, 2013). However, photobleaching experiments suggested the existence of at least three different actin pools in the nucleoplasm which may correspond to a monomeric and a polymeric actin state as well as actin bound to functional complexes (McDonald et al., 2006). Furthermore, drug mediated prevention of actin polymerization and utilization of a polymerization deficient actin-mutant reduced RNA polymerase I mediated transcription in vitro and in vivo (Ye et al., 2008), thus arguing for the requirement of polymerized actin for gene transcription. Nevertheless, the question whether the localization and identified functions of actin in the nucleus goes along with the assembly of polymeric nuclear actin filaments, comparable to those in the cytoplasm, was in dispute (Pederson and Aebi, 2002). This was mainly due to the fact that nuclear actin structures were hardly detectable because of its general low nuclear abundance compared to its cytosolic fraction (Baarlink et al., 2013). Moreover, dynamic actin filaments could not be easily visualized in the nuclei of living somatic cells, as many actin detection methods such as genetically encoded fluorescently labeled actin or actin-binding proteins in general negatively influence functionality and kinetics (Belin et al., 2014; Spracklen et al., 2014).

On the other hand, numerous actin-binding proteins, playing essential roles in cytoplasmic actin rearrangement, have been recently detected in the nucleus. Among the reported nuclear localized actin-binding proteins are for example the already before mentioned ARP2/3 complex (Yoo et al., 2007), its NPF N-WASP (Suetsugu and Takenawa, 2003; Wu et al., 2006) and myosins (de Lanerolle and Serebryannyy, 2011), as well as the p53-cofactor JMY (Shikama et al., 1999; Zuchero et al., 2012; Zuchero et al., 2009), profilin (Lederer et al., 2005; Söderberg et al., 2012) and the actin severing and disassembly regulators cofilin (Dopie et al., 2012; Obrdlik and Percipalle, 2011) or gelsolin (Archer et al., 2005).

Furthermore, during apoptosis a caspase-3 mediated C-terminal FHOD1 cleavage product has been reported to translocate to the nucleus (Ménard et al., 2006).

Overexpression of this cleavage product resulted in RNA polymerase I inhibition in HeLa cells. All in all, the nuclear localization of proteins generally involved in assembly and disassembly of F-actin implies the presence of dynamic nuclear F-actin structures. Moreover, the human formin Diaphanous 1 (hDia1) was co-purified from HeLa cells in a complex with exportin 6 together with profilin-bound actin and other actin-binding proteins, thus suggesting nucleocytoplasmic shuttling of hDia1 (Stüven et al., 2003). Additionally, it was discovered that mDia2, but not mDia1 and mDia3, accumulates in the nucleus upon treatment with the CRM1-dependent nuclear export blocking drug Leptomycin B (LMB) (Miki et al., 2009). Functional analysis of the mDia2 amino acid sequence revealed at least one functional NLS and NES in this particular formin. Based on these studies it was suggested that mDia2 continuously shuttles between the nuclear and the cytoplasmic compartment using a specific transport machinery composed of importin-α/β and CRM1 (Miki et al., 2009).

Worth mentioning, it is still under investigation if the activity-state of mDia affects its nuclear import. It has to be determined if there is a specialized nuclear mechanism of mDia activation or if formin activity is passively transduced towards the nucleus. Principally, mDia activation can occur prior to nuclear import in the cytoplasm or inside the nucleus upon entering the nuclear compartment. Generally, the majority of mDia resides in an autoinhibited state under unstimulated conditions. This suggests nuclear import of autoinhibited mDia, as CRM1 treatment leads to a rapid nuclear accumulation of mDia2 even without further stimulation. However, it remains unclear if mDia2 in its active open conformation is prevented from its nuclear import (Baarlink and Grosse, 2014; Plessner and Grosse, 2015).

Recently, the first tools for detailed and reliable visualization of endogenous nuclear actin structures in living somatic cells became available (Baarlink et al., 2013; Belin et al., 2013; Melak et al., 2017; Plessner et al., 2015). For example, a role for polymerized nuclear actin in the context of integrin-based cellular adhesion and mechanotransduction through the LINC complex was described using a nuclear

targeted cameloid nanobody fused to TagGFP2, called nuclear Actin-Chromobody (Plessner et al., 2015).

Although the occurrence of formins in the nucleus was reported previously (Miki et al., 2009; Ménard et al., 2006; Stüven et al., 2003), their detailed functions remained unknown for years. However, quite recently, functions of formins in the assembly of nuclear F-actin were detected (Baarlink et al., 2013; Belin et al., 2015). For instance, a role for nuclear formin activity was suggested in DNA repair. It was shown that DNA damage leads to formation of nuclear actin filaments. Those filaments were assembled by nuclear localized Formin-2 together with the actin nucleators Spire-1 and Spire-2 and promote clearance of double-strand DNA breaks (Belin et al., 2015).

1.5.1 Formin regulated nuclear actin network formation and MRTF/SRF transcriptional activity

Another recent study revealed nuclear mDia mediated signal induced regulation of actin filaments in the nucleus combined with alterations in MRTF-SRF transcriptional activity in mammalian cells (Baarlink et al., 2013). Using a nuclear targeted version of the actin probe LifeAct (Riedl et al., 2008), the dynamic assembly of a nuclear mDia dependent intranuclear actin network could be visualized upon stimulation with serum or LPA in living cells (Baarlink et al., 2013).

The regulation of MRTF-A is a complex interplay between cytosolic and nuclear actin rearrangement. Binding of nuclear G-actin to MRTF-A promotes its export into the cytoplasm. In turn, an excessive amount of G-actin in the cytosol impairs its nuclear import (Figure 6). Therefore, MRTF-A activity was suggested to be dependent on the formation and disruption of G-actin-MRTF-A complexes in both compartments, indirectly mediated by polymerization-induced depletion of the overall G-actin pool (Mouilleron et al., 2011; Pawłowski et al., 2010; Vartiainen et al., 2007). Recent studies furthermore suggested that MRTF-A activation also requires active polymerization of nuclear F-actin, rather than just equilibration of the nuclear and cytoplasmic actin

pools. Additionally, mDia promoted nuclear F-actin formation appears to be sufficient to drive MRTF-A/SRF dependent gene expression, although it was suggested to be an integral part of a global cellular actin polymerization response that controls MRTF-A/SRF activity (Baarlink et al., 2013).

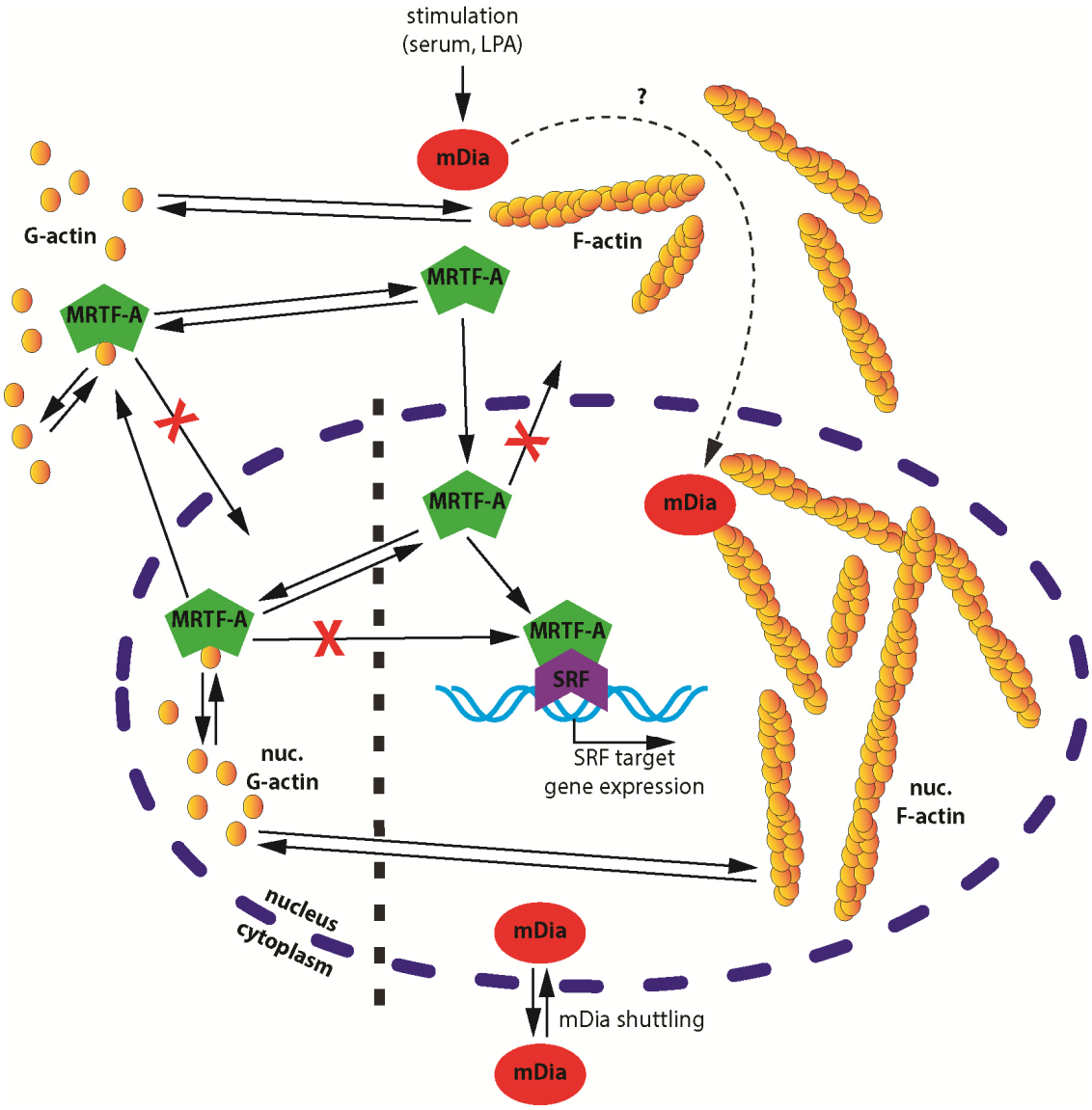

Figure 6: Nuclear F-actin formation by mDia regulates MRTF-A localization and activity

Signaling mediated dynamic assembly and disassembly of nuclear actin filaments is directly linked to MRTF-A activity. MRTF-A continuously shuttles between the nucleus and the cytoplasm in an actin polymerization and depolymerization dependent manner. The binding of nuclear actin monomer to MRTF-A drives its nuclear export to the cytoplasm. In turn, binding of cytoplasmic G-actin inhibits access to the NLS of MRTF-A and thus impairs its nuclear import. Increased intranuclear F-actin formation, for example mediated by mDia, which actively shuttles between the cytoplasmic and the nuclear

compartment, depletes the amount of available nuclear G-actin for binding to MRTF-A and prevents MRTF-A from being exported from the nucleus. In the cytoplasm, assembly of F-actin promotes release of G-actin from MRTF-A and mediates MRTF-A shuttling to the nucleus. Subsequently, MRTF-A co-activates SRF driven gene transcription. Upon nuclear F-actin disassembly, free G-actin binds again to MRTF-A and initiates its translocation to the cytoplasm, leading to inactivation of MRTF-A/SRF activity. Activation of nuclear mDia is sufficient to induce the assembly of nuclear F-actin structures and subsequent activation of MRTF-A/SRF activity. The image was adapted from (Baarlink and Grosse, 2014; Grosse and Vartiainen, 2013; Plessner and Grosse, 2015).

1.6 The formin INF2

Based on the results of previous publications it seems very likely that other formins, presumably members of the DRF family, might also perform a role in nuclear actin filament formation. One of the possible candidates to act in nuclear F-actin assembly was inverted formin 2 (INF2). Indeed, in a preliminary subcellular fractionation experiment, INF2 was also detected in the nucleus (H. Wang, unpublished data).

The domain architecture of INF2 (Figure 7A) features multiple similarities with formins of the DRF subfamily. The mainly regulatory N-terminus contains a DID and a dimerization domain, whereas the C-terminus comprises an FH1, FH2 and a DAD. Interestingly, the DAD resembles a highly conserved monomeric actin binding WH2 domain (Chhabra and Higgs, 2006).

INF2 is capable of conducting two quite opposite functions regarding actin dynamics: besides promoting the formation and elongation of actin filaments, INF2 is also able to mediate actin filament severing and to accelerate depolymerization. The F-actin severing and depolymerization activity was shown to require ATP hydrolysis and subsequent phosphate release from the filament (Chhabra and Higgs, 2006). It was suggested that both, FH2 binding and phosphate release result in local F-actin deformation which in turn allows the DAD/WH2 domain to bind adjacent actin protomers followed by severing and depolymerization of the filament (Figure 7B) (Gurel et al., 2014). This combination of barbed end elongation, filament severing and

DAD/WH2 mediated depolymerization leads to formation of short and rather transient F-actin structures under nearby steady-state conditions. The activity of profilin thereby helps to overcome the rate-limiting step of nucleotide exchange (ADP-actin to ATP-actin) upon release of G-actin from INF2, thus shifting the equilibrium toward polymerization and resulting in elongation of filaments (Gurel et al., 2015).

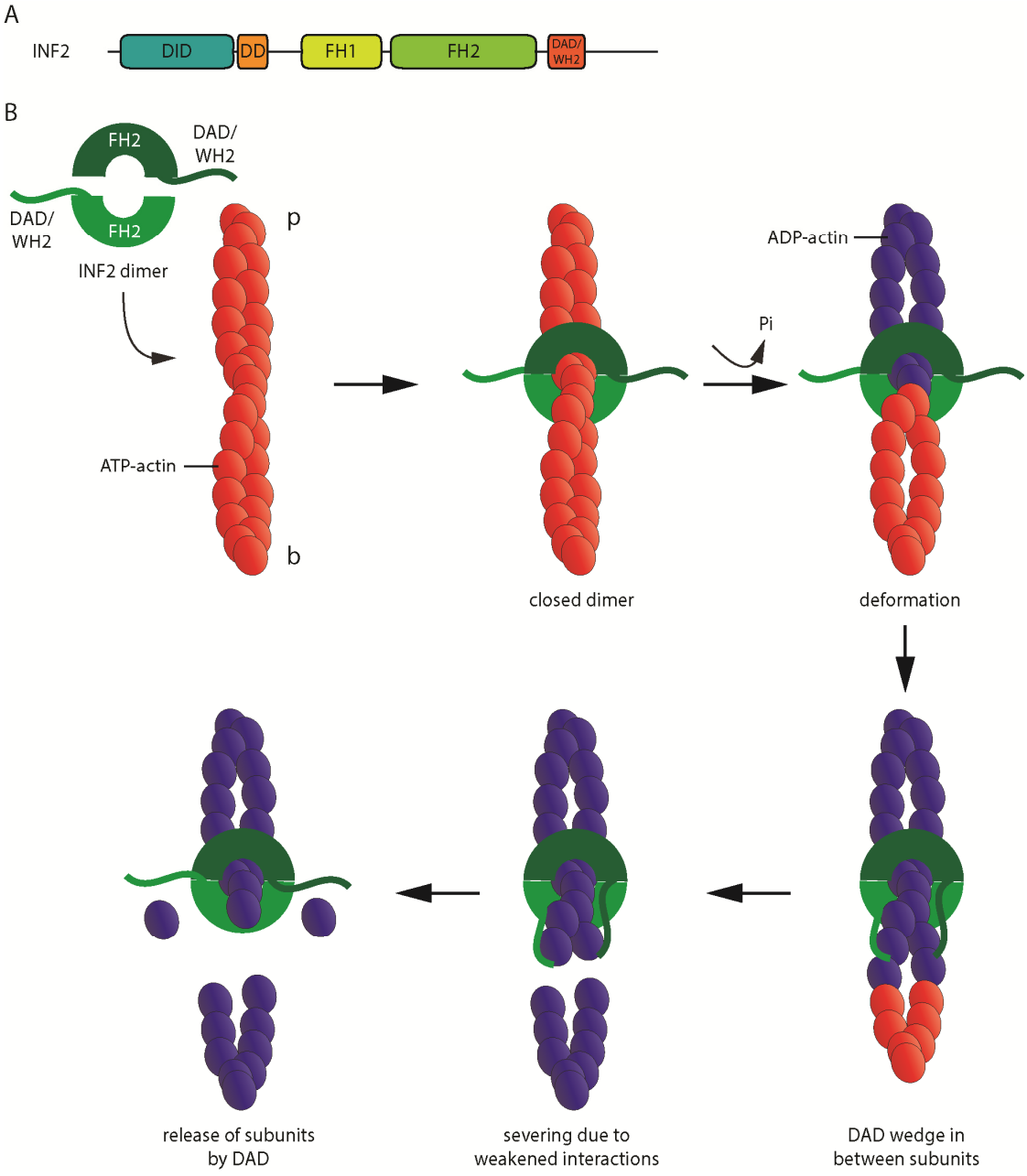

Figure 7: INF2 mediated severing and depolymerization of actin filaments

A) The cartoon illustrates the domain organization of INF2. **B)** A model for the INF2 mediated F-actin severing and depolymerization mechanism suggests that the partially dissociated INF2 dimer encircles

the filament either in a closed ring conformation or as an open dimer, arranged as a daisy chain. All severing and depolymerization steps in this model are displayed in the closed ring conformation, but could also be executed in an open dimer arrangement. Binding of the INF2 dimer leads to structural changes in the actin filament. Upon phosphate release, INF2 further deforms the filament close to its binding site, resulting in exposure of the DAD binding site of adjacent actin protomers. INF2-DAD/WH2 subsequently keys in and destabilizes F-actin. This leads to severing of the filament with INF2 remaining bound to the newly formed barbed end (b). The DAD/WH2-bound ADP-actin subunits are released subsequently. The image was adapted from (Gurel et al., 2014).

INF2 was shown to be autoinhibited by DID and DAD interaction. Remarkably, free actin monomers can compete with this interaction, thereby regulating actin polymerization as well as severing and depolymerization of actin filaments (Ramabhadran et al., 2013). Previous studies also implied binding of Cdc42 to INF2, thereby modulating its activity (Andrés-Delgado et al., 2010; Madrid et al., 2010). However, a direct interaction between INF2 and Cdc42 was rebutted and Cdc42 and INF2 were suggested to interact through additional proteins which serve as stabilizing factors for the DID and DAD interaction (Ramabhadran et al., 2013).

Mammalian INF2 exists as two splice variants, differing in cellular localization and functions due to their distinct C-terminus: INF2 and INF2-CAAX (Chhabra et al., 2009; Ramabhadran et al., 2011). Generally, the C-terminal CAAX box is defined by a cysteine residue followed by two aliphatic residues (AA) and any amino acid depending on its localization or substrate specificity. CAAX proteins usually undergo a posttranslational prenylation process by either adding a farnesyl or a geranylgeranyl residue to the cysteine for anchoring the proteins to membranes (Gao et al., 2009). INF2-CAAX is tightly bound to the endoplasmic reticulum (ER) (Chhabra et al., 2009) and modulates for example an actin dependent step during mitochondrial fission (Korobova et al., 2013). INF2 lacking the CAAX box on the other hand mainly localizes to the cytoplasm and mediates for instance organization of the Golgi (Ramabhadran et al., 2011).

A set of further INF2 functions has been described recently. In T-lymphocytes, INF2 regulates the transport of the src-family kinase lymphocyte-specific protein tyrosine kinase (Lck) to the plasma membrane. Thereby, Cdc42 was proposed as factor to bind

and activate INF2 (Andrés-Delgado et al., 2010). Additionally, basolateral-to-apical transcytosis and lumen formation in hepatocytes was suggested to be Cdc42 and INF2 dependent (Madrid et al., 2010). Furthermore, INF2 was linked to remodeling of the extracellular matrix in fibroblasts by promoting the formation of dorsal stress fibers and fibrillar focal adhesions (Skau et al., 2015). INF2 also modulates Ca^{2+}-dependent mechanosensing by mediation of a rapid and transient perinuclear actin polymerization upon mechanical stimulation. This perinuclear actin remodeling is necessary for a rapid intracellular response to external force (Shao et al., 2015). Last but not least, INF2 has recently been identified as key regulator for a process termed Calcium-mediated Actin Reset (CaAR), which includes a rapid and transient actin rearrangement in response to increased intracellular calcium levels. CaAR affects processes such as cell spreading, wound healing, organelle immobilization and alterations in SRF-mediated gene transcription (Wales et al., 2016).

Besides the direct regulation of actin polymerization and depolymerization, INF2 was also shown to antagonize Rho activated mDia signaling by heterodimeric interaction of INF2-DID and mDia-DAD (Sun et al., 2011). It has been demonstrated in cultured podocytes as well as in in vivo experiments that INF2 is an important modulator of Rho/mDia mediated actin dynamics, related to processes as lamellipodia formation and peripheral membrane trafficking (Sun et al., 2014; Sun et al., 2013). Additionally, a novel mechanism of serial formin activation was suggested, where mDia1 activates INF2 via interaction of mDia-DAD and INF2-DID and thereby regulates stable microtubules in migrating cells (Bartolini et al., 2016).

Several missense mutations in INF2 have been associated to the occurrence of the demyelinating neuropathy Charcot–Marie–Tooth (CMT). CMT often comes along with the renal disease Focal and segmental glomerulosclerosis (FSGS), which frequently leads to overt kidney failure in adolescence or adulthood (Barua et al., 2013; Boyer et al., 2011; Brown et al., 2010; Gbadegesin et al., 2012). All so far identified INF2 mutations are located in the DID. Some of these mutations, for instance E184K and R218Q, were described to inhibit the binding of INF2-DID to INF2-DAD and result in an

increased association with G-actin, the F-actin capping protein CapZ α-1 as well as profilin 2 (Rollason et al., 2016). Moreover, the mutations E184K and R218Q perturb the interaction of INF2-DID with mDia-DAD (Sun et al., 2011), leading to an impaired regulatory function of INF2 in terms of antagonizing Rho/mDia signaling (Sun et al., 2014; Sun et al., 2013). Generally, the previous findings suggest that the emergence of FSGS and CMT is at least partially linked to aberrant fine regulation of actin dynamics. Furthermore, E184K and R218Q also prevent the formation of stabilized detyrosinated microtubules. Hence, mutated INF2 mediated lack of microtubule stability may also be disease relevant (Bartolini et al., 2016). However, the precise contribution of mutated INF2 to the etiology of FSGS and CMT is still unknown.

2. Aim of this study

The appearance of monomeric actin in the nucleus of mammalian somatic cells, implicated in chromatin remodeling and the regulation of general eukaryotic gene transcription, was already widely accepted (de Lanerolle and Serebryannyy, 2011). In contrast, mainly due to limitations in detection, the existence of nuclear actin polymers remained elusive and was controversially discussed. Recently, specific nuclear actin probes have been described which enabled detailed visualization of F-actin structures in the nuclei of fixed and living cells (Baarlink et al., 2013; Belin et al., 2013; Melak et al., 2017; Plessner et al., 2015). Moreover, the discovery of several nuclear localized actin filament assembly proteins such as formins provided a first insight into regulation and function of actin polymerization in the nucleus (Baarlink et al., 2013; Belin et al., 2015).

However, many details about nuclear F-actin assembly and the contributing actin nucleation factors as well as detailed insight into the potential roles of nuclear actin filaments are still unknown. Thus, further progress in elucidating the exact mechanisms on the formation of nuclear actin filaments and resulting cellular functions is highly demanded.

The major aim of my thesis was to identify additional proteins which in terms of their intracellular localization and known actin-binding or actin-modulating properties are presumably involved in nuclear F-actin rearrangement.

Overexpression of an isolated mDia-DAD in cells sterically interfered with the DID-DAD binding and resulted in a release of the autoinhibited state and activation of mDia. This was followed by F-actin assembly and subsequent increase in MRTF/SRF activity (Alberts, 2001; Baarlink et al., 2013). The initial question was if overexpression of an isolated DID is also capable to interfere with the DID-DAD binding to promote release of formin autoinhibition. Indeed, overexpression of different DIDs and the investigation of the capability to activate their corresponding formin revealed that mDia-DID and INF2-DID perform comparably in terms of formin activation and

induction of SRF activity. Moreover, activation of INF2 could also be obtained by overexpression of the isolated INF2-DAD. Thus, we generated a powerful tool to control autoinhibition of endogenous INF2, allowing us to analyze the cellular impact of regulated INF2 activity.

Active mDia has been shown to mediate actin filament formation not only in the cytoplasm, but also inside the mammalian nucleus (Baarlink et al., 2013). Upon detection of endogenous INF2 in the nuclear extract by conducting subcellular fractionation experiments, we hypothesized that INF2 might also play a role in nuclear actin regulation.

The following questions were addressed and investigated, mainly by the use of fluorescence confocal microscopy in fixed or living cells as well as by biochemical approaches:

What are the nuclear import and export sequences enabling INF2 translocation to the nucleus and transport out of the nuclear compartment?

Does nuclear targeted INF2 activation induce the formation of F-actin structures in the nucleus?

Does nuclear INF2 activity affect subcellular localization of MRTF-A and subsequent MRTF/SRF transcriptional regulation?

Are the effects upon activation of INF2 by overexpression of its DAD specific for INF2 or due to involvement of other proteins, such as mDia formins?

Taken together, this study should extend our knowledge of factors involved in actin polymerization in the somatic cell nucleus.

3. Materials and Methods

3.1 Materials

Table 2: Reagents used in this study

Name	Supplier
2-Mercaptoethanol	Sigma-Aldrich
Acetic Acid	Roth
Agarose NEEO Ultra	Roth
Ammonium persulfate (APS)	Merck
Ampicillin	Roth
BES	Sigma
Bovine serum albumin (BSA)	Roth
Bromophenol blue	Roth
Calcium chloride (CaCl2)	Roth
Chloroform	Roth
Coomassie brilliant blue G250	Roth
DAPI	Sigma-Aldrich
Dimethyl sulfoxide (DMSO)	Roth
Dithiothreitol (DTT)	Roth
DMEM (HPSTA)	Capricorn Scientific
DNA ladder 1kb plus	Thermo Fisher Scientific
DNA loading dye 6x	Thermo Fisher Scientific
dNTPs	Promega
EGTA	Sigma-Aldrich
Enzymes for cloning	Thermo Fisher Scientific
Ethanol	Roth
Ethidium bromide	Roth
Ethylendiamintetraacetat (EDTA)	Roth
Fetal calf serum (FCS)	Thermo Fisher Scientific
FLAG (M2) conjugated agarose beads	Sigma-Aldrich
Fluorescent mounting medium	DAKO
Formaldehyde solution 37%	Roth
Fugene HD	Promega
GeneRuler 1kb plus DNA ladder	Thermo Fisher Scientific
Glucose	Roth
Glutaraldehyde	Sigma-Aldrich
Glycerol	Roth
H_2O_2	Sigma-Aldrich
HEPES	Roth
iQ SYBR-Green® Supermix	Bio-Rad
Isopropanol	Roth

Kanamycin	Roth
Lipofectamine LTX/Plus	Thermo Fisher Scientific
Lipofectamine RNAiMAX	Thermo Fisher Scientific
Magnesium chloride ($MgCl_2$)	Roth
Methanol	Roth
Milk powder (fat free)	Roth
Myc conjugated agarose beads	Sigma-Aldrich
NP-40	Merck
OptiMEM	Thermo Fisher Scientific
PageRuler Plus Prestained Protein Ladder	Thermo Fisher Scientific
Paraformaldehyde	Roth
Passive lysis buffer 5x	Promega
PCR primer	Sigma-Aldrich
Penicillin Streptomycin	PAA
Phalloidine (conjugated)	Thermo Fisher Scientific
Phosphate-buffered saline (PBS)	PAA
Phusion Hot Start II High-Fidelity DNA Polymerase	Thermo Fisher Scientific
Ponceau S solution	Sigma-Aldrich
Potassium chloride (KCl)	Roth
Protease inhibitor cocktail (COMPLETE)	Roche
Random hexamers	Thermo Fisher Scientific
RevertAid Reverse Transcriptase	Thermo Fisher Scientific
RiboLock RNase Inhibitor	Thermo Fisher Scientific
RotiPhorese® Gel 30 (Acrylamide-Bisacrylamide solution)	Roth
Saponine	Sigma-Aldrich
siRNA FlexiTube	QIAGEN
Sodium azide	Sigma-Aldrich
Sodium borohydride (NaBH4)	Sigma-Aldrich
Sodium chloride (NaCl)	Roth
Sodium deoxycholate	Sigma-Aldrich
Sodium dihydrogenphosphate ($Na_2H_2PO4 .H_2O$)	Roth
Sodium dodecyl sulphate (SDS)	Roth
Sodium hydroxide (NaOH)	Sigma-Aldrich
T4 DNA ligase	Thermo Fisher Scientific
Tetramethylethylenediamine (TEMED)	Roth
TRIS	Roth
Triton X-100 (TX-100)	Sigma-Aldrich
TRIzol®	Thermo Fisher Scientific
Trypsin-EDTA 0.05%	Capricorn Scientific
Tryptone	Roth
Tween-20	Roth
Yeast extract	Roth
2-(N-Morpholino)ethansulfonsäure (MES)	Sigma

Table 3: Standard solutions, buffers and bacterial growth medium

Solution	Composition	
BES-buffered saline (BBS) 2x	BES NaCl Na_2HPO_4 pH 6.95	50 mM 280 mM 1.5 mM
Blocking buffer for immunoblotting	Milk powder in TBST	5% (w/v)
Coomassie destaining solution	Acetic acid Methanol	10% (v/v) 20% (v/v)
Coomassie staining solution	Coomassie G250 Acetic acid Methanol	0.1% (w/v) 10% (v/v) 40% (v/v)
Cytoskeleton buffer	MES NaCL EGTA Glucose $MgCl_2$ pH 6.1	10 mM 150 mM 5 mM 5 mM 5 mM
Laemmli buffer 4x	Glycerol EDTA SDS 2-mercaptoethanol Bromophenol blue Tris-HCl pH 6.8	28% (v/v) 10 mM 5.7% (v/v) 4.7 mg/ml 3.5 mg/ml 286 mM
LB agar	NaCl Yeast extract Tryptone Agar	1% (w/v) 0.5% (w/v) 1% (w/v) 1.5% (w/v)
LB medium	NaCl Yeast extract Tryptone	1% (w/v) 0.5% (w/v) 1% (w/v)
PBS	Na2HPO4 KH2PO4 NaCl KCl pH 7.4	8 mM 1.5 mM 137 mM 2.7 mM
PBST	Tween 20 in PBS	1% (w/v)
Ponceau S staining solution	Ponceau S solution Acetic acid	0.5% (v/v) 3% (v/v)

RIPA buffer	Tris-HCl NaCl NP-40 EDTA SDS Na-Deoxycholate pH 8.0	50 mM 150 mM 1% (v/v) 2 mM 0.1% (w/v) 0.5% (w/v)
SDS-PAGE running buffer 1x	Glycine SDS Tris-HCl pH 8.3	192 mM 0.1% (w/v) 25 mM
SDS-PAGE separating gel	RotiPhorese® Gel 30 (v/v) TEMED SDS Tris-HCl APS pH 8.8	8–15% 9.5 µM 0.1% (w/v) 0.36 M 0.1% (w/v)
SDS-PAGE stacking gel	RotiPhorese® Gel 30 TEMED SDS Tris-HCl APS (w/v) pH 6.8	19% (v/v) 14.5 µM 0.1% (w/v) 0.12 M 0.15%
Subcellular fractionation – cell lysis buffer	HEPES KCl EGTA DTT NP-40 COMPLETE pH 7.9	10 mM 10 mM 0.1 mM 1 mM 0.5% (v/v) 1:20
Subcellular fractionation – nuclear extraction buffer	HEPES NaCl EDTA DTT COMPLETE pH 7.5	20 mM 400 mM 1 mM 1 mM 1:20
TBST buffer	NaCl Tris-HCl Tween-20 pH 7.5	500 mM 20 mM 1% (v/v)

Transfer buffer for immunoblotting	Glycine Tris-HCl Methanol pH 8.5	192 mM 25 mM 20% (v/v)
Tris-Acetat-EDTA (TAE) buffer	EDTA Tris-HCl Acetic acid pH 8.0	2 mM 40 mM 20 mM

Table 4: Antibodies and fluorescent dyes used in this work

Antibody	Supplier	Dilution (in blocking buffer)
Alexa Fluor conjugated 2nd AB	Thermo Fisher Scientific	IF 1:400
SNAP-Cell 647 SiR	New England BioLabs	IF 1:200
α-c-Myc, TRITC conjugated	Santa Cruz	IF 1:200
α-FLAG, HRP conjugated	Sigma-Aldrich	WB 1:3000
α-GFP	Santa Cruz	IF 1:400
α-HDAC2	Abcam	WB 1:5000
α-INF2	Proteintech	WB 1:1000, IF 1:100
α-Lamin A/C	Cell Signaling	IF 1:100
α-mDia1	BD	WB 1:1000, IF 1:100
α-mDia2	M. Innocenti Lab, NL	WB 1:1000
α-Mouse IgG, HRP conjugated	GE Healthcare	WB 1:5000
α-Myc, HRP conjugated	Sigma-Aldrich	WB 1:2500
α-Rabbit IgG, HRP conjugated	Bio-Rad	WB 1:5000
α-Tubulin	Cell Signaling	WB 1:5000
α–H3K4Me1	Abcam	IF 1:200
α-β Actin	Sigma-Aldrich	WB 1:3000

Table 5: Biochemical Kits used in this work

Name	Supplier
Dual-Luciferase® Reporter Assay System	Promega
NucleoSpin® gel and PCR clean-up	Marcherey-Nagel
NucleoSpin® Plasmid	Marcherey-Nagel
Pierce® ECL Western Blotting Substrate	Thermo Fisher Scientific
PureLink™ HiPure Plasmid Filter Maxiprep Kit	Thermo Fisher Scientific

Table 6: Special equipment, devices and working materials used in this study

Name	Supplier
Blue LED illumination device	In-house made

Centrifuge 5415R	Eppendorf
Forma Series II 3110 Water-Jacketed CO2 Incubators	Thermo Fisher Scientific
Glass bottom dishes 3.5 cm	MatTek
LSM 700 confocal microscope, 63x, 1.4 NA oil objective	Zeiss
Luminoskan™ Ascent Microplate Luminometer	Thermo Fisher Scientific
Mini-Trans-Blot System	Bio-Rad
NanoDrop 1000	Peqlab
Nikon Eclipse Ti microscope	Nikon
PowerPack 300	Bio-Rad
Protran Nitrocellulose Transfermembran 0.45 µm	Whatman
INFINITY gel documentation	Peqlab
T3 Thermocycler	Biometra
Thermomixer compact	Eppendorf
X-Ray film processor	Medical Index GmbH
X-Ray films	Kodak

Table 7: Software used for this study

Name	Supplier
Ascent™ Software	Thermo Fisher Scientific
Illustrator CS5	Adobe
ImageJ / Fiji	Open Source
MS Office 2010	Microsoft
Photoshop CS5	Adobe
Prism 6	Graph Pad Software
Serial Cloner 2.6.1	Serial Basics
Zen 2009 light edition	Zeiss
Zen 2012	Zeiss
Imaris 8.3.1	Bitplane

3.2 Cell Culture

3.2.1 General cell culture

HEK293, NIH3T3, HeLa, HT29 and LOX cells were maintained in DMEM (HPSTA – high glucose, stable glutamine and sodium pyruvate, Capricorn Scientific) supplemented with 10% fetal bovine serum (FCS) under standard conditions at 37°C in a 5% CO2 environment.

Table 8: Cell lines used in this study

Name	Type
HEK293	Human embryonic kidney cells
HeLa	Human cervical carcinoma cells
HT29	human colorectal adenocarcinoma cells
LOX	Human melanoma cells
NIH3T3	Mouse embryonic fibroblast cells

3.2.2 Transfection of DNA

In HEK293 cells, plasmids were transfected using the calcium phosphate method. Briefly, cells were pre-seeded in cell culture dishes 24 h before transfection. For a 3.5 cm dish, the DNA was diluted and mixed in 112.5 µl ultrapure bidest H_2O. 125 µl 2x BBS was added after mixing, followed by 12.5 µl $CaCl_2$. After gentle vortexting, the transfection mixture was incubated for 15 min at RT before adding it dropwise to the subconfluent cells. After around three hours upon transfection, the transfection medium was replaced with fresh 10% DMEM and cells were incubated overnight (o/n) at 37°C in a 5% CO2 environment before further application.

HeLa cells were transfected using Fugene HD (Promega) according to the manufacturer's instructions. The DNA was mixed in 100 µl serum free DMEM or 100 µl OptiMEM. 4 µL of Fugene HD was added and mixed. After 15 min of incubation at RT, the transfection mixture was added dropwise to the subconfluent cells, which were seeded in a 3.5 cm tissue culture dish the day before. Cells were incubated o/n at 37°C, 5% CO2 before carrying out further experiments.

The other cell lines used in this study (NIH3T3, LOX and HT29) were transfected using Lipofectamine LTX/Plus (Thermo Fisher Scientific) according to the manufacturer's protocol. The plasmids were mixed in 100 µl serum free DMEM or 100 µl OptiMEM and 2 µl Plus-reagent was added. Upon mixing, the solution was incubated for 5 min at RT. Subsequently, 4 µL LTX-reagent were added. The transfection mixture was then incubated for further 15 min and added to subconfluent pre-seeded cells in a 3.5 cm cell culture dish. Before carrying out further experiments, cells were incubated o/n (37°C, 5% CO2).

3.2.3 Transfection of siRNA

All siRNAs were purchased from Qiagen. The targeting sequences of siRNAs used in this work are indicated in table 9. siRNAs were transfected using Lipofectamine RNAiMAX (Thermo Fisher Scientific) following the manufacturer's instructions. For siRNA treatment of cells seeded in a 3.5 cm cell culture dish, 5 µL of the transfection reagent were diluted and mixed in 250 µL OptiMEM. In a separate tube, 2.5 µl siRNA of a 20 µM siRNA solution, corresponding to a final concentration of 10 nM, were diluted and mixed with 250 µL OptiMEM. Both solutions were then mixed together and incubated for 20 min at RT. Afterwards, the transfection mix was added to the subconfluent cells and incubated for 48 h at 37°C in a 5% CO2 environment before further application. If it was necessary, cells were split 24 h after siRNA transfection.

Table 9: siRNA targeting sequences (FlexiTube siRNA, QIAGEN)

Name	Sequence 5' to 3'
Mm_2610204M08Rik_1 (siINF2 #1)	CCGGAAGGAACAGATGGCAAA
Mm_2610204M08Rik_2 (siINF2 #2)	CTGGCAGAAGCTGCCATCCAA
Mm_2610204M08Rik_3 (siINF2 #3)	AAGCATGAGATTGAGAACCTA
Mm_2610204M08Rik_4 (siINF2 #4)	TAGGCTCTAGGGAACAAATAA
Mm_mDia1 #1_5	CAGGAACAGTATAACAAACTA
Mm_mDia2 #3_2	AAGGAGCTTAATTATAAATCTA

3.2.4 Photoactivation of LOV-INF2-DAD

Optogenetic activation of LOV-INF2-DAD derivatives was obtained by the incubation of cells at 37°C in a 5% CO2 atmosphere under constant illumination by blue LED for 3 hours. Upon illumination, cells were analyzed with a LSM 700 confocal microscope (Zeiss), equipped with a 63X, 1.4 NA oil objective and the ZEN 2012 software (Zeiss).

3.3 Molecular biological methods

3.3.1 DNA cloning and constructs

Expression vectors were generated by using standard cloning procedures. DNA fragments were obtained by PCR reactions using Phusion Hot Start II High-Fidelity DNA Polymerase in HF or CG buffer (Thermo Fisher Scientific) according to the manufacturer's instructions. Additionally, the PCR reaction contained 100 ng DNA template, 100 nM of each primer (forward and reverse), 2 – 3 µl DMSO (optional), and was filled with bidest H_2O to a total volume of 50 µl. The primers used in this study are summarized in Table 11. The DNA template was either cDNA from pre-existing plasmids or cDNA obtained by reverse transcription from the total mRNA amount of cells derived from mouse or human. The PCR reaction was conducted using a T3 Thermocycler (Biometra) with the following conditions:

denaturation	98°C	30 sec		
denaturation	98°C	10 sec		
annealing	X°C	30 sec	X: 55°C – 72°C	30 cycles total
extension	72°C	X sec	X: 30 sec – 3 min	
final extension	72°C	5 min		
storage	4°C			

The PCR products were separated on an agarose gel containing ethidium bromide and were visualized under UV light. The DNA fragment was then extracted from the agarose gel and digested together with the respective cloning vector using appropriate DNA restriction endonucleases. The respective restriction sites of the generated constructs can be seen in Table 11. All restriction enzymes were purchased from Thermo Fisher Scientific and the DNA digestion reactions were conducted according to the manufacturer's instructions. Upon digestion, the DNA was separated again on an agarose gel and extracted. Afterwards, the digested vector backbone and the DNA insert were combined at a ratio of around 1:3 or 1:4 and ligated using T4 ligase (Thermo Fisher Scientific) in accordance to the manufacturer's protocol. 6 µl of the ligation reaction were transformed into DH5α bacterial cells. Cells were then plated on

LB agar (containing either ampicillin or kanamycin) and incubated at 37°C o/n. Grown bacterial colonies were picked and incubated o/n in 3 ml liquid antibiotics containing LB medium. Plasmids were then extracted from bacterial cells by using the NucleoSpin® Plasmid Miniprep Kit (Marcherey-Nagel). The extracted plasmids were finally sent for DNA sequencing, conducted by Macrogen, Amsterdam, NLD.

Plasmids were expressed under the control of the EF-1α promotor as derivatives of pEF-pLink2 carrying N-terminal FLAG, FLAG- GFP, MYC, MYC-mCherry or MYC-TagBFP2 epitope tags. hINF2-DID (aa 32-266), hINF2-DAD-core (aa 941-1015) and hINF2-DAD (aa 965-1240) were amplified from human cDNA, based on the sequence of human INF2 (NCBI Reference Sequence: NP_001026884.3). hINF2-DAD-CAAX (aa 965-1249) was based on the human cDNA sequence of human INF2-CAAX (NP_071934.3). mINF2-DID (aa 32-267) was based on mouse INF2 (NP_940803.2). Other DID constructs comprise the following amino acids according to their respective mouse or human cDNA sequence: mDia1-DID (aa 129-369), mDia2-DID (aa 149-397), mDia3-DID (aa 163 – 399), hFMNL2-DID (aa 75-399), hFMNL2-DID (aa 71-391), hFMNL3-DID (aa 74-395), hFHOD1-DID (aa 115-341), hFHOD3-DID (aa 103-332). The SV40 large T antigen NLS (PPKKKRKV) was C-terminally fused with one linking glycine to restrict constructs to the nucleus. To enable nuclear export, known NES sequences of HIV-Rev (LPPLERLTL) and Stat3 (SLAAEFRHLQLK) were used. GFP-INF2 and GFP-INF2-CAAX (both in pEGFP-C1 vector backbone) were a gift from the Higgs-Lab. GFP-INF2-A149D and GFP-INF2-A149D-CAAX were generated by site-directed mutagenesis with a subsequent Dpn1 digestion step (2h at 37°C).

Table 10: Expression vectors and pre-existing constructs used in this study

Name	Comments
Actin-Chromobody-GFP-NLS	cloned by C. Baarlink, R. Grosse Lab, Marburg, D
Actin-Chromobody-SNAP	cloned by C. Baarlink, R. Grosse Lab, Marburg, D
Lamin-Chromobody-SNAP	cloned by C. Baarlink, R. Grosse Lab, Marburg, D
pEF-FLAG-mDia2-DAD-L1168G-NLS	cloned by C. Baarlink, R. Grosse Lab, Marburg, D
pAC-TagGFP	Chromotek
pLC-TagRFP	Chromotek
pEGFP-C1	Clontech

pEGFP-C1-hINF2	Gift from H. Higgs Lab, Hanover, USA
pEGFP-C1-hINF2-CAAX	Gift from H. Higgs Lab, Hanover, USA
LifeAct-GFP	Gift from M. Sixt Lab, Klosterneuburg, AUT
pRL-TK	Promega
MRTF-A-GFP	R. Treisman Lab, London, UK
pEF-pLINK2	R. Treisman Lab, London, UK
pGL3D.AFOS	R. Treisman Lab, London, UK

Table 11: Primers for cloning used in this study

Oligo name	Sequence 5' to 3'
mDia1DID fw	GCGCGCGCATGGACGAGCTGTACAAGGGCCAGAAAGAGAGC TCTAGGTCTGC
mDia2DID fw	GCGCGCGCATGGACGAGCTGTACAAGGGCAGTAGCCGACAG ATCTCACCTC
mDia1DID NLS SpeI rev	GCGCGCACTAGTCTACACCTTCCGCTTTTTCTTAGGCGGGCCT CCCTTCAGATCAAAGAAATC
mDia2DID NLS SpeI rev	GCGCGCACTAGTCTACACCTTCCGCTTTTTCTTAGGCGGGCCA GATGCTTCATCAAGTTCAGC
mDia1DID NLS SpeI rev	GCGCGCACTAGTCTATCCCTTCAGATCAAAGAAATC
mDia2DID NLS SpeI rev	GCGCGCACTAGTCTAAGATGCTTCATCAAGTTCAGC
EcoRI mCherry fw	GCGCGCGAATTCATGGTGAGCAAGGGCGAGGAGG
FHOD1 m fw DID	GCGCGCGCATGGACGAGCTGTACAAGGGCCAGCTCTCCGTGA GGGTCAATGC
FHOD1 m rev DID	GCGCGCACTAGTCTAAGCCTCTTCCATATCTCCATC
FHOD1 h fw DID	GCGCGCGCATGGACGAGCTGTACAAGGGCCAGCTCTCTGTGA GGGTCAACG
FHOD1 h rev DID	GCGCGCACTAGTCTAGATGTCTCCATCCTCCAATTTCAG
FHOD3 m fw DID	GCGCGCGCATGGACGAGCTGTACAAGGGCCAGCTGTCTGTG AGGGTCCATG
FHOD3 m rev DID	GCGCGCACTAGTCTACTCAGCTGTCTCATCACCATC
FHOD3 h fw DID	GCGCGCGCATGGACGAGCTGTACAAGGGCCAGCTGTCTGTG AGGGTCCATG
FHOD3 h rev DID	GCGCGCACTAGTCTACTCCGTGGTCTCATCGCCATC
FMNL1 m fw DID	GCGCGCGCATGGACGAGCTGTACAAGGGCCAAGTCAAGAAT CCCCCTGC
FMNL1 m rev DID	GCGCGCACTAGTCTACAACACTGCATTCTTCGTCTC
FMNL1 h fw DID	GCGCGCGCATGGACGAGCTGTACAAGGGCCAAGTCAAGAAT CCCCCCGCAG
FMNL1 h rev DID	GCGCGCACTAGTCTACAGCACAGCGTTCTTGGTCTC
FMNL2 m fw DID	GCGCGCGCATGGACGAGCTGTACAAGGGCCAGGTGAAGAAC CCTCCCCATAC
FMNL2 m rev DID	GCGCGCACTAGTCTACAAGGCAGCATTCTTGGTTTCTG

FMNL2 h fw DID	GCGCGCGCATGGACGAGCTGTACAAGGGCCAGGTGAAGAATCCTCCCCATAC
FMNL2 h rev DID	GCGCGCACTAGTCTACAAGGCAGCATTCTTAGTTTCAG
FMNL3 m fw DID	GCGCGCGCATGGACGAGCTGTACAAGGGCCAAGTAAAGAATCCTCCCCACAC
FMNL3 m rev DID	GCGCGCACTAGTCTACAGGGCTACATTCTTGGTTTCTG
FMNL3 h fw DID	GCGCGCGCATGGACGAGCTGTACAAGGGCCAGGTGAAGAATCCTCCCCAC
FMNL3 h rev DID	GCGCGCACTAGTCTACAGGGCTACATTCTTGGTCTC
INF2 m fw DID	GCGCGCGCATGGACGAGCTGTACAAGGGCAGCGCCGAGCCTGAGCTGTGC
INF2 m rev DID	GCGCGCACTAGTCTACCCATCGCTAATTCGCTGAAG
INF2 h fw DID	GCGCGCGCATGGACGAGCTGTACAAGGGCAGCGCGGACCCCGAGCTGTGC
INF2 h rev DID	GCGCGCACTAGTCTAGACCCCGCCAGAGACTCGCAG
mDia3 m fw DID	GCGCGCGCATGGACGAGCTGTACAAGGGCACCCTTTCTTCACAAGAATATG
mDia3 m rev DID	GCGCGCACTAGTCTAATTGAGACGGTGGGATAATTCAC
Diaph2 h fw DID	GCGCGCGCATGGACGAGCTGTACAAGGGCACCCTGTCTTCACAAGAATATG
Diaph2 h rev DID	GCGCGCACTAGTCTAATTGAGACGGTGTGATAATTCAG
BamH1 mCherry fw	GCGCGCGGATCCATGGTGAGCAAGGGCGAGGAGG
TagBFP2 EcoRI fw	GCGCGCAGGAATTCGATGAGCGAGCTGATTAAGGAGAAC
TagBFP2 XbaI rev	GCGCGCTCTAGACTAATTAAGCTTGTGCCCCAGTTTGC
mCh INF2 DAD short f	GCGCGCGCATGGACGAGCTGTACAAGGGCGGGAAGCAGGAGGAGGTGTG
hINF2DAD short SpeI r	GCGCGCACTAGTCTAGCTGCCCCCGTCGGTGTCC
hINF2DAD short NLS SpeI r	GCGCGCACTAGTCTACACCTTCCGCTTTTTCTTAGGCGGCCCGCTGCCCCCGTCGGTGTCC
INF2 m rev BcuI NLSDID	GCGCGCACTAGTCTACACCTTCCGCTTTTTCTTAGGCGGCCCCCCATCGCTAATTCGCTGAAG
INF2 h rev BcuI NLSDID	GCGCGCACTAGTCTACACCTTCCGCTTTTTCTTAGGCGGCCCGACCCCGCCAGAGACTCGCAG
hINF2 DAD fw	GCGCGCGCATGGACGAGCTGTACAAGGGCAAGCAGCAGCTGGCGGAGGAGG
hINF2 DAD BcuI rev	GCGCGCACTAGTCTACACAGGCTCTGTGGCTCTTGG
hINF2 DAD BcuI NLS rev	GCGCGCACTAGTCTACACCTTCCGCTTTTTCTTAGGCGGCCCCACAGGCTCTGTGGCTCTTGG
MluI BFP PWPXL fw	GCGCGCACGCGTCCTAGCGCTACCGGTCGCCACCATGGTGTCTAAGGGCGAAGAGCTGATTAAGGAGAACATGCAC
EcoRI BFP PWPXL rev	GCGCGCGAATTCCTATCGAGATCTGAGTCCGGAATTAAGCTTGTGCCCCAGTTTGC
PmeI MAL fw	GCGCGCGTTTAAACTAATGCTGCCCCCTTCCGTCATTGCTG

3xRPEL BFP fw	GCGCGCGTAAATTACCCAAAGGTAGCAGACAGTGGGATGGTGTCTAAGGGCGAAGAGCTG
BFP MluI rev	GCGCGCACGCGTATTAAGCTTGTGCCCCAGTTTGC
hINF2 EcoRI f	GCGCGCGAATTCATGTCGGTGAAGGAGGGCGCAC
LOV hINF2DAD 1	GCAGAAGAGATTGATGAGGCGGCAGGAGAGGACGGGAAGCCTGTCAG
LOV hINF2DAD 2	GCAGAAGAGATTGATGAGGCGGCAGAGGACGGGAAGCCTGTCAGGAAG
LOV hINF2DAD 3	GCAGAAGAGATTGATGAGGCGGCAGACGGGAAGCCTGTCAGGAAG
LOV hINF2DAD 4	GCAGAAGAGATTGATGAGGCGGCAGGGAAGCCTGTCAGGAAGG
LOV hINF2DAD 5	GCAGAAGAGATTGATGAGGCGGCAAAGGGGCCCGGGAAGCAGGAG
LOV hINF2DAD 6	GCAGAAGAGATTGATGAGGCGGCAGGGCCCGGGAAGCAGGAGGAG
LOV hINF2DAD 7	GCAGAAGAGATTGATGAGGCGGCACCCGGGAAGCAGGAGGAGGTG
LOV hINF2DAD 8	GCAGAAGAGATTGATGAGGCGGCAGGGAAGCAGGAGGAGGTGTGTG
LOV hINF2DAD 9	GCAGAAGAGATTGATGAGGCGGCAAAGCAGGAGGAGGTGTGTGTCATC
LOV hINF2DAD 10	GCAGAAGAGATTGATGAGGCGGCACAGGAGGAGGTGTGTGTCATC
LOV hINF2DAD 11	GCAGAAGAGATTGATGAGGCGGCAGAGGAGGTGTGTGTCATCGATG
LOV hINF2DAD 12	GCAGAAGAGATTGATGAGGCGGCAGAGGTGTGTGTCATCGATGC
LOV hINF2DAD 13	GCAGAAGAGATTGATGAGGCGGCAGTGTGTGTCATCGATGCCCTGCTG
LOV hINF2DAD 14	GCAGAAGAGATTGATGAGGCGGCATGTGTCATCGATGCCCTGCTG
LOV hINF2DAD 15	GCAGAAGAGATTGATGAGGCGGCAGTCATCGATGCCCTGCTGGCTG
LOV hINF2DAD I539E 1	GCAGAAGAGGAAGATGAGGCGGCAGGAGAGGACGGGAAGCCTGTCAG
LOV hINF2DAD I539E 2	GCAGAAGAGGAAGATGAGGCGGCAGAGGACGGGAAGCCTGTCAGGAAG
LOV hINF2DAD I539E 3	GCAGAAGAGGAAGATGAGGCGGCAGACGGGAAGCCTGTCAGGAAG
LOV hINF2DAD I539E 4	GCAGAAGAGGAAGATGAGGCGGCAGGGAAGCCTGTCAGGAAGG
LOV hINF2DAD I539E 5	GCAGAAGAGGAAGATGAGGCGGCAAAGGGGCCCGGGAAGCAGGAG

LOV hINF2DAD I539E 6	GCAGAAGAGGAAGATGAGGCGGCAGGGCCCGGGAAGCAGGAGGAG
LOV hINF2DAD I539E 7	GCAGAAGAGGAAGATGAGGCGGCACCCGGGAAGCAGGAGGAGGTG
LOV hINF2DAD I539E 8	GCAGAAGAGGAAGATGAGGCGGCAGGGAAGCAGGAGGAGGTGTGTG
LOV hINF2DAD I539E 9	GCAGAAGAGGAAGATGAGGCGGCAAAGCAGGAGGAGGTGTGTGTCATC
LOV hINF2DAD I539E 10	GCAGAAGAGGAAGATGAGGCGGCACAGGAGGAGGTGTGTGTCATC
LOV hINF2DAD I539E 11	GCAGAAGAGGAAGATGAGGCGGCAGAGGAGGTGTGTGTCATCGATG
LOV hINF2DAD I539E 12	GCAGAAGAGGAAGATGAGGCGGCAGAGGTGTGTGTCATCGATGC
LOV hINF2DAD I539E 13	GCAGAAGAGGAAGATGAGGCGGCAGTGTGTGTCATCGATGCCCTGCTG
LOV hINF2DAD I539E 14	GCAGAAGAGGAAGATGAGGCGGCATGTGTCATCGATGCCCTGCTG
LOV hINF2DAD I539E 15	GCAGAAGAGGAAGATGAGGCGGCAGTCATCGATGCCCTGCTGGCTG
EcoRI LOV fw	GCGCGCGAATTCGGCTTGGCTACTACACTTGAACG
mCh LOV fw	GCGCGCGCATGGACGAGCTGTACAAGGGCTTGGCTACTACACTTGAACG
EcoRI mDia1DID fw	GCGCGCGAATTCATGCAGAAAGAGAGCTCTAGGTCTGC
EcoRI mDia2 DID fw	GCGCGCGAATTCATGAGTAGCCGACAGATCTCACCTC
EcoRI hINF2 DAD fw	GCGCGCGAATTCATGAAGCAGCAGCTGGCGGAGGAGG
EcoRI hINF2 DADWH2	GCGCGCGAATTCATGGGGAAGCAGGAGGAGGTGTG
EcoRI hINF2 DID	GCGCGCGAATTCATGAGCGCGGACCCCGAGCTGTGC
BamHI mINF2 DID	GCGCGCGGATCCATGAGCGCCGAGCCTGAGCTGTGC
hINF2 DAD 3xLtoA	GAGGTGTGTGTCATCGATGCCGCTGCTGCTGACATCAGGAAGGGCTTCCAGGCTCGGAAGACAGCCCGGGGCCGCGGGGAC
hINF2 DID A149D	GAAGCAGGTGTTTGAGCTACTGGCTGACCTGTGCATCTACTCTCCCGAGGGCCAC
hINF2 FH2 I643A	CAAGAAGAGCCTGAACCTCAACGCATTCCTGAAGCAATTTAAGTGCTCCAACGAG
hINF2 FH2 K792A	GATCAGCACATTGCTGAAGCTCACGGAGACCGCATCCCAGCAGAACCGCGTGACGCTGCTGCAC
hINF2 +CAAX SpeI rev	GCGCGCACTAGTCTATCACTTGGCCTTGGGCCTGGGCCTGTTTGTTTTATTATCATC
hINF2 –CAAX SpeI rev	GCGCGCACTAGTCTATCACTTGGCCTTGGGCCTGGGCCTG
hINF2 DID E184K fw	CTTCAGCATTGTCATGAACAAGCTCTCCGGCAGCGACAAC
hINF2 DID E184K rev	GTTGTCGCTGCCGGAGAGCTTGTTCATGACAATGCTGAAG
hINF2 DID R218Q fw	CTGCGCGCGCGCACCCAGCTGCAAAACGAGTTTATCGGGCTG
hINF2 DID R218Q rev	CAGCCCGATAAACTCGTTTTGCAGCTGGGTGCGCGCGCGCAG

I2 A149D SDM fw	GTGTTTGAGCTACTGGCTGACCTGTGCATCTACTCTCC
I2 A149D SDM rev	GGAGAGTAGATGCACAGGTCAGCCAGTAGCTCAAACAC
EcoRI BFP fw	GCGCGCGAATTCATGGTGTCTAAGGGCGAAGAGCTG
BFP LOV fw	GCGCGCGCAAACTGGGGCACAAGCTTAATGGCTTGGCTACTACACTTGAACG
LOV GS hI2DAD 969	GCAGAAGAGATTGATGAGGCGGCAGGCGGTAGCGGAGGTTCTGAGGTGTGTGTCATCGATGC
LOV GS hI2DAD 970	GCAGAAGAGATTGATGAGGCGGCAGGCGGTAGCGGAGGTTCTGTGTGTGTCATCGATGCCCTGCTG
LOV GS hI2DAD 971	GCAGAAGAGATTGATGAGGCGGCAGGCGGTAGCGGAGGTTCTTGTGTCATCGATGCCCTGCTG
LOV GSGS hI2DAD 971	GCAGAAGAGATTGATGAGGCGGCAGGCAGCGGATCTTGTGTCATCGATGCCCTGCTG
LOV GS hI2DAD 971	GCAGAAGAGATTGATGAGGCGGCAGGTTCTTGTGTCATCGATGCCCTGCTG
LOV GGS hI2DAD 971	GCAGAAGAGATTGATGAGGCGGCAGGCGGTAGCTGTGTCATCGATGCCCTGCTG
hINF2 NLS1 fw	GCGCGCGAATTCCGGGCCAGGAAGGAGCCCAAG
hINF2 NLS1 rev	GCGCGCACTAGTCTAGCACTTAAATTGCTTCAGGAAG
hINF2 NLS2 fw	GCGCGCGAATTCTTCAGCACCATGAAGGCTTTC
hINF2 NLS2 rev	GCGCGCACTAGTCTACTTCCTCCTCTCTGCCTTCG
hINF2 NLS3 fw	GCGCGCGAATTCCGGGCCTCAAAGGGGACCGGGAAG
hINF2 NLS3 rev	GCGCGCACTAGTCTAGATCACACACAGTTTCTTTG
EcoRI hINF2 fw 2	ATATATGAATTCATGTCGGTGAAGGAGGGC
EcoRI hINF2 fw 3	ATATATGAATTCATGTCGGTGAAGGAGGGCGCACAG
hINF2 NLS1 mut fw	GCGCGCGAATTCCGGGCCGCTGCAGAGCCCAAGGAGATCACTTTC
hINF2 NLS2 mut rev	GCGCGCACTAGTCTAAGCTGCAGCCTCTGCCTTCGCCGCCTGCTCCTTC
hINF2 NLS3 mut fw	GCGCGCGAATTCCGGGCCTCAAAGGGGACCGGGGCTGCAGCTGCAGCTGCACCCTCCAGGAGCCAGGAAGAGGTTC
hINF2_2 NLS3 mut rev	GCGCGCACTAGTCTACTTGGCCTTGGGCCTGGGCCTGAG
hINF2 FH2 I643R	CGATGCCAAGAAGAGCCTGAACCTCAACAGATTCCTGAAGCAATTTAAGTGCTCCAACGAGGAGGTC
hINF2 FH2 K792A	GATCAGCACATTGCTGAAGCTCACGGAGACCGCATCCCAGCAGAACCGCGTGACGCTGCTGCAC
hINF2 NES1 fw	GCGCGCGAATTCCTGCTGGAGGCGCTGGCGCGGCTGTCGGGCCGCGGC
hINF2 NES1 rev	GCGCGCACTAGTCTAGCCGCGGCCCGACAGCCGCGCCAGCGCCTCCAGCAG
hINF2 NES2 fw	GCGCGCGAATTCCTGGCTCGCCTGCGAGACCTGGAG
hINF2 NES2 rev	GCGCGCACTAGTCTAAGCCTCCAGCTGGATCAGCAGGTC
hINF2 NES3 fw	GCGCGCGAATTCCTCCTTAAGCTCCTTCCCGAGAAGCACGAGATT

hINF2 NES3 rev	GCGCGCACTAGTCTAAATCTCGTGCTTCTCGGGAAGGAGCTTAAGGAG
hINF2 NES4 fw	GCGCGCGAATTCATGAAGGCTTTCCGGGACCTTTTCCTCCGCGCCCTG
hINF2 NES4 rev	GCGCGCACTAGTCTACAGGGCGCGGAGGAAAAGGTCCCGGAAAGCCTTCAT
hINF2 NES4 mut fw	GCGCGCGAATTCATGAAGGCTTTCCGGGACCTTTTCGGACGCGCCCTG
hINF2 NES4 mut rev	GCGCGCACTAGTCTACAGGGCGCGTCCGAAAAGGTCCCGGAAAGCCTTCAT
hINF2 DAD 3LA long	CAGGAGGAGGTGTGTGTCATCGATGCCGCTGCTGCTGACATCAGGAAGGGCTTCCAGGCTCGGAAGACAGCCCGGGGCCGCGGGGACACCGAC
hINF2 DID E184K rev long	GTAGGGCACGTTGTCGCTGCCGGAGAGCTTGTTCATGACAATGCTGAAGCGGTACTG
hINF2 DID R218Q rev long	CAGCAGCTGCAGCCCGATAAACTCGTTTTGCAGCTGGGTGCGCGCGCGCAGGTCCTC
hINF2 +CAAX EcoRI rev	GCGCGCGAATTCCTATTACTGGATCACACACAGTTTC
hINF2 –CAAX EcoRI rev	GCGCGCGAATTCCTATCACTTGGCCTTGGGCCTGGGCCTG

3.3.2 Agarose gel electrophoresis

The DNA samples (PCR fragments, digested vectors, etc.) were mixed with DNA loading dye and loaded onto 0.8% - 2% agarose gels (depending on the size of the DNA fragments) in 1x TAE buffer containing 10 µg/µl ethidium bromide. The DNA fragments were separated electrophoretically under constant voltage using a DNA electrophoresis chamber (BioRad). The separated DNA fragments were detected under UV light using an INFINITY gel documentation system (peQlab). Seperated DNA bands were cut from the gel and extracted by the NucleoSpin® gel and PCR clean-up kit (Marcherey-Nagel).

3.3.3 RNA isolation from cells

Target cells were washed with ice cold PBS and lysed by addition of 1 ml TRIzol reagent (Thermo Fisher Scientific) directly to the 3.5 cm cell culture dish. Cells were then collected in a tube and vortexed thoroughly. Afterwards, 200 µl Chloroform were added to the cell lysate, followed by 15 sec of rigorous vortexing and incubation for 2 min at 4°C. Samples were then centrifuged at 12,000 g for 15 min at 4°C to obtain

phase separation. The RNA, residing in the upper aqueous phase, was carefully transferred to a fresh tube and mixed with 500 µl isopropanol for RNA precipitation. After incubation for 30 min on ice, RNA was pelleted by centrifugation at 12,000g for 15 min at 4°C. The RNA pellet was washed carefully with 75% Ethanol and pelleted again at 12,000g for 5 min at 4°C. The pellet was then dried at RT and dissolved in 15 – 45 µl RNAse-free H_2O.

3.3.4 CRISPR/Cas9 mediated deletion of INF2

To delete both isoforms of the INF2 gene in NIH3T3 cells by using an all-in-one CRISPR/Cas9 vector system (Sakuma et al., 2014), cells were transfected with the pX330A-1x2 vector encoding for two different guide RNAs (gRNAs) directed towards the INF2 coding region. The vector additionally contains a 2A-eGFP fragment from pSpCas9(BB)-2A-GFP (Ran et al., 2013). The following oligonucleotides were taken into account: #1: CCCGAGTAGTTGACCACCGAGGG, #2: GCCCGAGTAGTTGACCACCGAGG, #14: CGCCTGGAGAGCAGCGATGGCGG, #15: TGGAGAGCAGCGATGGCGGCTGG. All sequences are localized in exon2. The particular gRNA combinations were used to obtain an all-in-one vector harboring double gRNA cassettes: #1 & #14 (Clone 2), #2 & #14 (Clone 3) and #2 & #15 (Clone 4). The empty vector was used to generate control cells. The successful INF2 gene deletion was validated by immunoblotting against endogenous INF2. The whole process of generating INF2-depleted NIH3T3 cells was planned and conducted by Eva-Maria Kleinschnitz with the aid of Andrea Wüstenhagen and Marga Losekam (all AG Grosse).

3.4 Immunofluorescence and microscopy

3.4.1 Immunofluorescence microscopy sample preparation and staining

Cells grown on glass coverslips were fixed with 3.7% formaldehyde in PBS for 10 min at room temperature (RT). Upon washing the coverslips three times with PBS, cells were permeabilized with 0.2% Triton X-100 in PBS (PBST) for 5 min at RT or, when

specifically indicated, with 0.05% Saponine in PBS for 5 min at RT. Afterwards, cells were blocked in 5% FCS/PBST (or 5% FCS/PBS, if permeabilized with Saponine) for 20 min at RT and subsequently incubated with the particular antibodies (antibodies used in this study see Table 4). Primary antibody incubations were performed in 5% FCS/PBS(T) for 60 min at RT, followed by three washing steps with PBS(T). If necessary, cells were incubated then with Alexa Fluor-labeled secondary antibodies in 5% FCS/PBS(T) for 60 min at RT, followed by an optional incubation step for 10 min with DAPI (50x in PBS(T)). After three final washing steps with PBS(T), the coverslips were mounted on glass slides with fluorescent mounting medium (DAKO).

3.4.2 Visualization of nuclear F-actin in fixed cells with phalloidin

Visualization of nuclear actin filaments using phalloidin was performed as described previously (Baarlink et al., 2013). Briefly, NIH3T3 cells were grown at low density on glass coverslips. Cells were washed once with PBS and initially fixed with 0.5% TX-100 and 0.25% Glutaraldehyde in cytoskeleton buffer for 1 min. A second fixation step was performed subsequently for 15 min with 2% Glutaraldehyde in cytoskeleton buffer. Upon washing the coverslips three times with cytoskeleton buffer, autofluorescence was quenched by treatment with 1 mg/ml freshly prepared $NaBH_4$ for 5 min at RT. Afterwards, cells were washed again three times with cytoskeleton buffer and incubated with Alexa Fluor 488 conjugated phalloidin (1:400 in cytoskeleton buffer) for 30 min. The coverslips were finally washed three times with cytoskeleton buffer and three times with ultrapure bidest H_2O, followed by mounting on a glass slide with fluorescent mounting medium.

3.4.3 Microscopy and image analysis

All images were collected with an LSM 700 confocal microscope (Zeiss), equipped with a 63X, 1.4 NA oil objective and the ZEN 2012 software (Zeiss). The images were later processed for contrast enhancement and background noise reduction with ZEN 2012 (Zeiss) or ImageJ/Fiji (National Institutes of Health).

To analyze the nucleocytoplasmic ratio of putative INF2-NES or INF2-NLS sequences, confocal Z-stacks of single cells were imaged and the maximum intensity projections were calculated with ZEN 2009 (Zeiss). The quantification of the nucleocytoplasmic ratio was performed by using ImageJ (National Institutes of Health), applying the IntensityRatioNucleiCytoplasm-Macro (http://dev.mri.cnrs.fr/projects/imagej-macros/wiki/Intensity_Ratio_Nuclei_Cytoplasm_Tool).

Nuclear fluorescence intensity measurements were conducted by analyzing confocal Z-stacks of α-INF2 and DAPI stained NIH3T3 cells (Control vs. INF2-deleted cells) with the Imaris 8.3.1 software (Bitplane). All images were taken with the same microscope settings. Quantitative analysis of the confocal images was done by Matthias Plessner (AG Grosse).

3.4.4 Live cell imaging

For live cell imaging, cells were grown and transfected in 3.5 cm glass bottom dishes (MatTek). Live cell imaging was performed at 37 °C in a CO2 (5%) humidified chamber using an LSM700 confocal microscope with a 63×/1.4 oil objective in combination with the ZEN 2012 software (Zeiss).

SNAP-Cell 647 SiR labeling was performed according to the manufacturer's protocol (New England Biolabs). Briefly, cells were pre-seeded on glass bottom dishes and transfected with the appropriate plasmids the day before analysis. Prior visualization under the confocal microscope, SNAP-Cell 647 SiR loading dye was applied 1:400 and cells were incubated for 30 min at 37 °C in 5% CO2.

3.5 Biochemical methods

3.5.1 SDS- polyacrylamide gel electrophoresis (SDS-PAGE) and protein immunoblotting (Western blot)

Proteins were denatured by adding 2x Laemmli buffer either directly to cells in cell culture plates or to already prepared samples from co-immunoprecipitation or fractionation experiments. The samples were then collected in a tube and boiled for 10 min at 95°C. Afterwards, the lysate was cleared by centrifugation at 16,000g for 10 min. The samples were then either immediately subjected to SDS-PAGE or stored at -20°C.

The denatured proteins were separated by SDS-PAGE using a Mini-PROTEAN III Cell gel system (Bio-rad). Therefore, the samples were loaded to a polyacrylamide gel, which had to be casted before. The separating gels were casted in concentrations of 8%, 10% or 13%, depending on the sizes of the proteins to be separated. The proteins were then electrophoretically separated by applying a constant voltage to the gel (80 V for proteins inside the stacking gel and 120 V upon entering the separating gel).

The separated proteins on the polyacrylamide gel were then transferred to a 0.45 µm nitrocellulose membrane (Whatman) by applying constant 350 mA for 1 h to 1.5 h using a Mini Trans-Blot® Electrophoretic Transfer Cell system (Bio-Rad). After successful protein transfer to the nitrocellulose membrane, checked by Ponceau S staining, membranes were incubated in blocking buffer (5% Milk in TBST) for 1 h at RT. The membrane was then incubated in blocking buffer containing the proper diluted primary antibody (see Table 4) either at 4°C o/n or for 1 h at RT. After washing the membrane three times for 10 min with TBST, it was incubated for 1 h at RT with secondary horseradish peroxidase (HRP)-conjugated antibodies diluted in blocking buffer. Membranes were then washed again three times for 10 min with TBST before analysis. Antibody labeled protein bands were detected by applying ECL reagent to the nitrocellulose membrane and exposing X-Ray films to the membrane inside a dark

room. Finally, the films were developed with an X-Ray film processor (Medical Index GmbH).

3.5.2 Co-immunoprecipitation

HEK293 or NIH3T3 cells were grown in 10 cm dishes and transfected with 2.5 µg of DNA. Upon a single wash with ice-cold PBS, cells were lysed in RIPA buffer supplemented with COMPLETE protease inhibitors. The lysate was incubated for 10 min on ice and centrifuged for 10 min at 12,000g at 4°C. The supernatant, containing the debris-cleared lysate, was incubated afterwards with α-FLAG pre-coupled agarose beads (Sigma-Aldrich) or α-MYC pre-coupled agarose beads (Sigma-Aldrich) for 1.5 h at 4°C. The beads were then washed three times with RIPA buffer and finally lysed in 2x Laemmli buffer. Prior boiling the samples for 5 min, they were subjected to SDS-PAGE and immunoblotting using HRP-conjugated α-FLAG or α-MYC antibodies.

3.5.3 Subcellular fractionation

The preparation of subcellular fractionations was adapted from (Kosugi et al., 2009). NIH3T3 cells were grown and transfected in a 10 cm cell culture plate. Prior lysis, cells were washed once with ice-cold PBS, dislodged and pelleted for 5 min at 800g. The cell pellet was resuspended in cell lysis buffer and allowed to swell on ice for 15-20 min with intermittent gentle vortexing. Finally, a 10 s vortexing step was conducted to disrupt all cell membranes. The supernatant, containing the cytoplasmic extract, was collected upon centrifugation of the total cell lysate for 10 min at 4°C at 12,000g. The pelleted nuclei were then washed once in cell lysis buffer before resuspension in nuclear lysis buffer, followed by incubation for 30 min on ice. The supernatant, now containing the nuclear extract, was collected after sedimentation of the remaining insoluble debris for 15 min at 4°C at 12,000g. 2x Laemmli sample buffer was then added to aliquots of the cytoplasmic and nuclear extracts. The samples were then subjected to SDS-PAGE with subsequent immunoblotting using appropriate primary antibodies and HRP-conjugated secondary antibodies. The purity of obtained extracts

was controlled by immunoblotting for α-tubulin or α-HDAC2 as cytoplasmic or nuclear markers, respectively.

3.5.4 MRTF/SRF luciferase reporter assay

MRTF/SRF luciferase reporter assays were performed as described before (Brandt et al., 2009) using pGL3D.AFOS and pRL-TK reporter plasmids. MRTF/SRF activity experiments were generally conducted in HEK cells, unless stated otherwise. Briefly, 4 to 5 h after transfection of pre-seeded cells with pGL3D.AFOS and pRL-TK, together with plasmids carrying the genes of interest, cells were starved in DMEM containing 0.25 % FCS for 16 to 24 hours before analysis. If alterations in MRTF/SRF transcriptional activity upon serum stimulation were measured, cells were stimulated prior analysis with 20% FCS for 6 hours.

For sample preparation, cells were washed once with PBS and lysed by the addition of 200 µl ice-cold passive lysis buffer (Promega) per 3.5 cm dish. Afterwards, cells were scraped and transferred to a tube, followed by incubation on ice for 20 min and centrifugation at 20,000 g for 10 min at 4°C. Dependent on the transfection efficiency, 5 to 20 µl of the debris cleared cell lysate were used for measurements. The reporter assays were performed using the Dual-Luciferase® Reporter Assay System Kit according to the manufacturer's protocol. The firefly and renilla luciferase signals were measured sequentially by a Luminoskan™ Ascent Microplate Luminometer (Thermo Scientific) using the Ascent™ Software (Thermo Scientific). Afterwards, the firefly signal was normalized to the renilla signal in each sample.

3.6 Statistics

Statistical analysis was performed using GraphPad Prism 6 (GraphPad Software). Data is displayed as mean (± SD). The statistical significance was evaluated using the unpaired Student t test. Statistical significance is defined at $P \leq 0.05$.

4. Results

Formin proteins represent the largest group within different classes of actin nucleators. Up to date, 15 formin members have been discovered in vertebrates which can further be divided into several subgroups. Among those subgroups, Diaphanous-related formins (DRFs) form the largest subset (Breitsprecher and Goode, 2013). Typically, DRFs exist in an autoinhibited state within cells, mediated by an interaction of the N-terminal diaphanous inhibitory domain (DID) and the C-terminal diaphanous autoregulatory domain (DAD) (Baarlink et al., 2010). Relieve of this intramolecular inhibition results in activation of formins and subsequent nucleation and elongation of unbranched actin filaments (Pruyne et al., 2002).

Recently, a role of formins in the formation of F-actin structures in mammalian somatic cell nuclei was described (Baarlink et al., 2013; Belin et al., 2015). However, the appearance of additional formins in the nucleus as well as their putative participation in the assembly of nuclear actin filaments remained elusive.

4.1 A novel approach to activate endogenous mDia formins

Previously, it was revealed that the overexpression of an isolated mDia-DAD competes with the intramolecular inhibitory interaction of DID and DAD of endogenous mDia formins, leading to the release of mDia autoinhibition and subsequent actin rearrangement (Alberts, 2001). Based on the finding that essential DAD-binding amino acids are mostly located on the concave surface of the Armadillo Repeat Region (ARR) (Otomo et al., 2005a), we wanted to analyze if expression of an isolated ARR (here referred to as DID) also inhibits mDia formins to revert to their intramolecular autoinhibited state (working model see Figure 8). This approach would expand the tools available for endogenous formin activation in *trans*. Thus, we generated constructs genetically encoding the DIDs of either mDia1 (aa 149-397), mDia2 (aa 129-369) or mDia3 (aa 163-399) and tested their functionality.

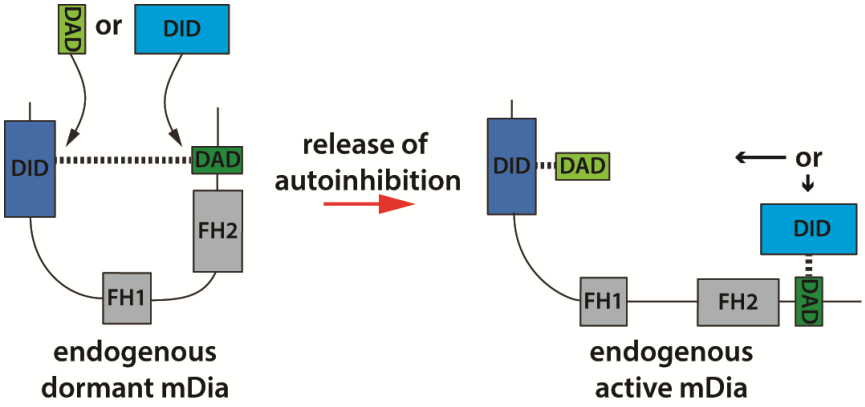

Figure 8: Release of formin autoinhibition by expression of DAD or DID

Cartoon illustrating the activation of endogenous mDia2 by overexpression of mDia2-DAD (Alberts, 2001) (light green) or mDia2-DID (light blue, amino acids 32 – 266, comprising the armadillo repeat region of mDia2). Overexpressed mDia2-DAD or -DID interferes with DID/DAD interaction in autoinhibited mDia2, thereby releasing its autoinhibition and promoting actin assembly.

4.1.1 Expression of the DID of mDia formins drives MRTF/SRF transcriptional activity

Activation of mDia caused by overexpression of its DAD mediates actin remodeling and subsequent MRTF/SRF transcriptional activity (Alberts, 2001). To analyze successful DID mediated activation of mDia formins, we investigated the effects of mDia-DID expression on actin dynamics by performing a luciferase reporter gene assay to examine SRF activity (SRF reporter gene assays were performed in serum starved HEK cells, unless stated otherwise). Indeed, expression of mDia1-DID, mDia2-DID or mDia3-DID led to a remarkable increase in SRF transcriptional activity, although the increase was not as striking as upon expression of mDia2-DAD (Figure 9A).

Furthermore, actin polymerization promotes the release of G-actin from MRTF-A, resulting in nuclear accumulation of MRTF-A (Vartiainen et al., 2007). Thus, we expected that overexpression of mDia-DID also mediates MRTF-A-shuttling to the nucleus. Indeed, the accumulation of MRTF-A-GFP in the nucleus of serum starved NIH3T3 cells could be visualized upon expression of mDia2-DID (Figure 9C, upper

panel). The DIDs of mDia1 and mDia3 have not been analyzed in terms of MRTF-A-shuttling.

4.1.2 The expression of mDia2-DID in the nucleus is capable of assembling a nuclear actin network

The dynamic regulation of MRTF/SRF transcriptional activity is dependent on actin inside the nucleus (Vartiainen et al., 2007). Recently, a role of nuclear mDia formins in the regulation of MRTF/SRF activity was described (Baarlink et al., 2013). Spatial activation of mDia2 mediated by expression of the nuclear targeted mDia2-DAD was shown to induce the assembly of a nuclear actin network followed by MRTF-A accumulation in the nucleus and subsequent increase in MRTF/SRF transcriptional activity (Baarlink et al., 2013).

Thus, we generated a nuclear targeted version of mDia2-DID (mDia2-DID-NLS) and analyzed the ability of the DID to activate endogenous mDia2 in the nucleus. Indeed, increased SRF activity (Figure 9B) and accumulation of MRTF-A-GFP in serum starved NIH3T3 cells (Figure 9C, lower panel) could be obtained upon expression of mDia2-DID-NLS. The effect in MRTF/SRF transcriptional regulation was not as prominent as upon activation of mDia2 by mDia2-DID (cf. Figure 9A). However, this more moderate effect comparing mDia2-DID-NLS to mDia2-DID mediated SRF-activity was expected as nuclear mDia activation by mDia2-DAD-L1168G-NLS also resulted in a marginal increase in SRF activity compared to mDia2 activation by mDia2-DAD (Figure 9B and (Baarlink et al., 2013), cf. Figure 9A). Furthermore, by using the nuclear actin probe Actin-Chromobody-TagGFP2-NLS (referred to as nuclear-Actin-Chromobody-GFP or short as nAC-GFP) (Plessner et al., 2015) we could obtain clearly visible nuclear actin filaments upon activation of mDia2 in the nucleus by mDia2-DID-NLS (Figure 9D).

Interestingly, co-expression of mDia2-DAD together with mDia2-DID prevented alterations in SRF activity (Figure 9E, left panel). The same effect could be obtained using nuclear targeted versions of mDia2-DAD and mDia2-DID (Figure 9E, right panel).

This suggests that both overexpressed constructs interact with each other within cells, thereby inhibiting their ability to release autoinhibition of endogenous mDia.

Taken together, these results strongly suggest that the expression of the isolated DID of mDia formins provides an additional tool to activate endogenous mDia by interacting with the DAD of the endogenous formin and thereby interfering with the intramolecular mDia autoinhibition.

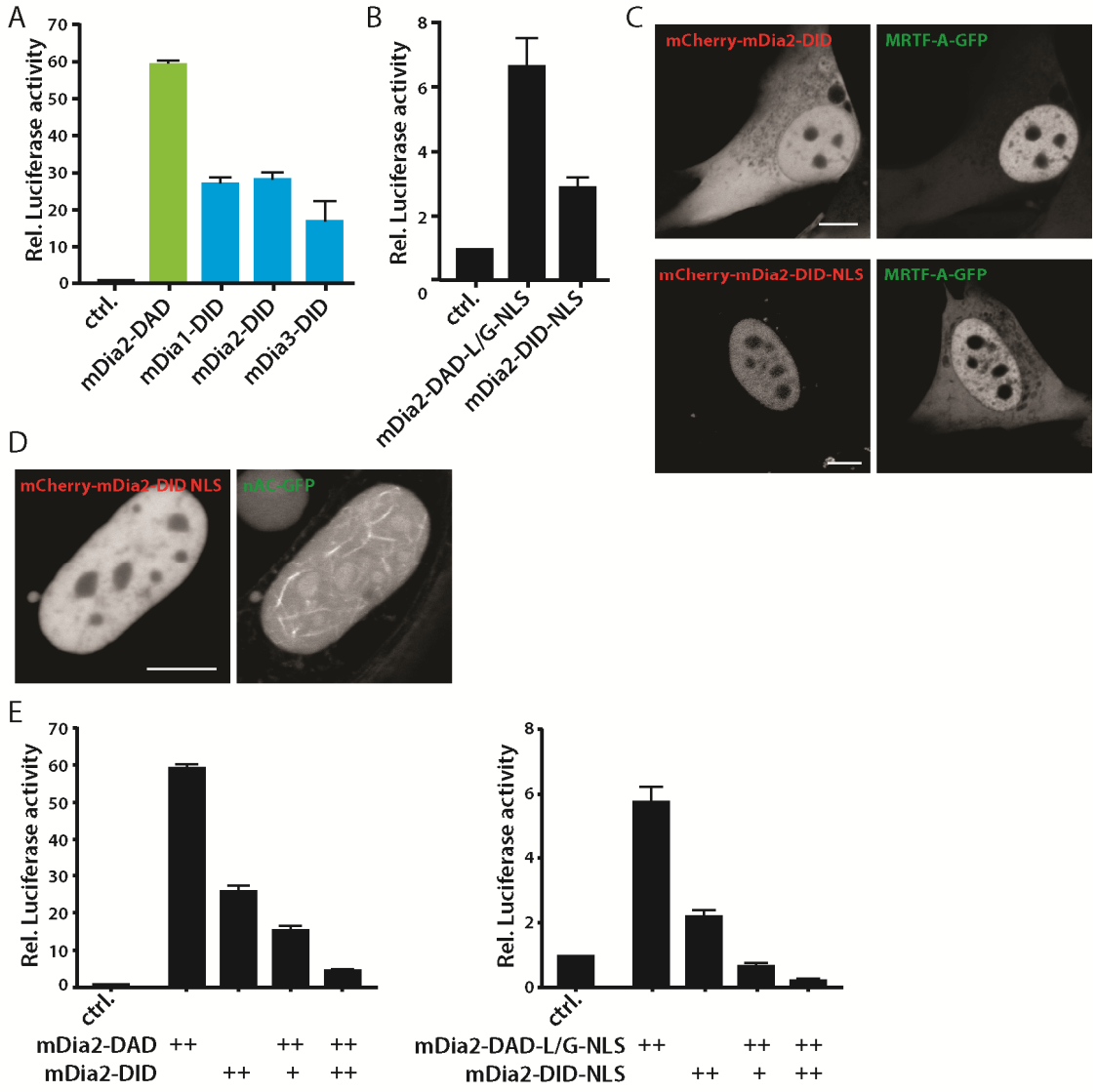

Figure 9: mDia-DID mediated regulation of actin dynamics and MRTF/SRF transcriptional activity

A) HEK cells were transfected with mDia1-DID, mDia2-DID or mDia3-DID together with the MRTF/SRF reporter 3DA.luc to analyze effects on SRF activity. mDia2-DAD was used as a positive control (and for

comparison). Transfected cells were grown under serum starved conditions (DMEM with 0.25 % FCS) before conducting the SRF reporter gene assay. Results are means ± SD (n=3). **B)** SRF activity in HEK cells expressing mDia2-DAD-L1168G-NLS (used as positive control) or mDia2-DID-NLS. Results are means ± SD (n=3). **C)** NIH3T3 cells were transfected with MRTF-A-GFP together with either mCherry-mDia2-DID or mCherry-mDia2-DID-NLS and imaged under serum starved conditions. Scale bar, 10 µm. **D)** Representative images show NIH3T3 cells expressing mCherry-mDia2-DID-NLS together with Actin-Chromobody-TagGFP2-NLS (= nuclear-Actin-Chromobody [nAC-GFP]). Scale bar, 10 µm. **E)** mDia2-DID inhibits mDia2-DAD driven SRF activity. HEK cells were transfected with 500 ng of either mDia2-DAD (left panel) or mDia2-DAD-L1168G-NLS (right panel). mDia2-DAD expressing cells were co-transfected with increasing amounts of mDia2-DID, whereas mDia2-DAD-L1168G-NLS expressing cells were transfected with mDia2-DID-NLS (+: 250 ng, ++: 500 ng). The transfected amount of DNA was filled to a total of 2 µg with empty vector. Results are means ± SD (n=3).

4.2 INF2 participates in actin dynamics and MRTF/SRF transcriptional activity

Next, we examined if the release of formin autoinhibition upon expression of the isolated DID is not restricted to mDia but rather if this elegant way of modulating endogenous formin activity ccould also be implemented in other DRFs.

4.2.1 INF2-DID and INF2-DAD expression results in increased SRF activity and MRTF-A accumulation to the nucleus

We conducted a MRTF/SRF reporter gene assay screen upon expression of DIDs of other DRFs (hFMNL1: aa 75-399, hFMNL2: aa 71-391, hFMNL3: aa 74-395, hFHOD1: aa 115-341, hFHOD3: aa 103-332 and hINF2: aa 32-266) to analyze if they behave in an mDia-DID comparable manner. A striking upregulation of SRF activity could be seen in serum starved HEK cells expressing hINF2-DID, whereas expression of the respective other DIDs showed no impact on MRTF/SRF regulation (Figure 10A). The DID of the mouse INF2 homologue, featuring 95% sequence homology to hINF2-DID, activated MRTF/SRF transcription similar to hINF2-DID (data not shown).

Furthermore, we wanted to analyze if INF2 autoinhibition could also be released by overexpression of its DAD. Thus, we generated three different versions of the INF2-DAD: INF2-DAD-core (containing the DAD/WH2 domain flanked by additional amino acids: aa 941-1015), hINF2-DAD (containing the full C-terminus of hINF2 starting N-terminal of the DAD/WH2: aa 965-1240) and hINF2-DAD-CAAX (containing the full C-terminus of hINF2-CAAX, aa 965-1249) (Figure 10B). Expression of either one of the INF2-DAD versions in HEK cells resulted in a striking upregulation of MRTF/SRF transcriptional activity (Figure 10C). However, expression of full length hINF2 or hINF2-CAAX alone displayed only moderate SRF activity, leading to the assumption that overexpressed full length INF2 mainly exists in an autoinhibited state in unstimulated cells. Co-expression of full length hINF2 or hINF2-CAAX together with the DAD of the respective isoform raised MRTF/SRF transcriptional activity almost to levels which were obtained by expression of constitutively active hINF2-A149D or hINF2-A149D-CAAX (Korobova et al., 2013; Ramabhadran et al., 2013) (Figure 10D). The INF2-DAD-core mediated increase in MRTF/SRF transcriptional activity could be suppressed by co-expression of hINF2-DID (Figure 10E).

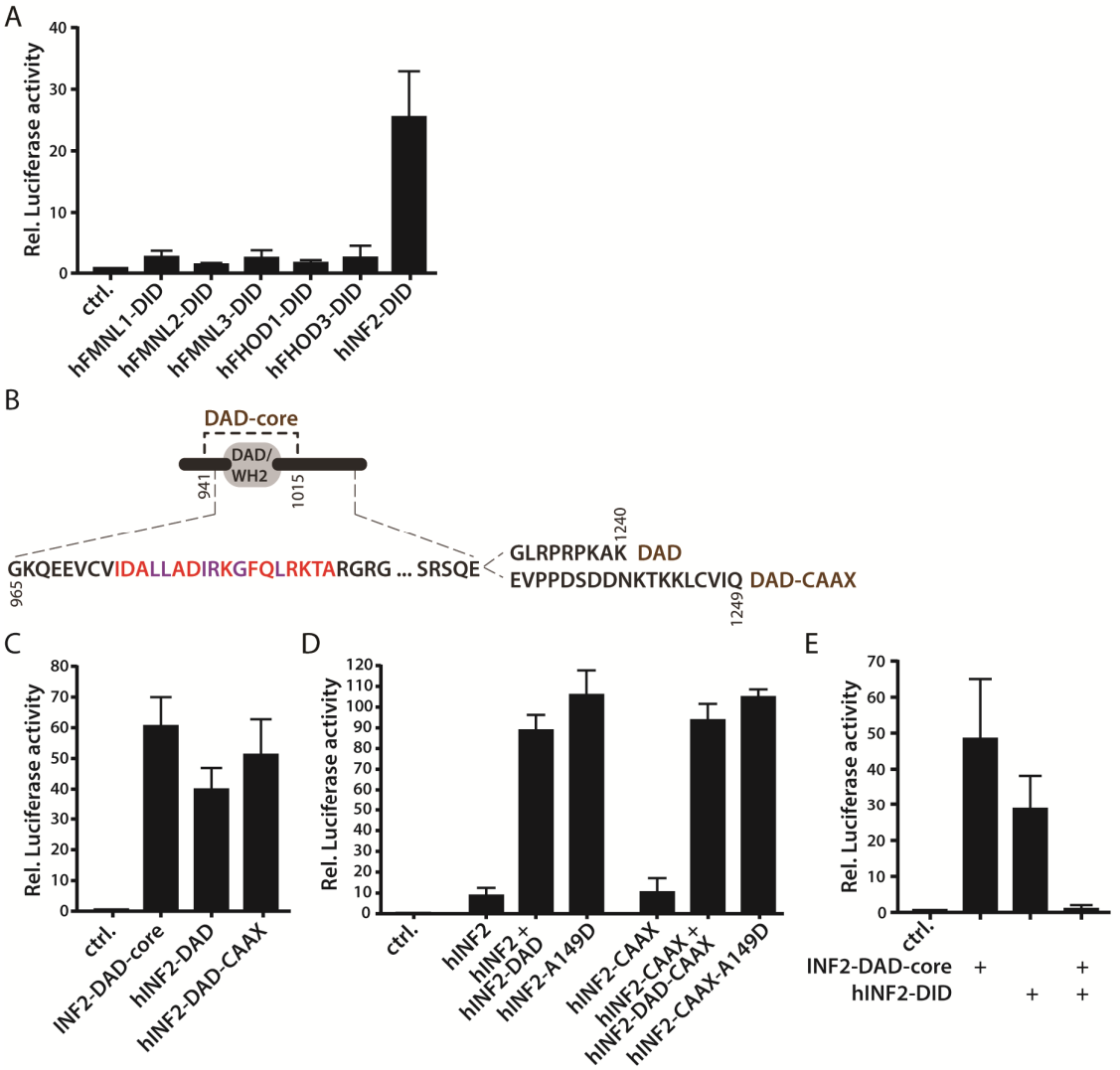

Figure 10: INF2-DID or INF2-DAD expression modulates SRF activity

A) SRF activity was compared upon transfection of HEK cells with the DID domain of distinct formins. Note that only the DID of INF2 (amino acids 32 – 266) shows a striking increase in MRTF/SRF dependent gene regulation. Results are means ± SD (n=3). **B)** The cartoon shows an illustration of the C-terminus of hINF2, comprising the DAD/WH2 domain (shown in red). Residues in purple indicate highly conserved amino acids among WH2 domains of other proteins (Chhabra and Higgs, 2006). Different variants of hINF2-DAD were used in this study: INF2-DAD-core (amino acids 941 – 1015), as well as the full C-termini of both hINF2 isoforms: hINF2-DAD (amino acids 965 – 1240) and hINF2-DAD-CAAX (amino acids 965 – 1249). **C)** HEK cells were transfected with INF2-DAD-core, hINF2-DAD or hINF2-DAD-CAAX and SRF activity was analyzed. Results are means ± SD (n=3). **D)** To analyze the efficiency of DAD mediated INF2 activation, SRF activity was measured in HEK cells expressing the respective isoforms of hINF2, hINF2 together with hINF2-DAD or constitutive active hINF2-A149D. 500 ng of each construct were transfected. Results are means ± SD (n=3). **E)** hINF2-DID inhibits INF2-DAD-core driven SRF activity. SRF

mediated transcription was measured in HEK cells transfected either with INF2-DAD-core or hINF2-DID alone or co-transfected with INF2-DAD-core together with equal amounts of hINF2-DID. Results are means ± SD (n=3).

Activation of hINF2 by its DID or DAD expression also resulted in translocation of MRTF-A-GFP to the nucleus in serum starved NIH3T3 cells (Figure 11A). For comparison, similar outcomes could be obtained upon expression of hINF2-A149D or hINF2-A149D-CAAX (Figure 11B) by observing nuclear accumulation of a truncated form of MRTF-A containing only the RPEL domain (Guettler et al., 2008) which controls the nucleocytoplasmic shuttling of MRTF-A.

Noteworthy, successful INF2-DAD mediated activation of endogenous INF2 was reported recently (Bartolini et al., 2016). Thereby a role of INF2 in the formation of stabilized detyrosinated microtubules was suggested.

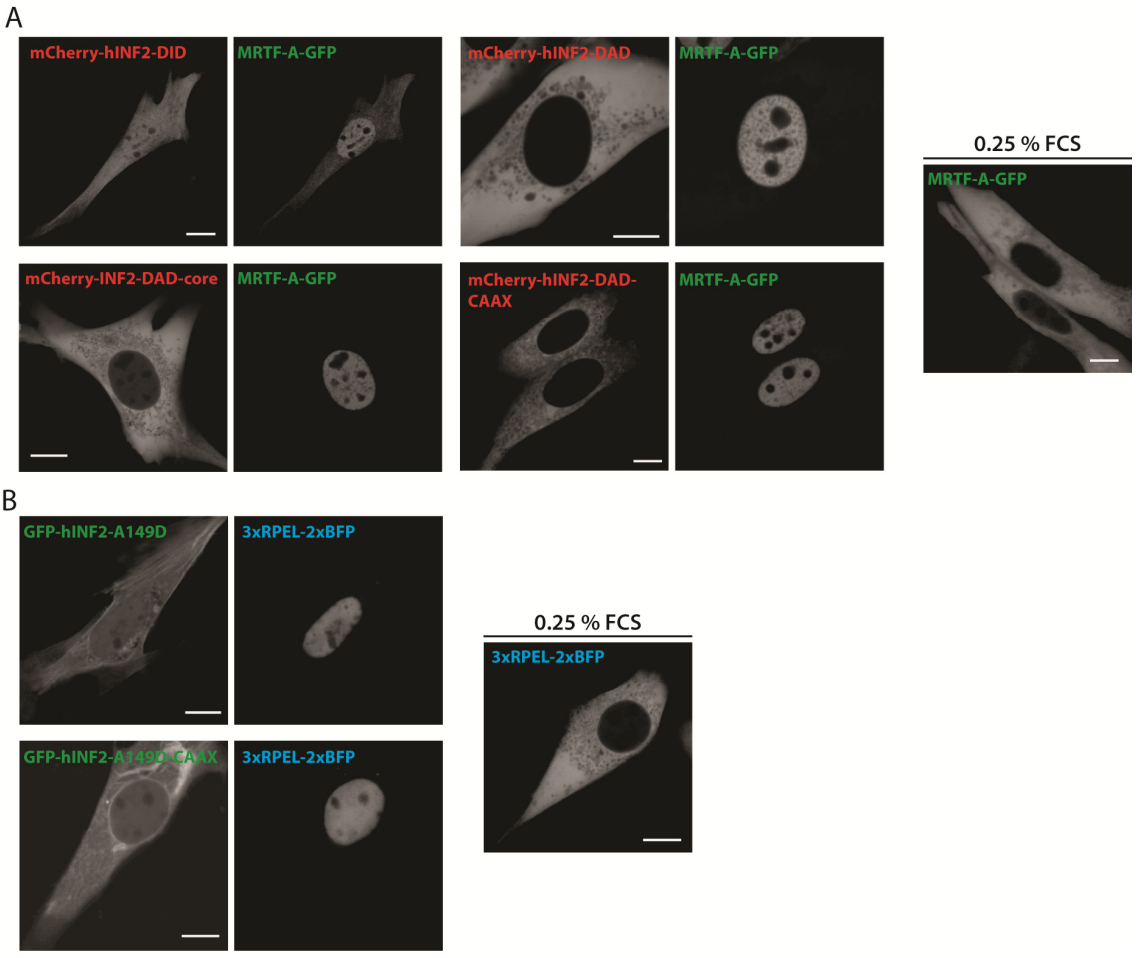

Figure 11: INF2-DID or INF2-DAD expression regulates translocation of MRTF-A to the nucleus

A) Serum starved NIH3T3 cells show MRTF-A-GFP localized to the nucleus upon expression of mCherry-hINF2-DID, mCherry-INF2-DAD-core as well as mCherry-hINF2-DAD or mCherry-hINF2-DAD-CAAX. The right panel shows the localization of MRTF-A-GFP in serum starved NIH3T3 cells (without INF2 activation). Scale bar, 10 µm. **B)** 3xRPEL 2xBFP was used as indicator for MAL shuttling in serum starved NIH3T3 cells with constitutive active INF2 (GFP-hINF2-A149D or GFP-hINF2-A149D-CAAX). The right panel shows the localization of 3xRPEL-2xBFP in serum starved NIH3T3 cells (without INF2 activation). Scale bar, 10 µm.

4.2.2 Distinct versions of INF2-DAD lead to selective activation of hINF2 isoforms

Selective activation of the respective hINF2 isoforms upon expression of hINF2-DAD or hINF2-DAD-CAAX could be shown by analyzing the effects on the reorganization of the actin cytoskeleton. Using LifeAct-GFP as actin detection probe, we observed that hINF2-DAD expression led to a distinct cytosolic actin pattern while hINF2-DAD-CAAX resulted in actin structures localizing to the ER surface (Figure 12A). The differential actin pattern could also be visualized in fixed NIH3T3 cells by phalloidin staining (Figure 12B). These differences are consistent with the previously reported distinct actin rearrangement upon expression of constitutively active INF2 isoforms ((Ramabhadran et al., 2013) and Figure 12C). Interestingly, hINF2-DAD-CAAX did not mediate actin rearrangement to the ER in HELA cells (data not shown) where the INF2-CAAX isoform could only be detected in very low amounts (Ramabhadran et al., 2011).

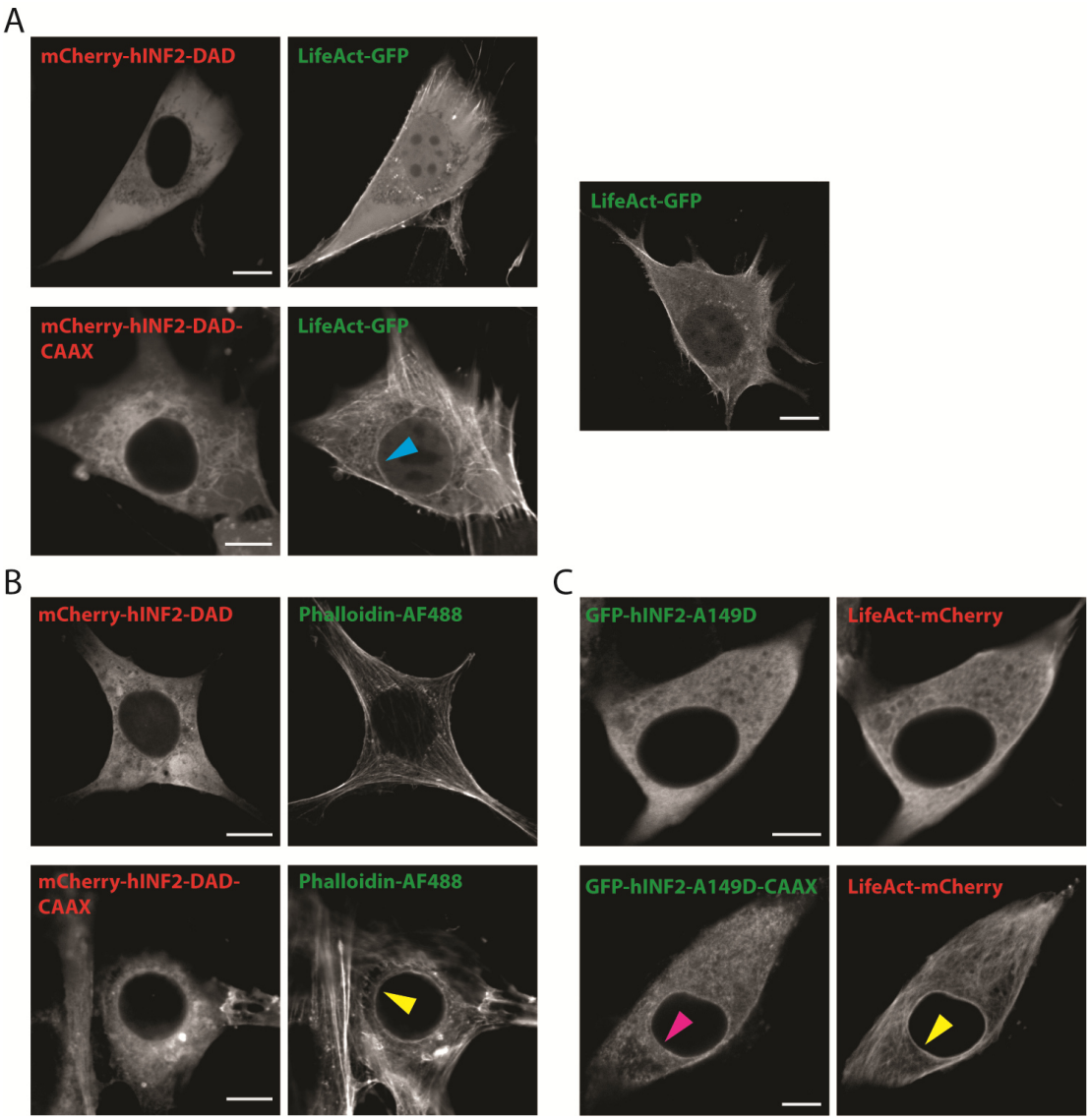

Figure 12: Differential isoform specific INF2-DAD derivatives selectively activate particular hINF2 isoforms

A) NIH3T3 cells expressing either mCherry-hINF2-DAD or mCherry-hINF2-DAD-CAAX together with LifeAct-GFP resemble a characteristic and distinct actin pattern (blue arrowhead: perinuclear actin ring upon activation of hINF2-CAAX). The right panel shows the actin pattern visualized by LifeAct-GFP in untransfected NIH3T3 cells. Scale bar, 10 µm. **B)** The distinct actin pattern upon expression of either INF2-DAD or INF2-DAD-CAAX can also be detected in fixed NIH3T3 cells. F-actin was labeled by Alexa Fluor 488 conjugated Phalloidin (Phalloidin AF488). The yellow arrowhead indicates the INF2-DAD-CAAX mediated characteristic perinuclear actin structure. Scale bar, 10 µm. **C)** Images show GFP-hINF2-A149D or GFP-hINF2-CAAX-A149D expressing NIH3T3 cells. LifeAct mCherry was co-transfected as a marker for Actin. Note the characteristic INF2-CAAX (pink arrowhead) and Actin (yellow arrowhead) pattern in the perinuclear region. Scale bar, 10 µm.

4.2.3 INF2-DID or INF2-DAD mediated effects on actin rearrangement and MRTF/SRF regulation are dependent on endogenous INF2

The above described INF2-DID or INF2-DAD mediated effects on cellular properties had to be characterized in terms of their specificity. Initially, point mutations were introduced in either the DID (A149D (Ramabhadran et al., 2013), E184K or R218Q (Brown et al., 2010)) or the DAD (L1008A, L1009A, L1018A [= 3LtoA] (Chhabra and Higgs, 2006)) which were suggested to disrupt INF2-DID/DAD binding and subsequent INF2 autoinhibition (Rollason et al., 2016). All mutations were shown to compensate for the increase in MRTF/SRF transcriptional activity induced by INF2-DID or INF2-DAD (Figure 13A). This functional deficits seems to be due to the loss of binding ability of mutated DID or DAD to their particular counterpart, as detected by Co-Immunoprecipitation (Figure 13B). hINF2-DID/DAD binding studies by Co-Immunoprecipitation were already conducted elsewhere (Rollason et al., 2016). However the length of the hINF2-DID construct in our study is remarkably shorter in length (aa 32-266, containing solely the ARR) than the construct used in (Rollason et al., 2016) (aa 14-343), therefore we decided to specify the binding abilities of the INF2-DID as well as DAD constructs used in this study.

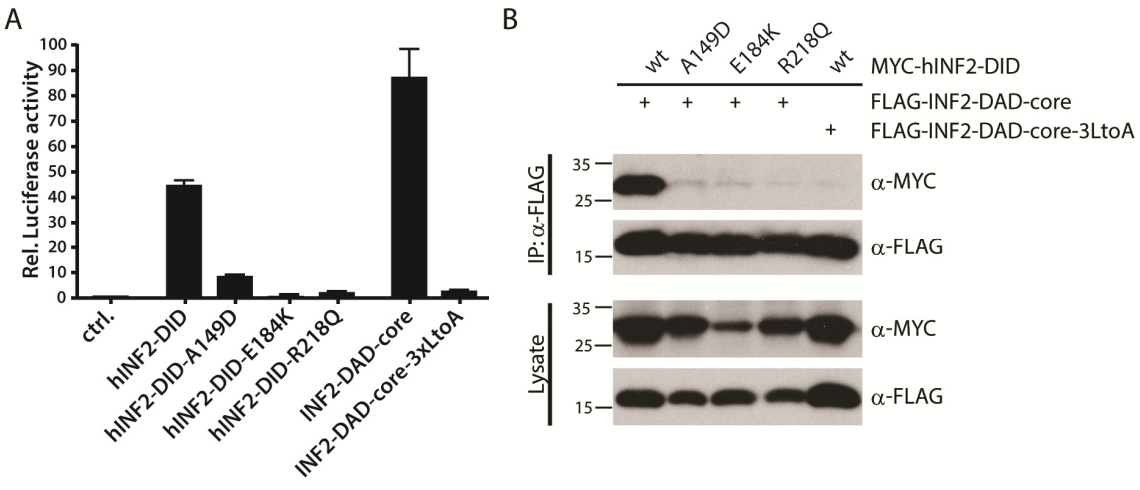

Figure 13: Mutations interfering with INF2-DID/DAD binding inhibit regulation of SRF activity

A) HEK cells were transfected with either hINF2-DID (wt, or with the mutations A149D, E184K or R218Q) or hINF2-DAD 'core' (wt or L1008A, L1009A, L1018A [= 3LtoA]). Measurements of SRF activity were conducted in serum starved cells. Results are means ± SD (n=3). **B)** Co-Immunoprecipitations from cells

expressing hINF2-DID (or derivatives) or INF2-DAD-core (or derivatives) were immunoblotted as indicated.

Furthermore, it had to be determined if the rearrangement of the actin structures upon overexpression of INF2-DAD or INF2-DAD-CAAX (cf. Figure 12A) were mediated by activation of the respective endogenous INF2 isoform or rather by the expression of the DAD itself or even by a putative influence of the DAD on other proteins. Thus, we tested if hINF2-DAD-CAAX overexpression affects the actin pattern in siRNA mediated INF2 knockdown cells compared to control cells (knockdown efficiency see Figure 14A). In siControl cells, the majority of hINF2-DAD-CAAX transfected cells showed characteristic active INF2-CAAX actin structures, whereas upon INF2 depletion, the amount of INF2-DAD-CAAX transfected cells featuring an ER localized actin pattern decreased strikingly (Figure 14B).

Moreover, we used the CRISPR/Cas9 system to obtain a complete deletion of INF2 in NIH3T3 cells. Efficient knockout of endogenous INF2 in different NIH3T3 clones was finally proven by immunoblotting (Figure 14C) as well as in selected clones by confocal microscopy using α-INF2-immunolabeling (Figure 14D). Interestingly, INF2 knockout led only to a decreased but not completely abolished INF2-DAD-core driven MRTF/SRF transcriptional activity (Figure 14E). Co-expression of INF2-DAD-core together with full length hINF2 could rescue the effect on SRF activity. Noteworthy, this co-expression in INF2-knockout cells resulted in lower SRF activity than in control cells. The difference might reflect the effect of activated endogenous INF2 in control cells which is depleted in INF2 knockout cells. The reduction of MRTF/SRF transcriptional activity upon INF2-DAD expression in INF2 depleted cells goes along with reduced MRTF-A-GFP accumulation in the nucleus (Figure 14F). Again, the reduced MRTF-A shuttling could be partially rescued upon co-expression of hINF2-DAD together with full length hINF2.

Noteworthy, INF2 depletion remarkably interfered with serum-induced SRF activity (Figure 14G). Thus, INF2 seems to be required to efficiently activate general SRF transcriptional activity by serum.

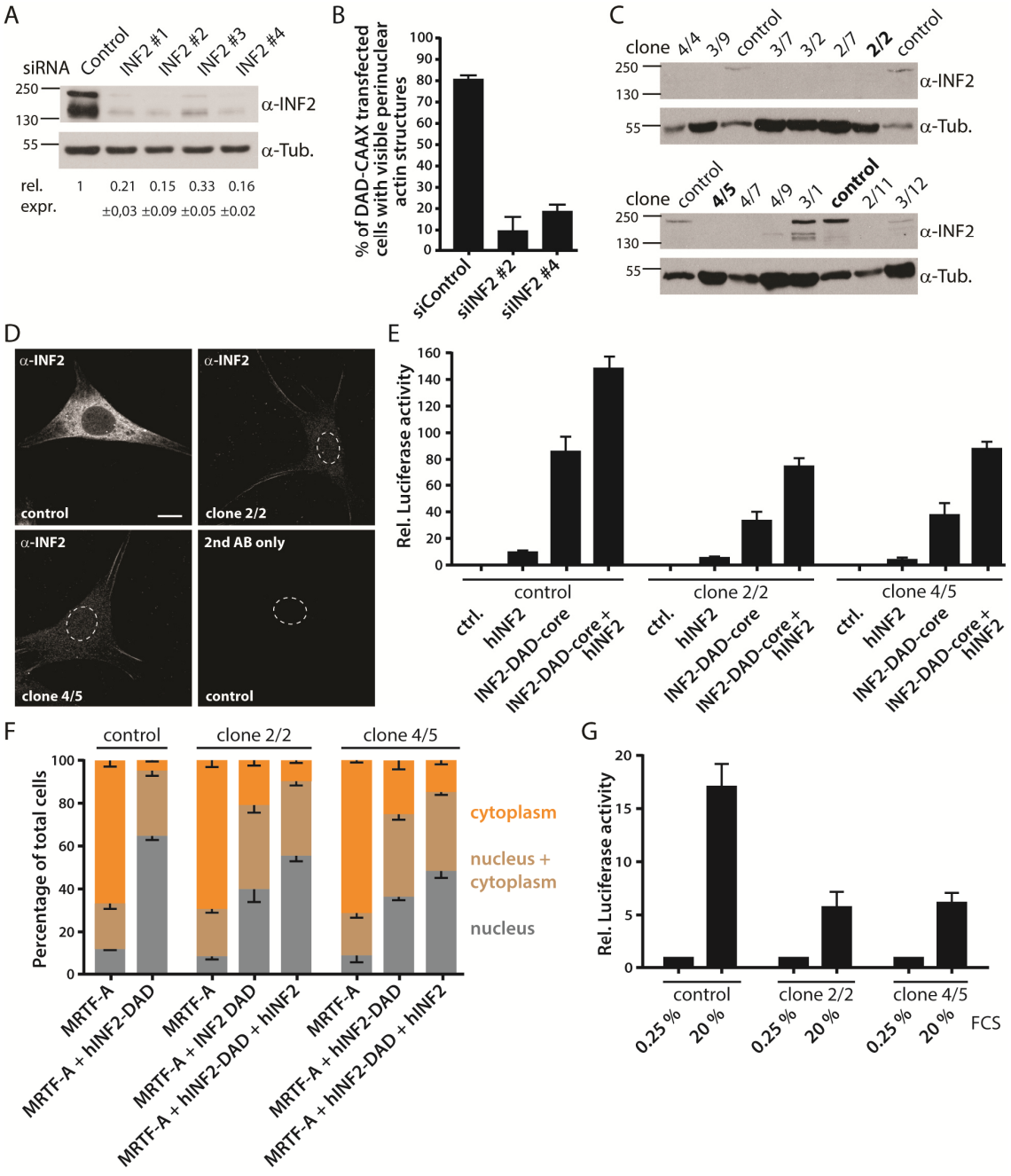

Figure 14: INF2-DID or INF2-DAD promoted effects on actin dynamics and MRTF/SRF regulation depend on endogenous INF2

A) Efficient siRNA mediated depletion of mINF2 in NIH3T3 cells was proven by immunoblotting against INF2 upon treatment with four different siRNA sequences. All four sequences are capable to silence both isoforms of INF2 simultaneously. α-Tubulin detection was used as loading control. **B)** INF2 silenced NIH3T3 cells were quantified for showing formation of characteristic hINF2-DAD-CAAX mediated F-actin structures, compared to siControl cells. Only cells expressing mCherry hINF2-DAD-CAAX were considered for quantification. Around 25 to 40 cells were analyzed for each condition in two

independent experiments. **C)** Efficient CRISPR/Cas9 mediated depletion of both isoforms of INF2 in NIH3T3 cells was proven by immunoblotting against INF2 in different clones (bold: clones used for further experiments). α-Tubulin detection was used as loading control. **D)** Representative confocal images (single z-stack section) illustrate α-INF2 immunolabeling of selected NIH3T3 INF2 knockout clones. White dashed lines delineate nuclear borders (cells were counterstained with DAPI – Data not shown). Scale bar, 10 µm. **E)** INF2 depleted NIH3T3 cells (control vs. clone 2/2 or 4/5) were transfected with either hINF2 alone, hINF2-DAD-core or hINF2-DAD-core together with hINF2. SRF activity was analyzed under serum starved conditions. Results are means ± SD (n=3). **F)** INF2 depleted NIH3T3 cells (control, clone 2/2 and clone 4/5) were transfected with either MRTF-A-GFP alone, MRTF-A-GFP together with mCherry-hINF2-DAD or MRTF-A-GFP together with mCherry-hINF2-DAD and MYC-hINF2 and imaged under serum starved conditions. Localization of MRTF-A-GFP was analyzed in around 55 to 100 cells for each condition in two independent experiments. **G)** NIH3T3 cells lacking INF2 were grown under serum starved conditions. Cells were stimulated with 20 % FCS 6 h before conducting the SRF reporter gene assay. Results are means ± SD (n=3).

4.3 INF2 localizes to the nucleus

Previous work revealed localization of mDia formins in the nucleus (Baarlink et al., 2013; Miki et al., 2009). We examined by subcellular fractionation if the formin INF2 also localizes to the nucleus. Indeed, immunoblotting revealed presence of endogenous INF2 in nuclear fractions of NIH3T3 cells (Figure 15A). Moreover, endogenous nuclear INF2 could also be detected by confocal microscopy. The nuclear INF2 fluorescence intensity was strikingly reduced in INF2 deleted cells compared to control cells (Figure 15B).

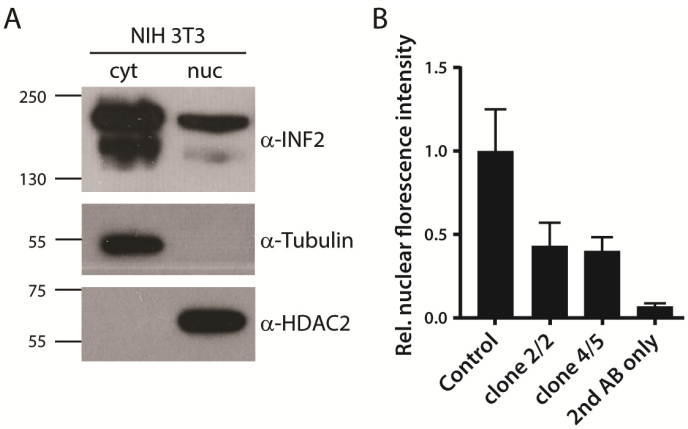

Figure 15: INF2 localizes to the nuclear compartment

A) Subcellular fractions of NIH3T3 cells were immunoblotted for endogenous INF2. α-Tubulin and α-HDAC blotting was used as control for successful fractionation. **B)** The relative nuclear fluorescence intensity upon α-INF2 immunolabeling was quantified from NIH3T3 control cells and INF2 deleted NIH3T3 cells. Additional staining of control cells without α-INF2 antibody served as control for unspecific 2nd antibody binding. The nucleus was highlighted with DAPI. Around 40 to 50 nuclei were analyzed for each condition in two independent experiments. Sample images are shown in Figure 14D. Results are means ± SD.

4.3.1 INF2 contains functional NLS and NES motifs

To gain details about the nuclear localization of INF2 we used the bioinformatics tool cNLS-Mapper (Kosugi et al., 2009) to detect putative nuclear localization sequences (NLS) in hINF2. Three putative NLS regions could be identified named NLS1 (aa 622 – 651), NLS2 (aa 910 – 941) and NLS3 (aa 1213-1240 in the isoform lacking the CAAX motif and aa 1213 – 1248 present in INF2-CAAX) (Figure 16A). Subsequently, we generated constructs expressing the isolated aa sequence of the identified NLS fused to a GFP fluorophore. To determine if these putative NLS are functional, we expressed the diverse GFP-NLS constructs in NIH3T3 cells and quantified the ratio between the nuclear and cytoplasmic GFP signal (Figure 16B, C). NLS1-GFP and NLS2-GFP did not show an increase in the nucleocytoplasmic GFP-signal ratio compared to the signal of GFP alone. However, the majority of the signal of GFP-NLS3 (in both isoforms) could be detected in the nuclear compartment. Mutations in the sequence of both NLS3 at six positively charged key residues (K1220A, R1221A, R1222A, K1223A, K1224A, and R1225A) efficiently inhibited nuclear accumulation of GFP-NLS3.

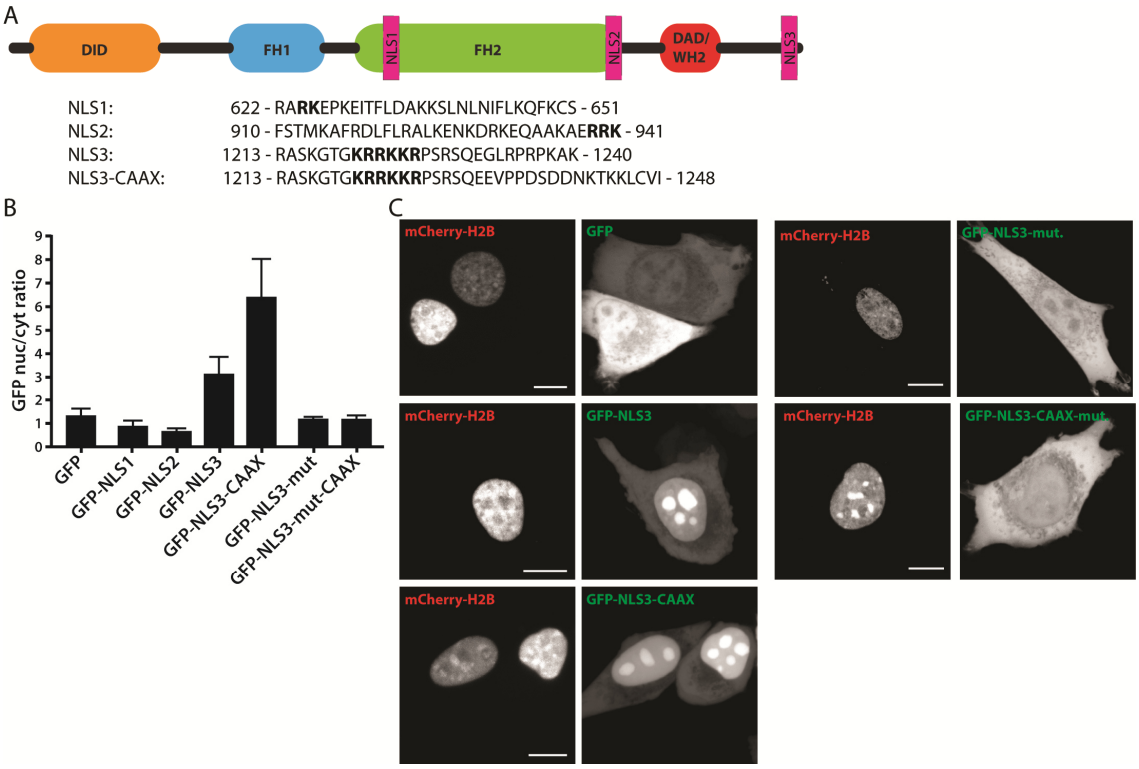

Figure 16: INF2 contains putative NLS-like sequences

A) Cartoon of distinct domains of hINF2 including three different putative nuclear localization sequences (NLS). Putative NLS were identified using cNLS mapper (Kosugi et al., 2009). Critical amino acids are highlighted in bold. Note the differences between the two isoforms in the sequence of NLS3. **B)** The ratio of the nuclear vs. the cytoplasmic GFP signal fused to each putative NLS as well as to the mutated NLS3 (K1220A, R1221A, R1222A, K1223A, K1224A, and R1225A). The average of 8 to 10 analyzed cells is shown. **C)** Left panel: Images of representative NIH3T3 cells show localization of GFP alone or GFP fused to the putative NLS3 (both isoforms). Right panel: Images display the localization of the K1220A, R1221A, R1222A, K1223A, K1224A, and R1225A mutant of NLS3 (of both INF2 isoforms) fused to GFP in NIH3T3 cells. mCherry-H2B was used as nuclear marker. Scale bar, 10 µm.

Furthermore, bioinformatic analysis using NetNES 1.1 Server (la Cour et al., 2004) of the hINF2 amino acid sequence revealed multiple putative nuclear export signals (NES) named NES1 (aa 77-88), NES2 (aa 230-247), NES3 (aa 675-685) and NES4 (aa 913-924) (Figure 17A). Constructs encoding the isolated NES-like sequence fused to GFP were generated and expressed in NIH3T3 cells. Analysis of their nucleocytoplasmic GFP-signal distribution revealed at least NES4 to be functional (Figure 17B, C). Interestingly, the amino acid sequence of NES4 in hINF2 shows some sequence homology to a well described NES-like sequence in the C-terminal mDia2 region containing the critical

residue L1168 (Miki et al., 2009) as well as to a putative NES sequence in FHOD1 (Ménard et al., 2006). In hINF2 the corresponding amino acid is L921. Mutation of L921 to Glycine blocks the export function of NES4.

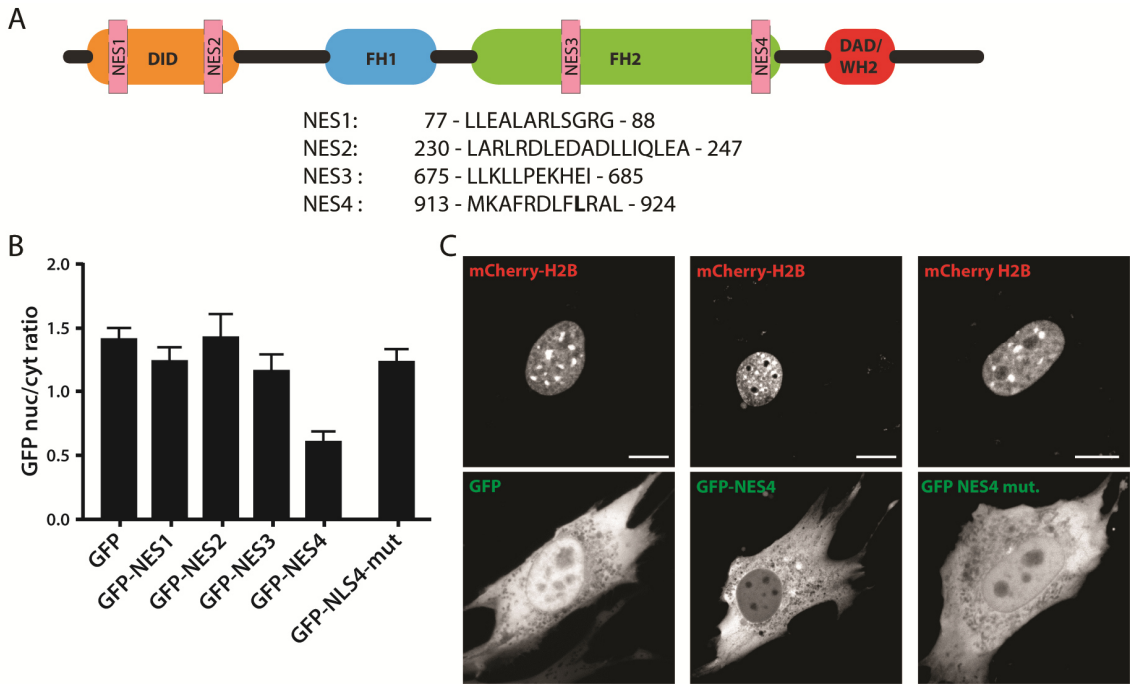

Figure 17: INF2 shows putative NES-like sequences

A) Cartoon showing the protein domain structure of hINF2. Putative NES-like sequences (shown in pink) were identified using NetNES 1.1 Server (la Cour et al., 2004). A putative critical amino acid in NES4 is shown in bold. **B)** The ratio of nuclear vs. cytoplasmic GFP signal fused to each putative NES as well as to mutated NES4 (L921G). The average of 8 to 10 analyzed cells is shown. **C)** Representative images of NIH3T3 cells show the localization of GFP alone and GFP fused to NES4 or mutated NES4 (L921G). mCherry H2B was used as nuclear marker. Scale bar, 10 µm.

These results suggest that INF2 contains functional NLS and NES motifs for putative nucleo-cytoplasmic shuttling. Previously, mDia2 was shown to continuously shuttle between the nucleus and the cytoplasm through a specific nuclear transport mechanism composed of importin-α/β and CRM1 (Miki et al., 2009). Notably, although isolated GFP-NES4 was enriched in the nucleus upon blocking CRM1 mediated nuclear export by leptomycin B (Figure 18A, B), neither endogenous hINF2 (Figure 18C) nor different full length hINF2 derivatives (Figure 18D) accumulated in the nucleus upon

LMB treatment. Thus we conclude that if INF2 continuously shuttles between the nucleus and the cytoplasm, it uses a nuclear transport machinery distinct from mDia2.

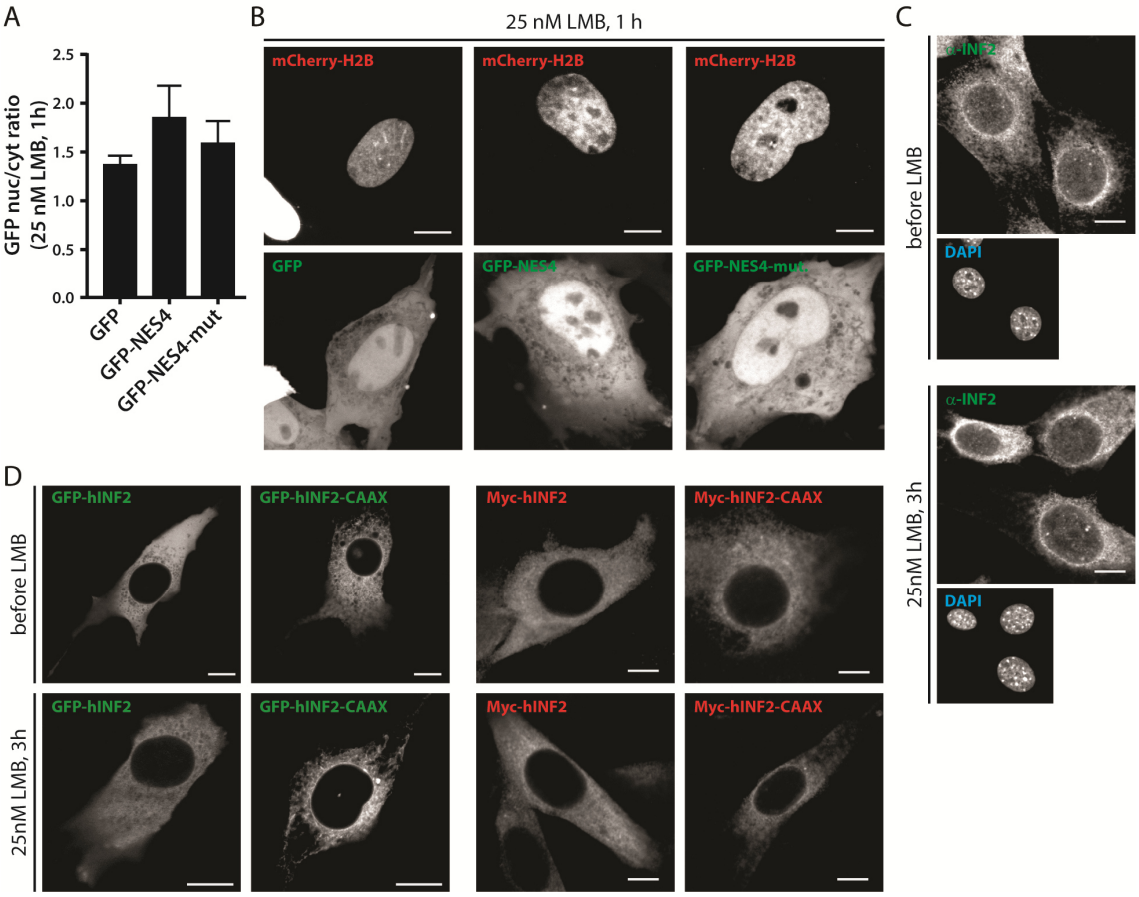

Figure 18: INF2 does not accumulate in the nucleus upon LMB treatment

A) Nucleocytoplasmic ratio of GFP-NES4 and GFP-NES4-L921G upon LMB treatment (25 nM, 1h). **B)** Representative images show the effect of LMB (25 nM, 1 h) on the localization of GFP fused to NES4 or the NES4-L921G mutant. Scale bar, 10 µm. **C-D)** Representative images show fixed NIH3T3 cells before or after treatment with 25 nM LMB for 3 hours. Cells were either immunostained for endogenous INF2 **(C)** or tagged versions of both hINF2 isoforms (GFP: left panel, MYC: right panel) were expressed and visualized **(D)**. Scale bar, 10 µm.

4.4 Nuclear INF2 regulates actin network assembly and MRTF/SRF activity

Activated nuclear mDia promotes the formation of a nuclear actin network and subsequent regulation of SRF dependent gene expression (Baarlink et al., 2013). As we could detect INF2 also in the nucleus, we thus analyzed if spatially restricted activation of INF2 affects nuclear actin polymerization.

4.4.1 Activation of INF2 within the nucleus leads to nuclear actin network assembly

To activate endogenous INF2 in the nucleus, we generated NLS tagged versions of hINF2-DID or INF2-DAD-core to release INF2 autoinhibition. Phalloidin staining revealed nuclear actin structures upon expression of either hINF2-DID-NLS or INF2-DAD-core-NLS in NIH3T3 cells (Figure 19A). Nuclear actin structures could also be obtained in living NIH3T3 cells by using the actin marker nAC-GFP upon expression of hINF2-DID-NLS or INF2-DAD-core-NLS (Figure 19B). Noteworthy, whereas a vast majority of INF2-DAD-core-NLS transfected cells displayed nuclear F-actin, fewer cells showed those structures upon hINF2-DID-NLS transfection. Expression of the DID binding deficient mutant INF2-DAD-core-3LtoA-NLS did not result in nuclear actin filament formation (Figure 19C), further underscoring the specificity of the approach. The formation of nuclear actin filaments upon INF2-DAD-core-NLS mediated activation of INF2 did not exclusively occur in NIH3T3 cells but could also be detected using nAC-GFP in diverse other cell lines such as HELA, LOX or HT29 (Figure 19D).

To refute the possibility that hINF2-DID-NLS or INF2-DAD-core-NLS overexpression is followed by an enrichment of actin monomers in the nucleus and thus leading to filament formation, subcellular fractionation experiments were conducted. However, no significant alterations in the abundance of endogenous actin in the nucleus could be obtained upon expression of neither nuclear hINF2-DID nor INF2-DAD-core (Figure 19E).

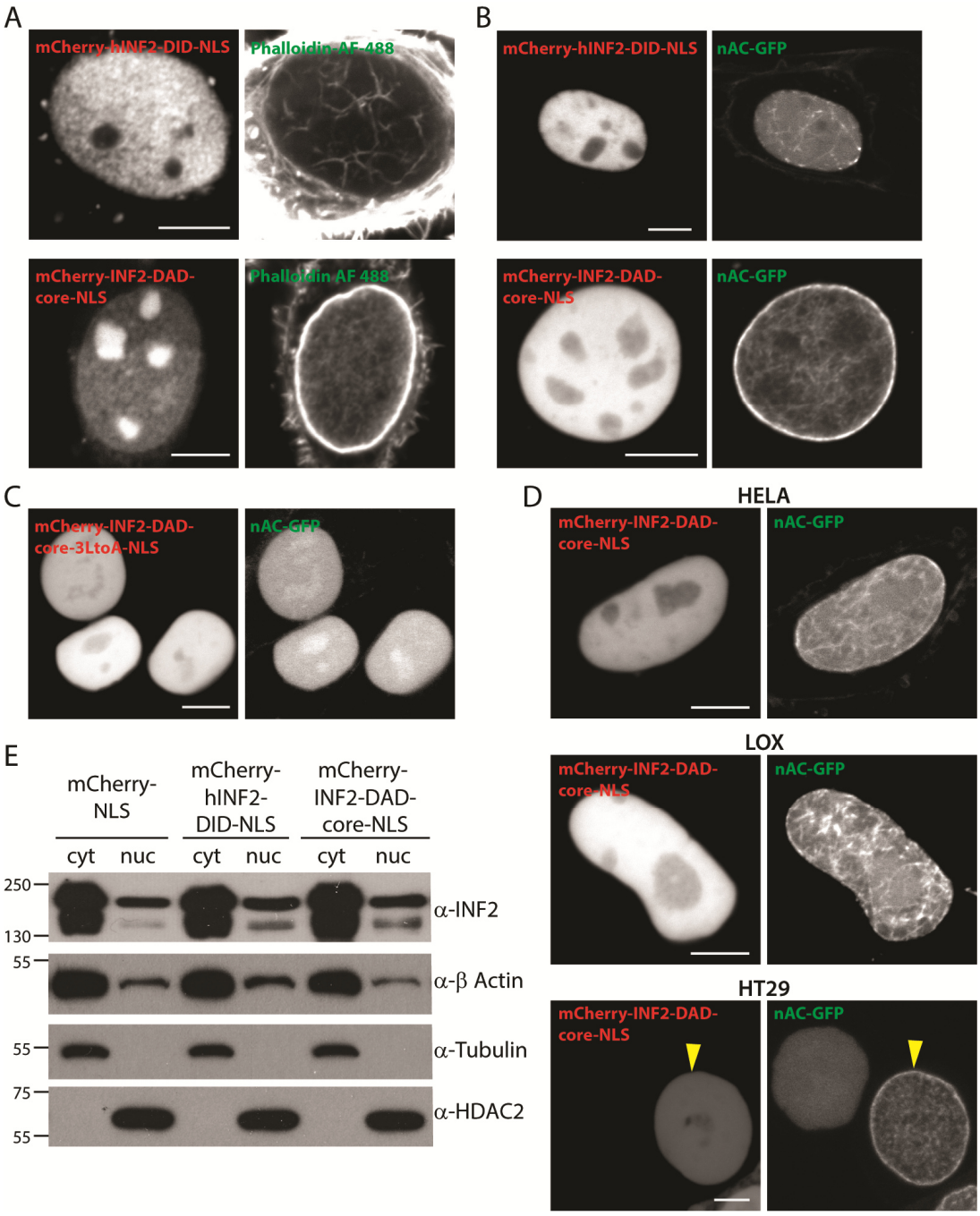

Figure 19: Activation of nuclear INF2 mediates formation of an actin network in the nucleus

A) Images show actin filaments visualized by Phalloidin-AF488 staining in fixed NIH3T3 cells expressing mCherry-hINF2-DID-NLS or mCherry-INF2-DAD-core-NLS. Note the distinctive nuclear actin structures visualized by Phalloidin-AF488. Scale bar, 10 µm. **B)** Nuclear actin structures upon expression of mCherry hINF2-DID-NLS or mCherry-INF2 DAD-core-NLS could also be visualized in living cells using nAC-GFP. Scale bar, 10 µm. **C)** NIH3T3 cells transfected with INF2-DAD-core-3LtoA-NLS do not show F-actin in the nucleus. Scale bar, 10 µm. **D)** Images show samples of nuclear actin structures visualized by nAC GFP in HELA, HT29 and LOX cells expressing mCherry-INF2-DAD-core-NLS. Note the differential actin pattern

comparing non-transfected to INF-2-DAD-core-NLS expressing (yellow arrowheads) cells. Scale bar, 10 µm. **E)** Immunoblotting for endogenous β-Actin upon subcellular fractionation does not reveal an accumulation of actin in the nucleus upon expression of either mCherry-hINF2-DID-NLS or mCherry-INF2-DAD-core-NLS compared to mCherry-NLS alone.

Noteworthy, a majority of INF2-DAD-core-NLS transfected cells exhibit a remarkable actin ring-like structure. However, in contrast to the INF2-CAAX mediated perinuclear actin ring (Ramabhadran et al., 2013), the INF2-DAD-core-NLS mediated actin ring-like structure at the nucleocytoplasmic border partially colocalizes with the nuclear lamina facing the nuclear interior (Figure 20A-C).

Furthermore, we confirmed the intranuclear localization of the actin ring by using Saponine permeabilization, which removes cholesterol from membranes while leaving the nuclear membrane, which does not contain cholesterol intact (Adam et al., 1990). Upon Saponine permeabilization, INF2-DAD-core-NLS mediated actin structures could not be detected in the nucleus of GFP-Actin-NLS expressing NIH3T3 cells by immunostaining against GFP, as antibodies are incapable of entering the nuclear interior under these conditions (Figure 20D). Contrariwise, nuclear actin structures could be visualized by α-GFP immunostaining when cells were permeabilized with TX-100. However, characteristic hINF2-DAD-CAAX mediated perinuclear actin structures could be detected in the cytoplasm in both permeabilization methods (data not shown).

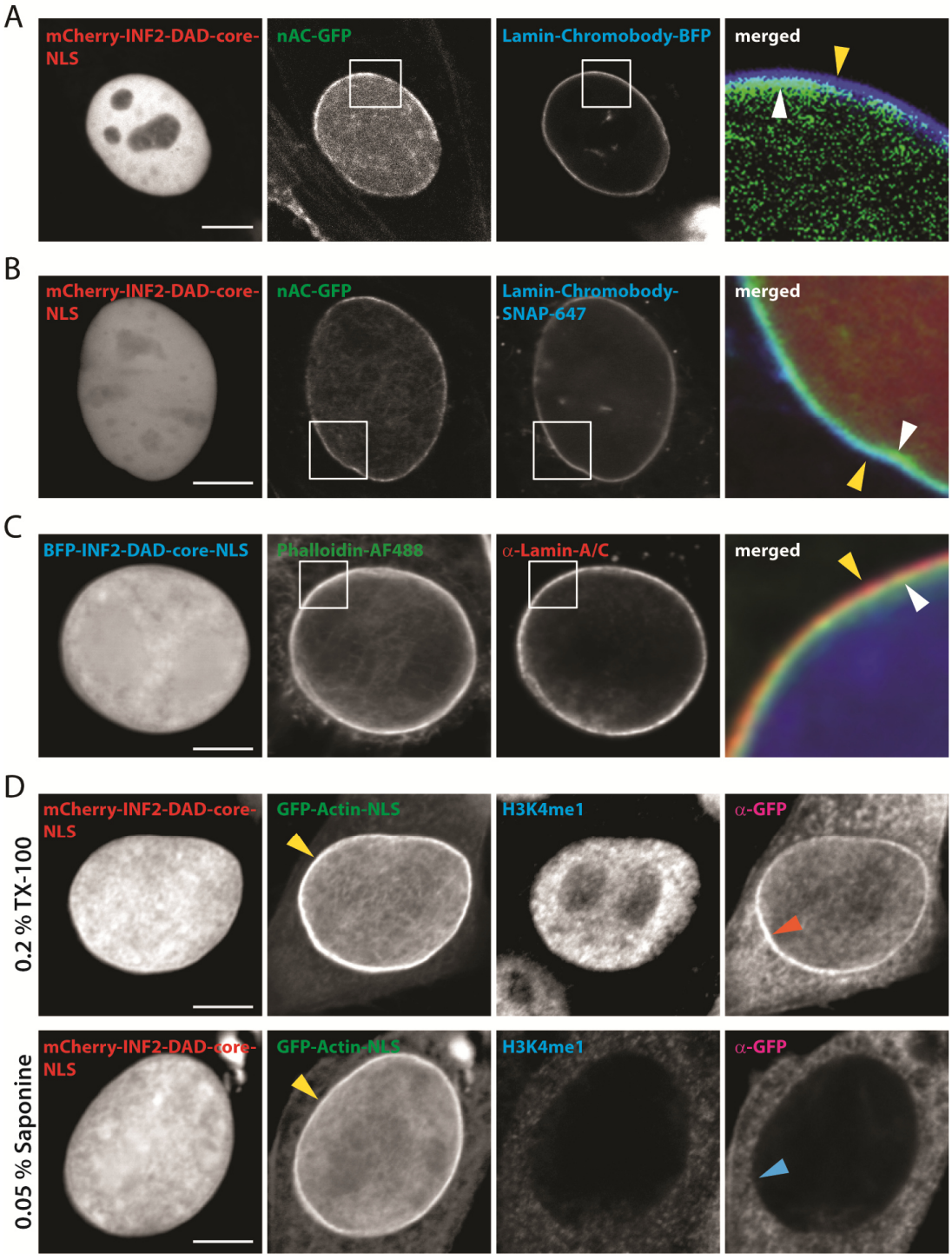

Figure 20: INF2-DAD-core-NLS expression promotes formation of a prominent sublaminar actin ring-like structure

A) NIH3T3 cells expressing nAC-GFP were transfected with Lamin-Chromobody-BFP and mCherry-INF2-DAD-core-NLS. White rectangles mark areas of higher magnification. The merged panel shows the localization of nAC GFP (white arrowhead) together with the Lamin-Chromobody-BFP signal (yellow arrowhead). Scale bar, 10 µm. **B)** NIH3T3 cells were transfected with mCherry-INF2-DAD-core-NLS

together with nAC-GFP and Lamin-Chromobody-SNAP (labeled with 647-SiR dye). An area of higher magnification (marked by white rectangles) is shown in the merged panel (white arrowhead: nAC GFP signal, yellow arrowhead: 647-SiR signal). Scale bar, 10 µm. **C)** Fixed NIH3T3 cells transiently expressing BFP-INF2-DAD-core-NLS were stained with Phalloidin-AF488 and for Lamin-A/C. The zoomed merged panel (correlating to white rectangles) displays nuclear actin structures (white arrowhead) and the nuclear lamina (yellow arrowhead). Scale bar, 10 µm. **D)** Fixed NIH3T3 cells expressing GFP-Actin-NLS and mCherry-INF2-DAD-core-NLS were permeabilized and stained as indicated. The yellow arrowheads point to remarkable INF2-DAD-core-NLS mediated ring-like nuclear actin structures detected by imaging the intramolecular GFP signal. Note that the ring-like structures could only be visualized by α-GFP immunolabelling upon cell permeabilization with 0.2 % TX-100 (orange arrowhead) but not upon 0.05 % Saponine treatment (blue arrowhead). Scale bar, 10 µm.

4.4.2 Nuclear INF2 activation affects MRTF/SRF transcriptional activity

Induction of INF2 mediated nuclear actin filaments also resulted in an increase in MRTF/SRF transcriptional activity (Figure 21A). Thereby, INF2-DAD-core-NLS expression upregulated SRF activity more effectively than hINF2-DID-NLS. Interestingly, the ability of translocation of MRTF-A to the nucleus was more effective upon DID mediated INF2 activation compared to DAD mediated activation (Figure 21B).

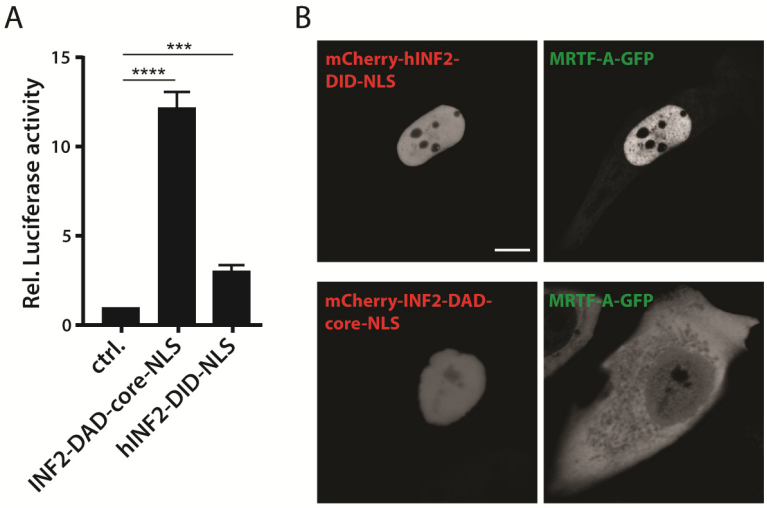

Figure 21: Active nuclear INF2 mediates MRTF translocation and affects SRF activity

A) HEK cells were transfected with INF2-DAD-core-NLS or hINF2-DID-NLS and SRF activity was measured. Results are means ± SD (n=3). ***: P<0.001, ****: P<0.0001, Student's t-test. **B)** NIH3T3 cells were

transfected with MRTF-A-GFP and either mCherry-INF2-DAD-core-NLS or mCherry-hINF2-DID-NLS. Cells were analyzed then for the localization of MRTF-A-GFP. Scale bar, 10 µm.

4.4.3 INF2-DAD mediated nuclear actin network assembly is INF2 dependent

Measurements of MRTF/SRF transcriptional regulation in HEK cells expressing equal amounts of hINF2-DID-NLS or INF2-DAD-core-NLS together revealed compensation of the effects on SRF activity mediated by expression of hINF2-DID-NLS or INF2-DAD-core-NLS alone (Figure 22A). Additionally, INF2-DAD-core-NLS expressing NIH3T3 cells were co-transfected together with hINF2-DID-NLS and analyzed for nuclear actin filament formation by fluorescence microscopy (Figure 22B). The percentage of NIH3T3 cells displaying nuclear actin structures mediated by INF2-DAD-core-NLS was reduced dramatically upon co-expression with hINF2-DID-NLS. However, this reduction could not be obtained upon transfection with the impaired DAD binding mutant hINF2-DID-A149D-NLS.

Furthermore, INF2 knockdown by siRNA in NIH3T3 cells led to a significant decrease of cells showing nuclear actin structures after transfection with INF2-DAD-core-NLS (Figure 22C). However, actin filaments in the nucleus could still be detected in a remarkable amount of cells. This could be explained by inhomogeneous siRNA mediated INF2 depletion within all analyzed cell. Thus, nuclear F-actin assembly upon INF2-DAD-core-NLS expression was analyzed in CRISPR/Cas9 mediated INF2 deleted NIH3T3 cells. Interestingly, even a complete knockout of INF2 did not entirely inhibit INF2-DAD-core-NLS driven formation of nuclear actin structures (Figure 22D). The results were rather comparable to the siINF2 knockdown cells.

Worth mentioning, mutations of highly conserved INF2-FH2 residues (I643A and/or K792A) (Andrés-Delgado et al., 2010; Ramabhadran et al., 2012), which were shown to be essential for barbed end binding and actin polymerization in other formins (Shimada et al., 2004; Xu et al., 2004), did not abolish INF2-DAD-core-NLS mediated

nuclear actin filament formation but rather led to the formation of thick nucleus spanning actin bundles (Data not shown).

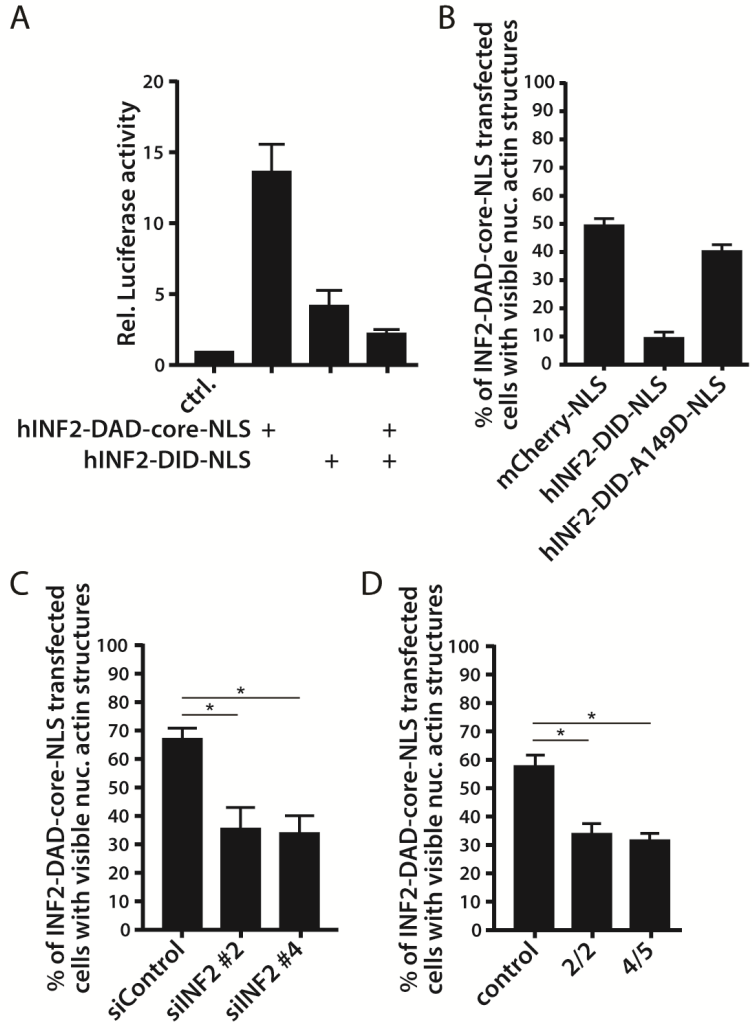

Figure 22: Nuclear actin network assembly mediated by INF2-DAD depends on endogenous INF2

A) SRF mediated transcription was measured in HEK cells transfected with either INF2-core-NLS or hINF2-DID-NLS alone or co-transfected with INF2-DAD-core-NLS together with equal amounts of hINF2-DID-NLS. Results are means ± SD (n=3). **: P<0.01, ***: P<0.001, Student's t-test. **B)** NIH3T3 cells expressing nAC-GFP together with BFP-INF2-DAD-core-NLS and either mCherry-NLS (as control), mCherry-hINF2-DID-NLS or hINF2-DID-A149D-NLS were analyzed and quantified in terms of nuclear actin filament formation. Only cells expressing both BFP-INF2-DAD-core-NLS and the hINF2-DID derivate were considered for quantification. Around 110 to 190 cells were analyzed for each condition in two independent experiments. *: P<0.05, **: P<0.01, Student's t-test. **C)** INF2 silenced NIH3T3 cells were quantified for showing formation of INF2-DAD-core-NLS mediated nuclear actin filaments (visualized by co-transfection with nAC-GFP), compared to siControl cells. Only cells expressing mCherry-hINF2-DAD-

core-NLS were considered for quantification. Around 90 to 120 cells were analyzed for each condition in two independent experiments. *: P<0.05, Student's t-test. **D)** INF2 deleted NIH3T3 cells showing INF2-DAD-core-NLS-mediated nuclear actin filaments were quantified and compared to NIH3T3 CRISPR control cells. Around 60 to 140 cells were analyzed for each condition in two independent experiments. *: P<0.05, Student's t-test.

4.4.4 Activation of endogenous INF2 partially modulates the activity of mDia1/2 formins

Depletion of INF2 did not fully inhibit INF2-DAD-core mediated effects, leading to the assumption that some of the effects might be, at least partially, unspecific, e. g. due to interaction or activation of other actin nucleators such as other formins. For example, INF2-DID has been shown to directly interact with the DAD of mDia proteins and thereby plays a role in modulation of mDia mediated Rho signaling and SRF activity (Sun et al., 2014; Sun et al., 2011) as well as in the regulation of stable microtubules (Bartolini et al., 2016).

Double-knockdown of mDia1 and mDia2 diminished the formation of nuclear actin filaments upon transfection with INF2-DAD-core-NLS (Figure 23A), although the effect was very minor compared to knockdown of INF2. Interestingly, triple-knockdown of INF2, together with mDia1 and mDia2 did not significantly further reduce INF2-DAD-core-NLS mediated formation of nuclear F-actin when compared to INF2 alone (Figure 23A, compare to Figure 22C). Double- and triple-knockdown efficiency was proven by immunoblotting (Figure 23A, upper panel).

Also a complete CRISPR/Cas9 mediated INF2 deletion in NIH3T3 cells did not completely inhibit INF2-DAD-core-NLS driven formation of nuclear actin structures (Figure 23B). Furthermore, double-knockdown of mDia1 and mDia2 in CRISPR/Cas9 control cells showed a moderate reduction in nuclei containing F-actin structures compared to siControl cells. INF2-depleted clones treated with simDia1 and simDia2 did not display significant reduction of cells showing nuclear actin filaments as detected upon INF2-depletion alone (Figure 23B).

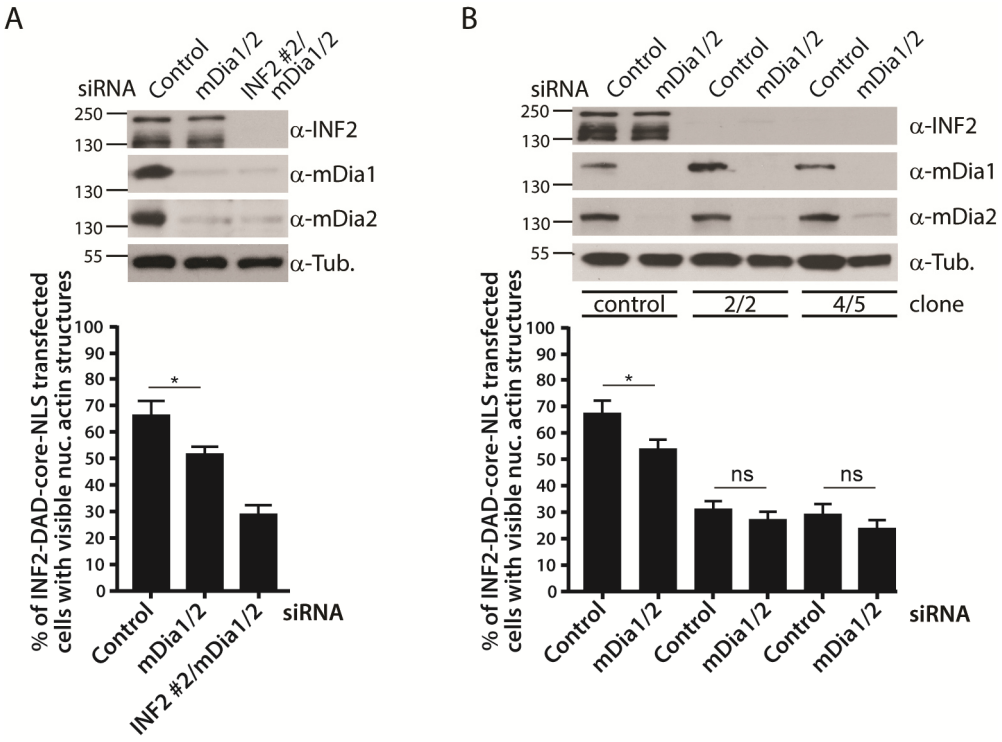

Figure 23: Active INF2 mediated nuclear F-actin assembly is partially modulated through mDia

A) Upper panel: Immunoblots for INF2, mDia1 and mDia2 from siRNA treated cells. Lower panel: simDia1/simDia2 or siINF2/simDia1/simDia2 treated NIH3T3 cells were transfected with INF2-DAD-core-NLS and quantified in terms of nuclear actin filament formation. Around 100 to 170 cells were analyzed for each condition in two independent experiments. *: $P<0.05$, Student's t-test. **B)** Upper panel: Immunoblots for INF2, mDia1 and mDia2 from siRNA treated INF2 depleted cells. Lower panel: INF2 depleted NIH3T3 cells were treated with siRNA against mDia1 and mDia2. Cells expressing INF2-DAD-core-NLS were quantified concerning the formation of F-actin in the nucleus. Around 130 to 230 cells were analyzed for each condition in two independent experiments. ns: $P>0.05$, *: $P<0.05$, Student's t-test.

Additionally, we examined if the proposed INF2–mDia interaction (Sun et al., 2011) also influences hINF2-DID or INF2-DAD mediated effects on SRF activity. An increase in SRF activity upon expression of either mDia2-DAD or hINF2-DID alone could be compromised upon expression of both constructs together. In contrast, mDia2-DID and hiNF2-DAD co-expression showed an additive upregulation in MRTF/SRF transcriptional activity (Figure 24A). Similar tendencies in alterations of SRF activity were obtained using nuclear localized DID/DAD derivatives (Figure 24B).

INF2-DAD-core-NLS mediated nuclear F-actin formation was dramatically reduced upon co-expression with hINF2-DID-NLS (Figure 22B). In contrast, co-expression of INF2-DAD-core-NLS with either mDia1-DID-NLS or mDia2-DID-NLS resulted only in a minor reduction of cells displaying an INF2-DAD-core-NLS induced nuclear actin network compared to control cells (Figure 24C). According to the assumption that INF2-DAD induced effects on actin filament formation are partially caused by interaction with mDia proteins, expressing a dominant negative (dn) form of mDia, which is deficient in binding of the FH2 domain to actin, should reduce the number of cells showing INF2-DAD driven rearrangement of the actin cytoskeleton. Therefore, nuclear mDia1-I845R (Shimada et al., 2004) or mDia2-I704A (Harris et al., 2006) was expressed together with INF2-DAD-core-NLS in NIH3T3 cells and the number of transfected cells with visible nuclear actin filaments was determined. However, neither dn-mDia1-NLS nor dn-mDia2-NLS expression significantly depleted the percentage of cells displaying a nuclear actin network compared to control cells (Figure 24C).

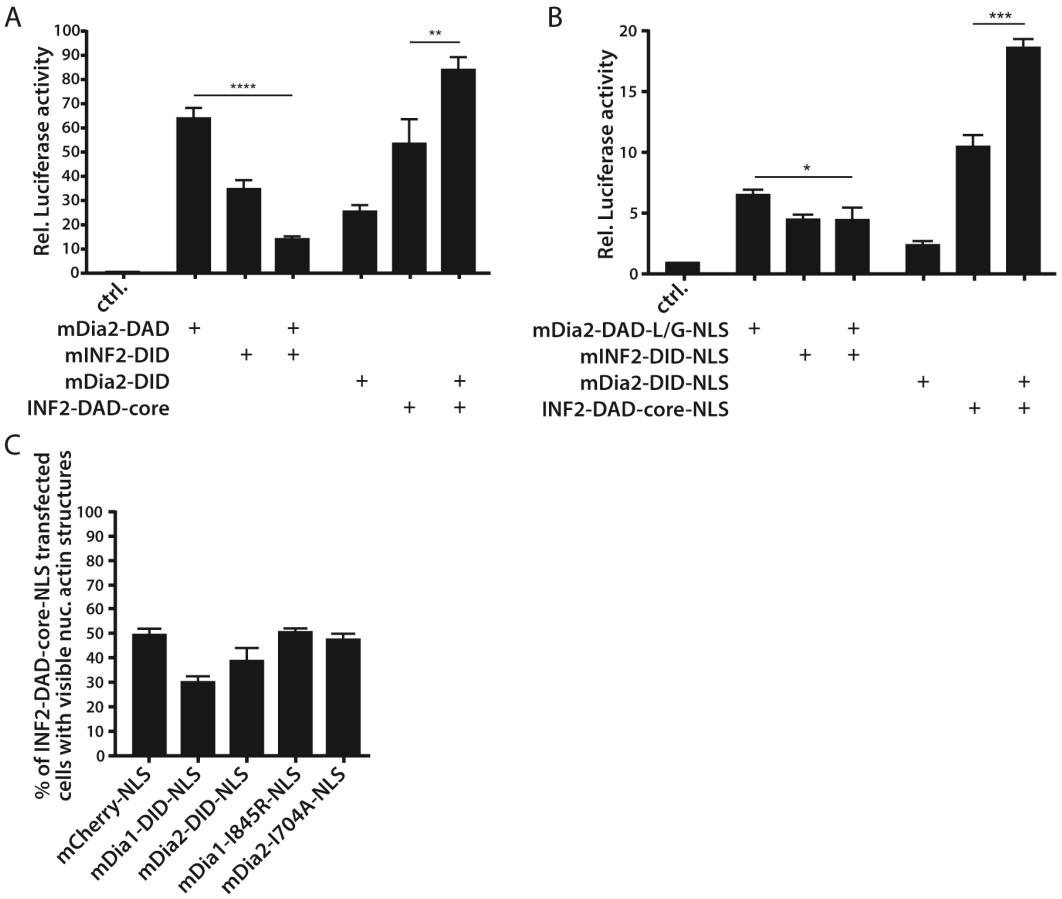

Figure 24: mDia2-DAD interferes with INF2-DID mediated SRF modulation

A) MRTF/SRF transcriptional activity was measured in HEK cells transfected with either mDia2-DAD or mINF2-DID alone or co-transfected with mDia2-DAD together with equal amounts of mINF2-DID. A similar experiment was conducted in HEK cells expressing mDia2-DID or INF2-DAD-core or both constructs together. Results are means ± SD (n=3). **: P<0.01, ****: P<0.0001, Student's t-test. **B)** As (A), but cells were transfected with the respective NLS tagged DID or DAD versions. Results are means ± SD (n=3). *: P<0.05, ***: P<0.001, Student's t-test. **C)** NIH3T3 cells expressing nAC-GFP together with BFP-INF2-DAD-core-NLS and either mCherry-NLS, mCherry-mDia1-DID-NLS, mCherry-mDia2-DID-NLS, RFP-mDia1-I845R-NLS or RFP-mDia2-I704A-NLS were analyzed and quantified in terms of nuclear actin filament formation. Only cells expressing all constructs were considered for quantification. Around 100 to 170 cells were analyzed for each condition in two independent experiments. ns: P>0.05, *: P<0.05, Student's t-test.

Taken together, these results suggest that active endogenous INF2, besides its direct impact on actin rearrangement, also partially modulates the activity of mDia1/2 formins. This modulation also occurs in the nuclear compartment.

4.4.5 Spatiotemporal activation of endogenous INF2 by a photoactivatable LOV-INF2-DAD/WH2 fusion protein mediates nuclear accumulation of MRTF-A and induces nuclear actin filament formation

The sustained presence of a formin induced nuclear actin network, for instance mediated INF2-DAD-core-NLS expression, might lead to unexpected and unwanted functional and morphological impacts on cells. Thus, an optogenetic tool, was introduced to activate endogenous INF2 in a spatially and temporally regulated manner to avoid potential unwanted effects in further experiments. The main idea, based on previous approaches to generate photoactivatable DADs of mDia1 or mDia2 (Baarlink et al., 2013; Rao et al., 2013), was that the photoactivatable LOV (light, oxygen, voltage) Jα-domain (aa 403-543) of *Avena sativa* phototropin-1 (AsLOV2) (Harper et al., 2003) was fused to the DAD of INF2, thereby inhibiting its binding properties of INF2-DAD to endogenous INF2 when the LOV domain is in its closed

conformation. Upon illumination with blue light, unwinding of the Jα-helix would subsequently release inhibition of the DAD, leading to activation of INF2.

To achieve this, the LOV domain was fused to INF2-DAD/WH2, a region within INF2-DAD-core, possessing similar features as INF2-DAD-core in terms of influencing SRF activity or driving nuclear actin filament formation when targeted to the nucleus.

Initially a series of derivatives was generated containing successive truncations at the N-terminus of INF2-DAD/WH2 (Figure 25A). To validate successful caching of INF2 DAD/WH2 activity, these INF2-DAD/WH2 derivatives were fused to a light-insensitive 'dark-state' version of AsLOV2, containing the point mutation C450A (Harper et al., 2003), and SRF activity was measured upon transfection of cells with the respective construct. The expression of the constructs starting with aa 967, 968, 969, 970 and 971 caused only a minor activation of MRTF-SRF transcription, hence arguing for successful INF2-DAD/WH2 caging (Figure 25B). The selected 'dark-state' LOV-INF2-DAD/WH2 constructs (967, 968, 969, 970 and 971) were then compared to their 'lit-state' counterparts, mimicking the permanently unfolded state of the LOV domain. The 'lit-state' of AsLOV2 is characterized by the point mutation I539E in the Jα helix (Harper et al., 2004). INF2-DAD/WH2 derivatives 969, 970 and 971 thereby demonstrated the most significant variance in the extent of MRTF-SRF transcriptional regulation comparing 'dark state' vs. 'lit state' (Figure 25C). Alterations in SRF activity were accompanied by accumulation of MRTF-A in the nucleus upon photoactivation of LOV-INF2-DAD/WH2 by illumination of cells with blue LED for 3h (Figure 25D).

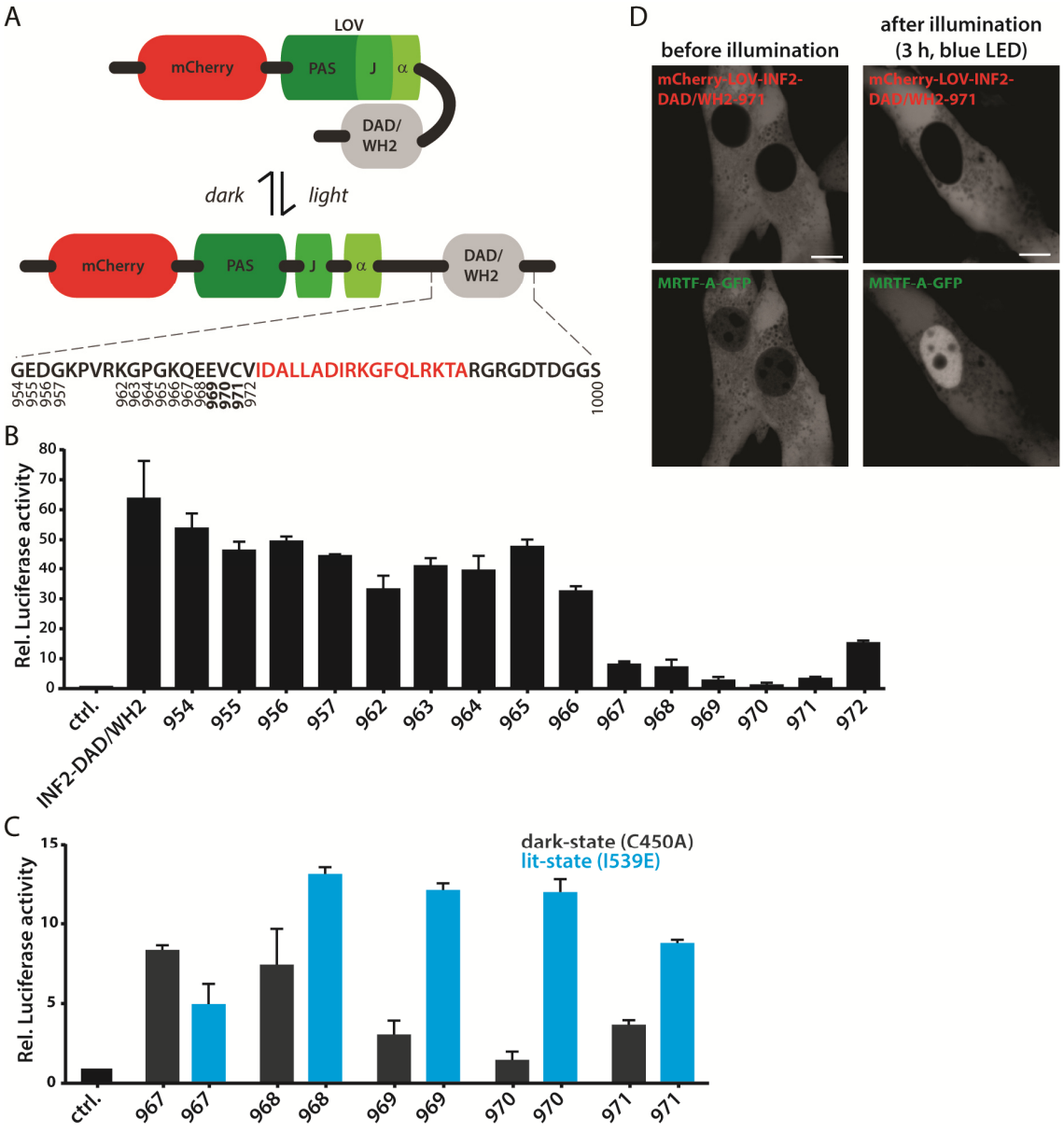

Figure 25: Screening for a photoactivatable LOV-INF2-DAD/WH2 fusion protein

A) Cartoon illustrating the suggested ability of LOV2 fused to INF2-DAD/WH2 to activate endogenous INF2 by light irradiation. The LOV2 domain of phototropin1 consists of a Per-ARNT-Sim (PAS) domain and a C-terminal Jα-helix. Upon illumination with blue light, which leads to unfolding of the Jα-helix, the INF2-DAD/WH2 domain is subsequently uncaged. The magnification shows a scheme of different LOV-INF2-DAD/WH2 constructs, which were generated by fusion of the LOV2 domain to successive N-terminal truncations of the INF2-DAD/WH2 domain (shown in red). Numbers indicate the positions of amino acid residues in hINF2. Numbers in bold represent the truncations which showed the most promising differences in SRF activity when comparing the respective 'lit state' construct (LOV2 mutation I539E) compared to its 'dark state' counterpart (LOV2 mutation C450A) (cf. Figure 25C). **B)** HEK cells expressing 'dark state' mutants of different LOV-INF2-DAD/WH2 fusion proteins were analyzed for their

ability to stimulate SRF transcriptional activity to define a subset of constructs showing successful caching of the DAD/WH2 domain. The expression of INF2-DAD/WH2 serves as negative control. Results are means ± SD (n=3). **C)** MRTF/SRF activity was analyzed in HEK cells transfected with selected 'lit state' LOV-INF2-DAD/WH2 constructs compared to their 'dark state' counterparts. Results are means ± SD (n=3). **D)** Images show NIH3T3 cells expressing mCherry-LOV-INF2-DAD/WH2-971 together with MRTF-A-GFP. Images were taken before and after 3 hours of blue LED illumination. Scale bar, 10 µm.

Photoactivatable release of INF2 autoinhibition restricted to the nucleus was obtained by fusing an NLS to LOV-GS-INF2-DAD/WH2-971 (containing an additional GS-linker sequence between the LOV-domain and INF2-DAD/WH2 starting with aa 971) (Figure 26A). A remarkable increase in the number of LOV-GS-INF2-DAD/WH2-971-NLS transfected cells containing nuclear F-actin structures could be visualized upon illumination of cells for 3 hours with blue LED (Figure 26B).

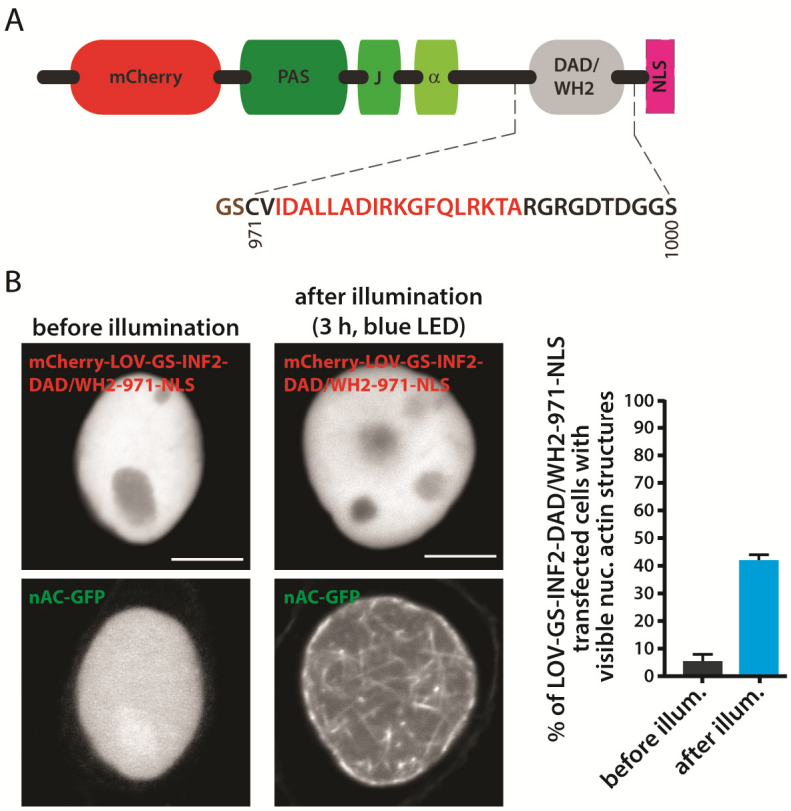

Figure 26: Spatiotemporal release of INF2 autoinhibition by using an optogenetic tool induces nuclear actin filament formation

A) Model illustrating a nuclear photoactivatable INF2-DAD/WH2 construct. An additional GS linker sequence between the LOV2 domain and INF2-DAD/WH2-NLS was inserted. **B)** nAC-GFP and mCherry-

LOV-GS-INF2-DAD/WH2-971-NLS co-transfected NIH3T3 cells were quantified in terms of showing nuclear actin filaments (right panel). Images were taken before and after illumination for 3 hours with blue LED. Around 60 to 110 cells were analyzed for each condition in two independent experiments. Left panel: Images display representative cells before and after illumination. Scale bar, 10 µm.

4.4.6 The dynamics of INF2-DAD mediated nuclear actin network formation

The formation of a prominent nuclear F-actin network mediated by photoactivatable nuclear mDia2-DAD was initiated already within a few minutes upon intervallic irradiation with 488 nm using confocal microscopy (Baarlink et al., 2013). However, investigating the dynamics of nuclear actin filament formation by utilization of LOV-GS-INF2-DAD/WH2-971-NLS did not reveal visible nuclear F-actin within this short range of time. In contrast, nuclear actin rearrangement did not occur before around one hour of constant illumination with blue LED. Thus, it was impossible to visualize nuclear actin rearrangement live by confocal microscope, as upon this rather long period of continuous illumination cycles the fluorescent signal of nAC-GFP was already bleached.

Generally, active INF2 in the cytoplasm did not result in nuclear actin network assembly (Figure 27A, B). To analyze the dynamics of INF2-DAD-core-NLS mediated release of INF2 autoinhibition in the nucleus and subsequent nuclear actin filament formation, two NES and one NLS was fused to obtain NES-mCherry-NES-INF2-DAD-core-NES-NLS (Figure 27C). This construct was supposed to continuously shuttle between the cytoplasm and the nucleus in a CRM1 dependent manner, displaying the majority of the protein localized to the cytoplasm under steady state conditions. Indeed, treatment of cells with 25 nM LMB resulted in a rapid accumulation of NES-mCherry-NES-INF2-DAD-core-NES-NLS in the nuclear compartment within a few minutes. However, de novo generation of nuclear actin filaments could be detected around 15 to 30 minutes upon LMB treatment. Around 1 hour after addition of LMB, nuclei finally showed the INF2-DAD-core-NLS mediated characteristic actin pattern (Figure 27D). In contrast, nuclear F-actin formation occurred already within a few

minutes upon LMB mediated nuclear translocation of mDia2-DAD (Baarlink et al., 2013).

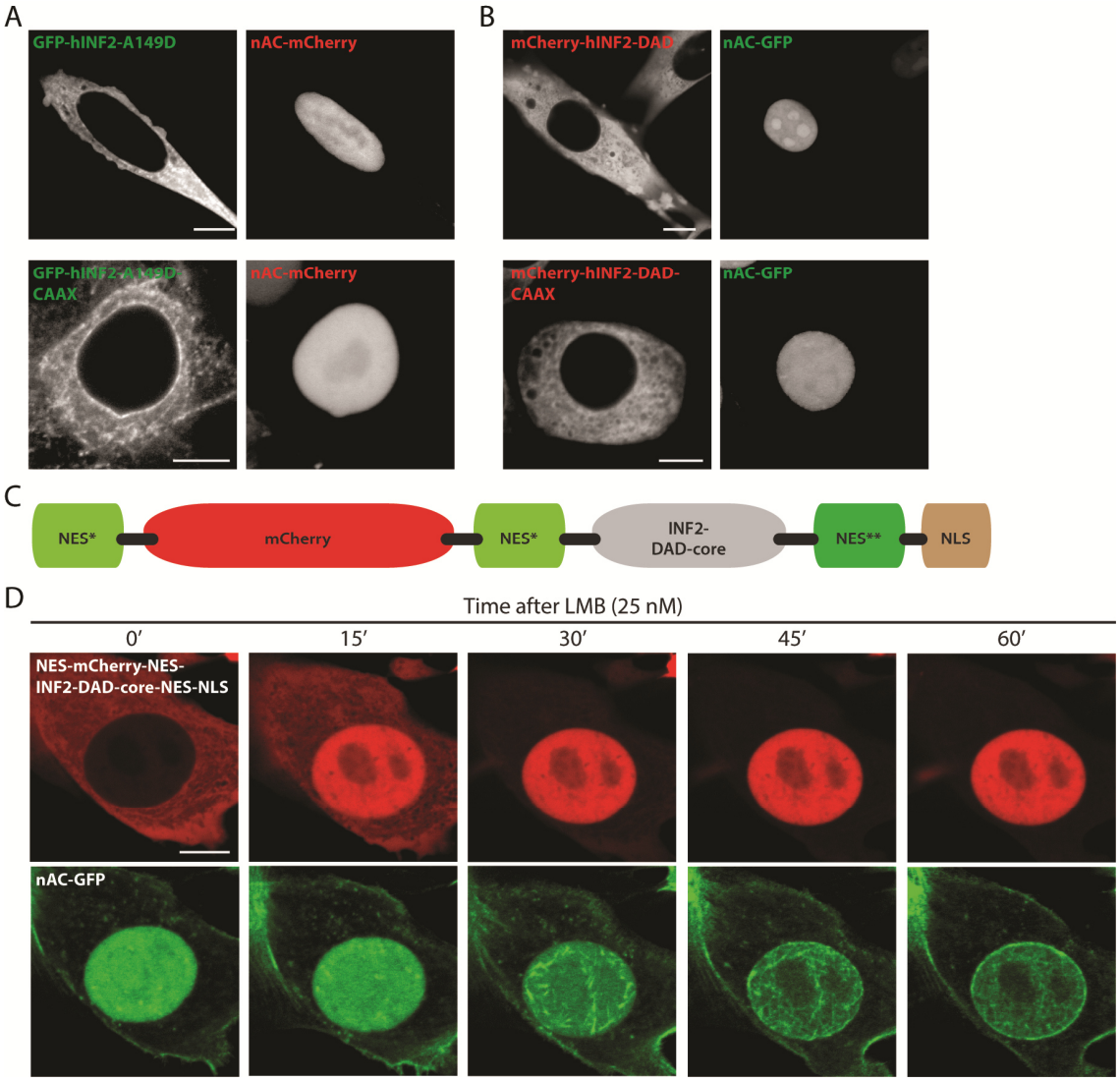

Figure 27: The dynamics of nuclear F-actin assembly mediated by INF2-DAD

A-B) Images show NIH3T3 cells with active INF2 (either achieved **(A)** by expression of constitutive active hINF2 or hINF2-CAAX or **(B)** by expression of the respective hINF2-DAD isoform) were co-transfected with nAC as marker for nuclear actin and analyzed for the formation of nuclear actin filaments. Scale bar, 10 µm. **C)** Model of a nucleocytoplasmic shuttling INF2-DAD-core construct. Different NES (NES*: NES of STAT3 - SLAAEFRHLQLK, NES**: NES of HIV-Rev - LPPLERLTL) and the NLS from the SV40 large T antigen (PPKKKRKV) were added to obtain NES-mCherry-NES-INF2-DAD-core-NES-NLS. **D)** NIH3T3 cells expressing NES-mCherry-NES-INF2-DAD-core-NES-NLS together with nAC-GFP were treated with 25 nM LMB and monitored over time. Representative video stills display dynamic nuclear accumulation of NES-

mCherry-NES-INF2-DAD-core-NES-NLS upon LMB treatment and subsequent spatiotemporal nuclear F-actin assembly. Scale bar, 10 µm.

However, LMB treatment leads to accumulation of a wide variety of different proteins in the nucleus. Thus, to exclude the possibility that nuclear actin filament formation is mediated by other factors than INF2-DAD, a nucleocytoplasmic shuttling version of the DID binding deficient mutant INF2-DAD-core-3LtoA was generated. Interestingly, no nuclear actin network could be detected in most cells upon LMB mediated nuclear translocation of NES-mCherry-NES-INF2-DAD-core-3LtoA-NES-NLS to the nucleus (Figure 28A, B).

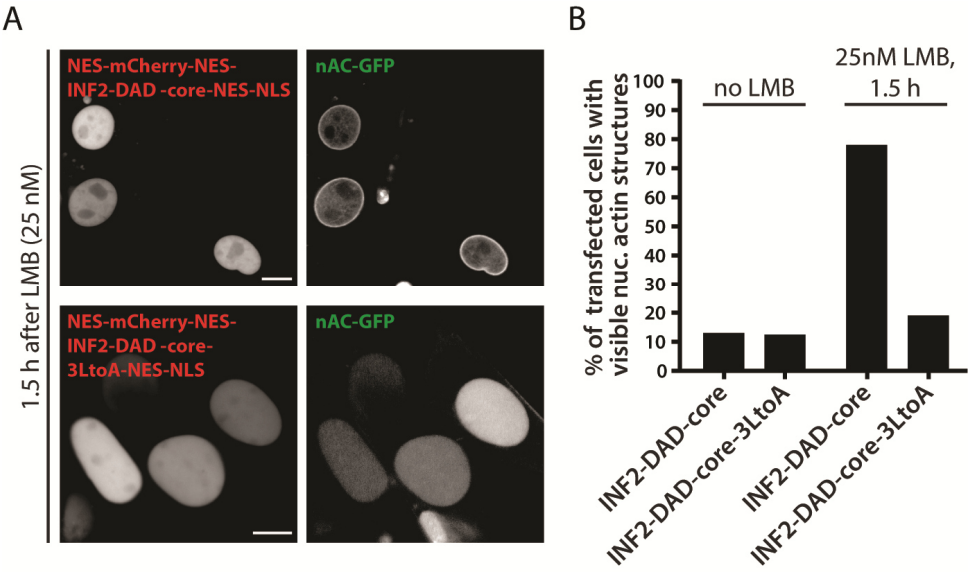

Figure 28: Actin filament formation in the nucleus upon LMB treatment depends on INF2-DAD expression

A) The images show representative NES-mCherry-NES-INF2-DAD-core-NES-NLS and nAC-GFP expressing cells after 1.5 h after addition of 25 nM LMB. **B)** NIH3T3 cells expressing NES-mCherry-NES-INF2-DAD-core-NES-NLS were quantified in terms of visible nuclear actin structures before and upon treatment with 25 nM LMB. nAC-GFP was used as marker for nuclear actin. Around 60 to 120 cells were analyzed for each condition.

5. Discussion

While the appearance of monomeric or short oligomeric actin in the nucleus and its role in processes like general transcriptional regulation or chromatin remodeling has been described previously (de Lanerolle and Serebryannyy, 2011; Gieni and Hendzel, 2009; Percipalle, 2013), the existence and functions of F-actin in somatic cell nuclei remained widely enigmatic (Pederson, 2008; Pederson and Aebi, 2002). However, recent work has provided visual evidence for endogenous polymeric and filamentous actin structures in the nucleus in both, fixed and living mammalian cells (Baarlink et al., 2013; Belin et al., 2013; Plessner et al., 2015). Additionally, several regulatory proteins involved in actin polymerization, such as the ARP2/3 complex (Yoo et al., 2007), N-WASP (Suetsugu and Takenawa, 2003) or members of the formin family (Belin et al., 2015; Miki et al., 2009; Ménard et al., 2006; Stüven et al., 2003) have been detected inside the nucleus and some of their nuclear functions have already been described. For example, our group has shown in a previous study that nuclear mDia activity regulates the SRF coactivator MRTF-A (Baarlink et al., 2013), an integral transcriptional cofactor, which is directly controlled by actin dynamics (Olson and Nordheim, 2010).

In general, to analyze formin mediated actin dynamics a directed regulation of formin autoinhibition and resultant formin activity is crucial. Former studies achieved spatially and/or temporally regulated activity of mDia formins by expression of the isolated DAD peptide which was shown to interfere with the intramolecular DID/DAD binding and consequently with the autoinhibited state of the formin (Alberts, 2001; Baarlink et al., 2013; Rao et al., 2013). The major advantage of this system is the exclusive modulation of the endogenous formin as there is no use to overexpress the full length protein or even a constitutively active version. In contrast, a putative disadvantage could be that the DID and DAD regions among certain formin families show highly conserved elements. Thus, cross-activation of related formins cannot be excluded and has not been intensely tested so far. In this study we expand the toolbox to activate endogenous mDia by demonstrating a successful autoinhibition release upon the expression of a peptide composed of the isolated five armadillo repeats of the DID

motif. Furthermore, a modification in the activity status of formins by expression of isolated DAD or DID peptides was not restricted to mDia formins but could also be implemented in at least INF2.

It was shown recently, that INF2 modulates MRTF/SRF transcriptional activity in a Ca^{2+} dependent manner, distinct from Rho, ROCK and mDia mediated SRF activation (Wales et al., 2016). In this work, the ability to regulate INF2 in a controlled manner led further to the discovery that actin rearrangement driven by INF2-DID or INF2-DAD expression results in a potent modulation of MRTF/SRF transcriptional activity. Additionally, we adduce evidence that INF2 plays an essential role in the physiological serum response in cells, as a depletion of INF2 strikingly impeded SRF activity induced by serum. Moreover, we provide additional layers of complexity concerning the assembly of nuclear F-actin structures and resultant MRTF-A/SRF regulation. In particular, a small but distinct amount of INF2 could be biochemically identified in nuclear fractions. The nuclear localization of endogenous INF2 was additionally confirmed by confocal microscopy. Concomitantly, the activation of endogenous INF2 restricted to the nuclear compartment results in nuclear actin filament formation. INF2 mediated F-actin assembly in the nucleus was followed by nuclear accumulation of MRTF-A and subsequent regulation of MRTF/SRF transcriptional activity. Hence, it can be hypothesized that in general the cellular actin response to serum and other stimuli depends on a tightly regulated signaling network. It involves a complex interplay of numerous factors, including the formin INF2, spanning from receptors at the cell surface which transmit extracellular cues up to transcription factors regulating gene expression in the nuclear compartment.

Previous studies have indicated DID/DAD interactions between closely related formins with the ability to regulate their activity *in trans* (Copeland et al., 2007; Sun et al., 2011; Vaillant et al., 2008). Thus, another important part of this study was to reveal if the effects on actin rearrangement and SRF activity mediated by the expression of INF2-DID or INF2-DAD are the result of direct interference with the autoinhibition of endogenous INF2 or rather due to an impact on other actin nucleation factors.

Addressing this question, multiple aspects in terms of specific modulation of endogenous INF2 autoinhibition were investigated.

The two INF2 isoforms in mammalian cells were shown to differ in their far C-terminus, which is dependent for its cellular localization (Chhabra et al., 2009; Ramabhadran et al., 2011). Here, we could show that the expression of the isoform specific INF2 C-terminus (including the DAD) promotes the assembly of differential actin patterns which resemble the identical phenotype as achieved upon expression of the respective full length constitutive active INF2 isoform (Ramabhadran et al., 2013). Thus, we suggest that INF2-DAD interferes with DID/DAD binding of INF2 and subsequently activates endogenous INF2. INF2 activation can be obtained in an isoform- and thus site-specific manner, leading to the formation of distinct F-actin phenotypes.

Worth mentioning, the DAD of INF2 resembles a WH2 motif and was reported to sequester actin monomers. However, polymerization activity has not been reported for the isolated C-terminus of INF2, which includes the DAD/WH2 domain (Chhabra and Higgs, 2006). Thus, and because of the fact that INF2 contains only a single G-actin binding WH2 motif, we propose that the re-organization of cytoplasmic and nuclear F-actin upon INF2-DAD expression is mediated rather by activation of the endogenous formin than by a hypothetic intrinsic actin nucleation activity of the WH2 domain upon binding to G-actin. Theoretically, it could also be hypothesized that visible actin structures are simply the result of site-specific accumulation of actin monomers bound to the WH2 domain of INF2. In our study we refute this assumption as hINF2-DAD or especially hINF2-DAD-CAAX promoted cytoplasmic F-actin structures as well as INF2-DAD-core-NLS driven nuclear actin filaments can clearly be visualized in fixed cells by phalloidin staining. Phalloidin was shown to exclusively bind F-actin and not G-actin with high affinity (Vandekerckhove et al., 1985; Wulf et al., 1979). Furthermore, the pattern of nuclear INF2-DAD mediated F-actin does not resemble the pattern of the expressed INF2-DAD-core-NLS, which is diffusely distributed within the nuclear compartment.

In contrast to wild type INF2-DAD-core, the expression of INF2-DAD-core featuring a triple Leucine to Alanine mutation (3LtoA) (Chhabra and Higgs, 2006) did not drive MRTF/SRF transcriptional activity. These mutations, all residing in the INF2-DAD/WH2 domain, were characterized to abrogate binding of the WH2 motif to actin monomers and inhibit actin severing and depolymerization activity of INF2 (Chhabra and Higgs, 2006; Ramabhadran et al., 2012). Moreover, they prevent DID-DAD binding, thus blocking the autoinhibitory interaction of INF2 (Chhabra et al., 2009). Worth mentioning, a recent study showed a competitive G-actin binding between the RPEL motifs of MRTF-A and different WH2 domains isolated from N-WASP, WAVE2, Spire2 or Cobl, resulting in activation of MRTF-A/SRF transcriptional activity. This WH2 domain mediated alteration of SRF activity was shown to occur independently of their role in actin filament formation (Weissbach et al., 2016). Thus, we cannot completely rule out an at least partial impact of the isolated INF2-DAD or more precisely of its intrinsic WH2 domain on the modulation of MRTF-A/SRF activity by competitive binding to G-actin. However, we detected a striking impairment of MRTF-A translocation to the nucleus and reduced SRF activity in cells lacking INF2 upon expressing the DAD of INF2. Noteworthy, the impairment could at least partially be rescued by re-introducing full length INF2 into cells. This argues for a major contribution of endogenous INF2 to facilitate INF2-DAD driven effects on MRTF/SRF transcriptional activity rather than MRTF-A regulation by competitive binding of G-actin to the INF2-DAD inhering WH2 motif.

Additionally, we could also show that SRF activity driven by the expression of the isolated hINF2-DID gets diminished upon the introduction of diverse single point mutations to the DID construct (A149D, E184K or R218Q). These point mutations were shown to interfere with DID/DAD binding of INF2 (Brown et al., 2010; Ramabhadran et al., 2013; Rollason et al., 2016). Thus, we suggest that the mutated DID constructs are incapable of releasing INF2 autoinhibition. Interestingly, the point mutations E184K and R218Q were also described in cases of the renal disease FSGS (Brown et al., 2010).

Furthermore, we introduced the 3LtoA mutation in the nuclear targeted version of INF2-DAD-core. Thereby we revealed that the formation of a nuclear F-actin network cannot be detected upon expression of INF2-DAD-core-3LtoA-NLS. In contrast, the expression of unmodified INF2-DAD-core-NLS resulted in the assembly of nuclear actin filaments in the majority of transfected cells. Interestingly, INF2-DAD-core-NLS driven filament formation was frequently accompanied by the assembly of a very prominent actin ring-like structure partially colocalizing with the interior side of the nuclear lamina. We could determine that this actin ring is different from the INF2-CAAX mediated perinuclear actin ring.

The fraction of cells displaying nuclear actin filaments upon INF2-DAD-core-NLS expression could be strikingly reduced upon co-expression with hINF2-DID-NLS but not with the DAD binding deficient mutant hINF2-DID-A149D-NLS. Thus we conclude that expression of the isolated DID peptide in part sterically interferes with binding of the expressed DAD (and vice versa) to the endogenous formin and thereby restricts release of formin autoinhibition. In accordance, co-expression of INF2-DID together with INF2-DAD-core also compensates for the effect on SRF activity compared to single expression of the respective proteins.

Consistent with the assumption that expression of INF2-DAD-CAAX specifically affects the activity status of endogenous INF2-CAAX, a decreased amount of INF2 depleted cells showed formation of an active INF2-CAAX typical actin pattern after expression of hINF2-DAD-CAAX when compared to wild type cells. Additionally, the percentage of cells displaying INF2-DAD-core-NLS mediated nuclear actin filament formation was significantly reduced upon INF2 knockdown by siRNA. However, a distinct amount of siRNA mediated INF2 knockdown cells expressing INF2-DAD-core-NLS still showed nuclear actin filaments. The most plausible general explanation therefore would be that not all cells got affected by siRNA treatment. These cells would still express INF2 and thus they are unimpededly able to form INF2 mediated F-actin in the nucleus. In turn, we also analyzed INF2-DAD-core-NLS mediated nuclear F-actin formation in cells completely lacking INF2 mediated by the CRISPR/CAS system. However, although

immunoblotting revealed a complete loss of INF2, a certain amount of INF2 knockout cells also still displayed nuclear actin structures in response to INF2-DAD expression. Taken together, this suggests that cells can either partially compensate for the loss of INF2 or that the INF2-DAD may functionally interact with other actin nucleation factors, probably with other related formins, at least in the nucleus.

Noteworthy, a heterodimerization between closely related formins has been described in previous studies. For example, it was shown that heterodimerization of full-length mDia1 and mDia2 occurs by DID/DAD interaction but not by their dimerization motif and FH2 domain. This DID/DAD interaction is able to act *in trans* to inhibit formin activity (Copeland et al., 2007). In turn, in addition to a described DID/DAD interaction, also the FH2 and the dimerization domain of the formins FRL2 and FRL3 (also known as FMNL3 and FMNL2) are able to form hetero-oligomers (Vaillant et al., 2008).

A recent study revealed that also the only partially related formins INF2 and mDia can form heterodimers via INF2-DID and mDia-DAD (Sun et al., 2011), Thus, we analyzed if co-expression of the DID and the DAD of either INF2 or mDia2 show additive or antagonistic effects in terms of their ability to activate MRTF/SRF mediated gene transcription. We revealed that co-expression of mDia2-DAD and mINF2-DID remarkably reduced SRF activity. This suggests mainly two possible scenarios: either 1) a direct interaction occurs between the overexpressed proteins and thereby preventing them to release autoinhibition of the respective endogenous formins, or 2) INF2-DID interferes with the autoinhibition of endogenous INF2 (or mDia), whereas mDia-DAD activates endogenous mDia (or INF2) but both active formins subsequently negatively regulate each other's impact on actin rearrangement and SRF activity. The latter option has been described for mDia and INF2. It was discovered that INF2 antagonizes Rho activated actin polymerization activity of mDia signaling by an interaction of INF2-DID with the DAD sequence of mDia1, mDia2 or mDia3 (Sun et al., 2011). Furthermore, experiments in cultured podocytes as well as *in vivo* experiments revealed that active INF2 is an important antagonist of mDia1 and mDia2 mediated

actin dynamics, related to processes as the formation of lamellipodia and peripheral membrane trafficking (Sun et al., 2014; Sun et al., 2013).

Contrariwise, co-expression of mDia2-DID together with INF2-DAD-core showed a synergistic effect in terms of SRF activation. Hence, we suggest, in contrast to mDia-DAD and INF2-DID, that INF2-DAD does not directly interact with mDia-DID. Thus, they do not prevent each other from interfering with the autoinhibition of endogenous INF2 of mDia. Moreover, endogenous active INF2 cannot antagonize mDia activity in this situation, as the intramolecular INF2-DID and mDia-DAD are occupied by the overexpressed INF2-DAD and mDia-DID, respectively.

Furthermore, we investigated if the number of cells displaying a nuclear F-actin network upon expression of INF2-DAD-core-NLS gets reduced when cells co-express mDia1-DID or mDia2-DID. Indeed, the number of cells with visible nuclear actin structures was diminished, although to a much more moderate extent than upon co-expression of INF2-DAD-core-NLS together with hINF2-DID. This suggests that expression of mDia1-DID or mDia2-DID interferes with INF2-DAD mediated activation of endogenous INF2. However, as a direct interaction between the DID of mDia formins and the DAD of INF2 was not reported (Sun et al., 2011), we hypothesize that both expressed constructs act independently from each other, thereby negatively modulating the formation of nuclear actin filaments. Hence, simultaneous nuclear activation of endogenous INF2 and endogenous mDia by INF2-DAD-core and mDia2-DID might prevent each other from the formation of visible F-actin structures in the nucleus, although they do not counteract in terms of MRTF/SRF regulation.

Moreover, co-expression of INF2-DAD-core-NLS together with nuclear targeted, dominant negative derivatives of mDia, mDia1-I845R (Shimada et al., 2004) or mDia2-I704A (Harris et al., 2006) did neither alter the number of cells displaying INF2-DAD-core-NLS mediated nuclear F-actin nor the actin pattern itself (data not shown). This result additionally underscores the hypothesis that INF2-DAD does not directly affect mDia mediated actin rearrangement. In turn we also analyzed the impact on nuclear full length INF2 derivatives possessing mutated FH2 residues (I643A and/or K792A)

(Andrés-Delgado et al., 2010; Ramabhadran et al., 2012). In other formins, the respective mutations were described to be essential for actin binding and polymerization (Shimada et al., 2004; Xu et al., 2004). Interestingly, nuclear expression of INF2-I643A, INF2-K792A or INF2-I643A/K792A in combination with INF2-DAD-core-NLS did not abolish the formation of nuclear F-actin structures, but rather resulted in the formation of thick and elongated actin bundles (data not shown). This rather unforeseen phenotype can be explained by the multiple diverging effects described for these mutations in the FH2 domain of INF2. A recent study has shown that INF2-I643A does not show decreased barbed end binding but that it rather causes tight capping of a subset of filaments. Furthermore, the I643A mutation possesses a minor inhibitory effect on actin polymerization activity but it causes almost a complete abolishment of severing and depolymerization activity. Also the INF2-K792A mutant affects both polymerization and severing/depolymerization activity, although to a much smaller degree than INF2-I643A. Moreover, INF2-K792A has similar barbed end affinity as wild type INF2, but it was shown to decelerate the rate of processive elongation (Ramabhadran et al., 2012). Therefore, we conclude that the formation of nuclear actin filaments mediated by INF2 activity is dependent on both, its polymerization as well as its depolymerization/severing capabilities.

Furthermore, we analyzed if siRNA mediated depletion of mDia1 and mDia2 also affects the assembly of nuclear F-actin upon expression of INF2-DAD-core-NLS. Indeed, simultaneous suppression of both, mDia1 and mDia2, negatively influenced nuclear actin filaments triggered by expression of INF2-DAD, although to a much more moderate extent than INF2 knockdown and INF2 depletion does. Interestingly, simultaneous depletion of INF2 together with mDia1 and mDia2 also did not completely abolish INF2-DAD-core-NLS mediated nuclear F-actin formation but led to a similar result as INF2 depletion alone. These experiments provide evidence that by and large the effects of INF2-DAD seem to be specific for INF2 and are unlikely to occur mainly due to crosstalk with other formins. Thereby, we suggest that INF2-DAD interferes specifically with INF2 autoinhibition, whereas activated INF2 additionally seems to execute regulatory effects on nuclear F-actin formation through interaction

with mDia formins. Noteworthy, synergistic effects between INF2 and mDia have not been described so far, although they cannot be entirely ruled out. Moreover, our results also point towards a potential role for additional so far unidentified factors in INF2-mediated nuclear actin filament formation.

In a nutshell, we discover here that the formin INF2 is an actin nucleation factor with the ability to form a nuclear actin network upon spatially restricted release of autoinhibition inside the nucleus. One direct consequence of nuclear INF2 activation is the translocation of the SRF cofactor MRTF-A to the nucleus followed by modulation of MRTF/SRF mediated gene transcription. Moreover, this work suggests a putative crosstalk between the formins INF2 and mDia as well as other unknown proteins inside the nuclear compartment. Thus, INF2 may play an important cellular role for fine-tuning or adjusting the multiple and complex levels of signal regulations of MRTF-A (Panayiotou et al., 2016; Vartiainen et al., 2007). However, conducting follow-up studies on INF2 driven actin dynamics, it has to be generally kept in mind that INF2 also possess a potent actin severing and depolymerization activity, thus massively broadening the scope for interpretations. Therefore, further studies have to be implemented addressing the exact cellular functions of nuclear INF2 together with the precise cross-regulation of other proteins.

INF2 mediated regulation of actin turnover was suggested to be involved in diseases affecting the peripheral nervous system (CMT) and the kidney glomerulus (FSGS) (Boyer et al., 2011; Brown et al., 2010; Subramanian et al., 2016). All so far identified disease-causing point mutations reside in the DID of INF2. Some of them were shown to result in dysfunctional INF2 autoinhibition (Rollason et al., 2016) and in impaired INF2-DID/mDia-DAD interaction (Sun et al., 2014; Sun et al., 2013). Both effects were suggested to lead to imbalanced actin dynamics and disruption of actin based processes. Based on our findings that INF2 plays an essential role in the physiological serum response and that INF2 mediated nuclear F-actin formation is sufficient to drive MRTF/SRF transcriptional activity, a disease-relevant role for mutated INF2 in the nuclear compartment is hypothetically possible. For example, perturbed nuclear actin

rearrangement caused by mutated INF2 might alter the localization and activity of MRTF-A and thus leading to a deregulated transcription of SRF target genes. This deregulated MRTF/SRF transcriptional activity might theoretically contribute to the onset of FSGS or CMT.

Another aspect which remains to be elucidated is the detailed transport mechanism which is in charge of regulating the hypothesized nuclear localization of INF2. Although formins such as mDia (Copeland et al., 2007; Miki et al., 2009) or FMN2 (Belin et al., 2015), but also INF2, as we now revealed by subcellular fractionation experiments, can be detected in the nuclear compartment, they usually reside predominantly in the cytoplasm under steady-state conditions. Thus, we suggest that INF2 continuously undergoes nucleocytoplasmic shuttling, which occurs through either direct interaction of INF2 with the nuclear import or export machinery or through co-import and co-export in a complex with other proteins.

Continuous shuttling between the nuclear compartment and the cytoplasm has been recently shown for mDia1 and mDia2. To accomplish nuclear entry, full-length mDia2 was suggested to bind directly to importin-α via an N-terminal bipartite NLS and gets imported into the nucleus by an importin-α/β complex (Miki et al., 2009). In turn, the nuclear import mechanism of mDia1 has not been fully characterized, although the protein was detected in nuclear fractions (Baarlink et al., 2013). A putative C-terminal NLS was reported for mDia1 (Copeland et al., 2007). However, whether this NLS is functional in full-length mDia1 remains to be tested. Moreover, mDia2, but not mDia1, was shown to be exported from the nucleus in a CRM1 dependent manner. It rapidly accumulates in the nucleus within minutes upon blocking CRM1-dependent nuclear export by using LMB (Miki et al., 2009). In contrast, mDia1 was speculated to become constantly co-exported with profilin and actin via an exportin 6 dependent pathway, as they appeared together in a purified nuclear exportin 6 complex (Stüven et al., 2003).

Despite the detection of nuclear INF2 localization, we currently do not know by which mechanism INF2 is translocated to and from nucleus. Bioinformatic analysis of the hINF2 amino acid sequence revealed several putative NLS and NES sequences. At least

one of the detected putative NLS (termed NLS3) and NES (termed NES4) sequences was shown to be functional when the peptide was isolated and fused to GFP. Interestingly, expression of GFP-NES4 furthermore revealed nuclear enrichment upon treatment with LMB, thus its export is at least partially dependent on CRM1. However, it still has to be determined if NLS3 and NES4 are also functional in a full length context. We could already reveal that CRM1 mediated nuclear export does not seem to play a role in the shuttling of endogenous INF2 as treatment of cells with LMB did not result in nuclear accumulation of the full-length protein. Thus, we suggest that INF2 contains functional NLS and NES motifs to undergo continuous nucleocytoplasmic shuttling by using a so far unidentified nuclear transport machinery. It remains a future challenge to identify the detailed transport mechanisms which are in charge of regulating the nuclear entry and export of INF2.

6. References

Adam, S.A., R.S. Marr, and L. Gerace. 1990. Nuclear protein import in permeabilized mammalian cells requires soluble cytoplasmic factors. *J Cell Biol*. 111:807-816.

Ahuja, R., R. Pinyol, N. Reichenbach, L. Custer, J. Klingensmith, M.M. Kessels, and B. Qualmann. 2007. Cordon-bleu is an actin nucleation factor and controls neuronal morphology. *Cell*. 131:337-350.

Alberts, A.S. 2001. Identification of a carboxyl-terminal diaphanous-related formin homology protein autoregulatory domain. *J Biol Chem*. 276:2824-2830.

Andrés-Delgado, L., O.M. Antón, R. Madrid, J.A. Byrne, and M.A. Alonso. 2010. Formin INF2 regulates MAL-mediated transport of Lck to the plasma membrane of human T lymphocytes. *Blood*. 116:5919-5929.

Archer, S.K., C. Claudianos, and H.D. Campbell. 2005. Evolution of the gelsolin family of actin-binding proteins as novel transcriptional coactivators. *Bioessays*. 27:388-396.

Baarlink, C., D. Brandt, and R. Grosse. 2010. SnapShot: Formins. *Cell*. 142:172, 172.e171.

Baarlink, C., and R. Grosse. 2014. Formin' actin in the nucleus. *Nucleus*. 5:15-20.

Baarlink, C., H. Wang, and R. Grosse. 2013. Nuclear actin network assembly by formins regulates the SRF coactivator MAL. *Science*. 340:864-867.

Bartolini, F., L. Andres-Delgado, X. Qu, S. Nik, N. Ramalingam, L. Kremer, M.A. Alonso, and G.G. Gundersen. 2016. An mDia1-INF2 formin activation cascade facilitated by IQGAP1 regulates stable microtubules in migrating cells. *Mol Biol Cell*.

Barua, M., E.J. Brown, V.T. Charoonratana, G. Genovese, H. Sun, and M.R. Pollak. 2013. Mutations in the INF2 gene account for a significant proportion of familial but not sporadic focal and segmental glomerulosclerosis. *Kidney Int*. 83:316-322.

Begg, D.A., R. Rodewald, and L.I. Rebhun. 1978. The visualization of actin filament polarity in thin sections. Evidence for the uniform polarity of membrane-associated filaments. *J Cell Biol*. 79:846-852.

Beli, P., D. Mascheroni, D. Xu, and M. Innocenti. 2008. WAVE and Arp2/3 jointly inhibit filopodium formation by entering into a complex with mDia2. *Nat Cell Biol*. 10:849-857.

Belin, B.J., B.A. Cimini, E.H. Blackburn, and R.D. Mullins. 2013. Visualization of actin filaments and monomers in somatic cell nuclei. *Mol Biol Cell*. 24:982-994.

Belin, B.J., L.M. Goins, and R.D. Mullins. 2014. Comparative analysis of tools for live cell imaging of actin network architecture. *Bioarchitecture*. 4:189-202.

Belin, B.J., T. Lee, and R.D. Mullins. 2015. Correction: DNA damage induces nuclear actin filament assembly by Formin-2 and Spire-1/2 that promotes efficient DNA repair. *Elife*. 4.

Bi, E., and S.H. Zigmond. 1999. Actin polymerization: Where the WASP stings. *Curr Biol*. 9:R160-163.

Blanchoin, L., K.J. Amann, H.N. Higgs, J.B. Marchand, D.A. Kaiser, and T.D. Pollard. 2000. Direct observation of dendritic actin filament networks nucleated by Arp2/3 complex and WASP/Scar proteins. *Nature*. 404:1007-1011.

Boyer, O., F. Nevo, E. Plaisier, B. Funalot, O. Gribouval, G. Benoit, E. Huynh Cong, C. Arrondel, M.J. Tête, R. Montjean, L. Richard, A. Karras, C. Pouteil-Noble, L. Balafrej, A. Bonnardeaux, G. Canaud, C. Charasse, J. Dantal, G. Deschenes, P. Deteix, O. Dubourg, P. Petiot, D. Pouthier, E. Leguern, A. Guiochon-Mantel, I. Broutin, M.C. Gubler, S. Saunier, P. Ronco, J.M. Vallat, M.A. Alonso, C. Antignac, and G. Mollet. 2011. INF2 mutations in Charcot-Marie-Tooth disease with glomerulopathy. *N Engl J Med*. 365:2377-2388.

Brandt, D.T., C. Baarlink, T.M. Kitzing, E. Kremmer, J. Ivaska, P. Nollau, and R. Grosse. 2009. SCAI acts as a suppressor of cancer cell invasion through the transcriptional control of beta1-integrin. *Nat Cell Biol*. 11:557-568.

Breitsprecher, D., and B.L. Goode. 2013. Formins at a glance. *J Cell Sci*. 126:1-7.

Brown, E.J., J.S. Schlöndorff, D.J. Becker, H. Tsukaguchi, S.J. Tonna, A.L. Uscinski, H.N. Higgs, J.M. Henderson, and M.R. Pollak. 2010. Mutations in the formin gene INF2 cause focal segmental glomerulosclerosis. *Nat Genet*. 42:72-76.

Buchwalter, G., C. Gross, and B. Wasylyk. 2004. Ets ternary complex transcription factors. *Gene*. 324:1-14.

Bugyi, B., and M.F. Carlier. 2010. Control of actin filament treadmilling in cell motility. *Annu Rev Biophys*. 39:449-470.

Bunnell, T.M., B.J. Burbach, Y. Shimizu, and J.M. Ervasti. 2011. β-Actin specifically controls cell growth, migration, and the G-actin pool. *Mol Biol Cell*. 22:4047-4058.

Campellone, K.G., and M.D. Welch. 2010. A nucleator arms race: cellular control of actin assembly. *Nat Rev Mol Cell Biol*. 11:237-251.

Castrillon, D.H., and S.A. Wasserman. 1994. Diaphanous is required for cytokinesis in Drosophila and shares domains of similarity with the products of the limb deformity gene. *Development*. 120:3367-3377.

Cheng, L., J. Zhang, S. Ahmad, L. Rozier, H. Yu, H. Deng, and Y. Mao. 2011. Aurora B regulates formin mDia3 in achieving metaphase chromosome alignment. *Dev Cell*. 20:342-352.

Chereau, D., M. Boczkowska, A. Skwarek-Maruszewska, I. Fujiwara, D.B. Hayes, G. Rebowski, P. Lappalainen, T.D. Pollard, and R. Dominguez. 2008. Leiomodin is an actin filament nucleator in muscle cells. *Science*. 320:239-243.

Chesarone, M., C.J. Gould, J.B. Moseley, and B.L. Goode. 2009. Displacement of formins from growing barbed ends by bud14 is critical for actin cable architecture and function. *Dev Cell*. 16:292-302.

Chesarone, M.A., and B.L. Goode. 2009. Actin nucleation and elongation factors: mechanisms and interplay. *Curr Opin Cell Biol*. 21:28-37.

Chesarone-Cataldo, M., C. Guérin, J.H. Yu, R. Wedlich-Soldner, L. Blanchoin, and B.L. Goode. 2011. The myosin passenger protein Smy1 controls actin cable structure and dynamics by acting as a formin damper. *Dev Cell*. 21:217-230.

Chhabra, E.S., and H.N. Higgs. 2006. INF2 Is a WASP homology 2 motif-containing formin that severs actin filaments and accelerates both polymerization and depolymerization. *J Biol Chem*. 281:26754-26767.

Chhabra, E.S., V. Ramabhadran, S.A. Gerber, and H.N. Higgs. 2009. INF2 is an endoplasmic reticulum-associated formin protein. *J Cell Sci*. 122:1430-1440.

Cooper, S.J., N.D. Trinklein, L. Nguyen, and R.M. Myers. 2007. Serum response factor binding sites differ in three human cell types. *Genome Res*. 17:136-144.

Copeland, J.W., and R. Treisman. 2002. The diaphanous-related formin mDia1 controls serum response factor activity through its effects on actin polymerization. *Mol Biol Cell*. 13:4088-4099.

Copeland, S.J., B.J. Green, S. Burchat, G.A. Papalia, D. Banner, and J.W. Copeland. 2007. The diaphanous inhibitory domain/diaphanous autoregulatory domain interaction is able to mediate heterodimerization between mDia1 and mDia2. *J Biol Chem*. 282:30120-30130.

Dahl, K.N., and A. Kalinowski. 2011. Nucleoskeleton mechanics at a glance. *J Cell Sci*. 124:675-678.

de Lanerolle, P., and L. Serebryannyy. 2011. Nuclear actin and myosins: life without filaments. *Nat Cell Biol*. 13:1282-1288.

DeRosier, D.J., and L.G. Tilney. 2000. F-actin bundles are derivatives of microvilli: What does this tell us about how bundles might form? *J Cell Biol*. 148:1-6.

Dominguez, R., and K.C. Holmes. 2011. Actin structure and function. *Annu Rev Biophys*. 40:169-186.

Dopie, J., K.P. Skarp, E.K. Rajakylä, K. Tanhuanpää, and M.K. Vartiainen. 2012. Active maintenance of nuclear actin by importin 9 supports transcription. *Proc Natl Acad Sci U S A*. 109:E544-552.

Dubreuil, R.R. 1991. Structure and evolution of the actin crosslinking proteins. *Bioessays*. 13:219-226.

Eisenmann, K.M., E.S. Harris, S.M. Kitchen, H.A. Holman, H.N. Higgs, and A.S. Alberts. 2007. Dia-interacting protein modulates formin-mediated actin assembly at the cell cortex. *Curr Biol*. 17:579-591.

Emmons, S., H. Phan, J. Calley, W. Chen, B. James, and L. Manseau. 1995. Cappuccino, a Drosophila maternal effect gene required for polarity of the egg and embryo, is related to the vertebrate limb deformity locus. *Genes Dev*. 9:2482-2494.

Fackler, O.T., and R. Grosse. 2008. Cell motility through plasma membrane blebbing. *J Cell Biol*. 181:879-884.

Fenn, S., D. Breitsprecher, C.B. Gerhold, G. Witte, J. Faix, and K.P. Hopfner. 2011. Structural biochemistry of nuclear actin-related proteins 4 and 8 reveals their interaction with actin. *EMBO J*. 30:2153-2166.

Fletcher, D.A., and R.D. Mullins. 2010. Cell mechanics and the cytoskeleton. *Nature*. 463:485-492.

Floyd, S., N. Whiffin, M.P. Gavilan, S. Kutscheidt, M. De Luca, C. Marcozzi, M. Min, J. Watkins, K. Chung, O.T. Fackler, and C. Lindon. 2013. Spatiotemporal organization of Aurora-B by APC/CCdh1 after mitosis coordinates cell spreading through FHOD1. *J Cell Sci*. 126:2845-2856.

Fukuhara, S., H. Chikumi, and J.S. Gutkind. 2000. Leukemia-associated Rho guanine nucleotide exchange factor (LARG) links heterotrimeric G proteins of the G(12) family to Rho. *FEBS Lett*. 485:183-188.

Gao, J., J. Liao, and G.Y. Yang. 2009. CAAX-box protein, prenylation process and carcinogenesis. *Am J Transl Res*. 1:312-325.

Gasman, S., Y. Kalaidzidis, and M. Zerial. 2003. RhoD regulates endosome dynamics through Diaphanous-related Formin and Src tyrosine kinase. *Nat Cell Biol*. 5:195-204.

Gbadegesin, R.A., P.J. Lavin, G. Hall, B. Bartkowiak, A. Homstad, R. Jiang, G. Wu, A. Byrd, K. Lynn, N. Wolfish, C. Ottati, P. Stevens, D. Howell, P. Conlon, and M.P. Winn. 2012. Inverted formin 2 mutations with variable expression in patients with sporadic and hereditary focal and segmental glomerulosclerosis. *Kidney Int*. 81:94-99.

Gieni, R.S., and M.J. Hendzel. 2009. Actin dynamics and functions in the interphase nucleus: moving toward an understanding of nuclear polymeric actin. *Biochem Cell Biol*. 87:283-306.

Gimona, M., R. Buccione, S.A. Courtneidge, and S. Linder. 2008. Assembly and biological role of podosomes and invadopodia. *Curr Opin Cell Biol*. 20:235-241.

Gineitis, D., and R. Treisman. 2001. Differential usage of signal transduction pathways defines two types of serum response factor target gene. *J Biol Chem*. 276:24531-24539.

Glotzer, M. 2001. Animal cell cytokinesis. *Annu Rev Cell Dev Biol*. 17:351-386.

Goley, E.D., and M.D. Welch. 2006. The ARP2/3 complex: an actin nucleator comes of age. *Nat Rev Mol Cell Biol*. 7:713-726.

Goode, B.L., and M.J. Eck. 2007. Mechanism and function of formins in the control of actin assembly. *Annu Rev Biochem*. 76:593-627.

Gould, C.J., S. Maiti, A. Michelot, B.R. Graziano, L. Blanchoin, and B.L. Goode. 2011. The formin DAD domain plays dual roles in autoinhibition and actin nucleation. *Curr Biol*. 21:384-390.

Goulimari, P., H. Knieling, U. Engel, and R. Grosse. 2008. LARG and mDia1 link Galpha12/13 to cell polarity and microtubule dynamics. *Mol Biol Cell*. 19:30-40.

Grikscheit, K., T. Frank, Y. Wang, and R. Grosse. 2015. Junctional actin assembly is mediated by Formin-like 2 downstream of Rac1. *J Cell Biol*. 209:367-376.

Grosse, R., J.W. Copeland, T.P. Newsome, M. Way, and R. Treisman. 2003. A role for VASP in RhoA-Diaphanous signalling to actin dynamics and SRF activity. *EMBO J*. 22:3050-3061.

Grosse, R., and M.K. Vartiainen. 2013. To be or not to be assembled: progressing into nuclear actin filaments. *Nat Rev Mol Cell Biol*. 14:693-697.

Gualdrini, F., C. Esnault, S. Horswell, A. Stewart, N. Matthews, and R. Treisman. 2016. SRF Co-factors Control the Balance between Cell Proliferation and Contractility. *Mol Cell*.

Guettler, S., M.K. Vartiainen, F. Miralles, B. Larijani, and R. Treisman. 2008. RPEL motifs link the serum response factor cofactor MAL but not myocardin to Rho signaling via actin binding. *Mol Cell Biol*. 28:732-742.

Gurel, P.S., M. A, B. Guo, R. Shu, D.F. Mierke, and H.N. Higgs. 2015. Assembly and turnover of short actin filaments by the formin INF2 and profilin. *J Biol Chem*. 290:22494-22506.

Gurel, P.S., P. Ge, E.E. Grintsevich, R. Shu, L. Blanchoin, Z.H. Zhou, E. Reisler, and H.N. Higgs. 2014. INF2-mediated severing through actin filament encirclement and disruption. *Curr Biol*. 24:156-164.

Habas, R., Y. Kato, and X. He. 2001. Wnt/Frizzled activation of Rho regulates vertebrate gastrulation and requires a novel Formin homology protein Daam1. *Cell*. 107:843-854.

Han, Y., E. Eppinger, I.G. Schuster, L.U. Weigand, X. Liang, E. Kremmer, C. Peschel, and A.M. Krackhardt. 2009. Formin-like 1 (FMNL1) is regulated by N-terminal myristoylation and induces polarized membrane blebbing. *J Biol Chem*. 284:33409-33417.

Harata, M., Y. Zhang, D.J. Stillman, D. Matsui, Y. Oma, K. Nishimori, and R. Mochizuki. 2002. Correlation between chromatin association and transcriptional regulation for the Act3p/Arp4 nuclear actin-related protein of Saccharomyces cerevisiae. *Nucleic Acids Res*. 30:1743-1750.

Harper, S.M., J.M. Christie, and K.H. Gardner. 2004. Disruption of the LOV-Jalpha helix interaction activates phototropin kinase activity. *Biochemistry*. 43:16184-16192.

Harper, S.M., L.C. Neil, and K.H. Gardner. 2003. Structural basis of a phototropin light switch. *Science*. 301:1541-1544.

Harris, E.S., I. Rouiller, D. Hanein, and H.N. Higgs. 2006. Mechanistic differences in actin bundling activity of two mammalian formins, FRL1 and mDia2. *J Biol Chem*. 281:14383-14392.

Heimsath, E.G., and H.N. Higgs. 2012. The C terminus of formin FMNL3 accelerates actin polymerization and contains a WH2 domain-like sequence that binds both monomers and filament barbed ends. *J Biol Chem*. 287:3087-3098.

Higashida, C., T. Miyoshi, A. Fujita, F. Oceguera-Yanez, J. Monypenny, Y. Andou, S. Narumiya, and N. Watanabe. 2004. Actin polymerization-driven molecular movement of mDia1 in living cells. *Science*. 303:2007-2010.

Higgs, H.N. 2005. Formin proteins: a domain-based approach. *Trends Biochem Sci*. 30:342-353.

Hofmann, W.A., L. Stojiljkovic, B. Fuchsova, G.M. Vargas, E. Mavrommatis, V. Philimonenko, K. Kysela, J.A. Goodrich, J.L. Lessard, T.J. Hope, P. Hozak, and P. de Lanerolle. 2004. Actin is part of pre-initiation complexes and is necessary for transcription by RNA polymerase II. *Nat Cell Biol*. 6:1094-1101.

Hofmann, W.A., G.M. Vargas, R. Ramchandran, L. Stojiljkovic, J.A. Goodrich, and P. de Lanerolle. 2006. Nuclear myosin I is necessary for the formation of the first phosphodiester bond during transcription initiation by RNA polymerase II. *J Cell Biochem*. 99:1001-1009.

Holmes, K.C., D. Popp, W. Gebhard, and W. Kabsch. 1990. Atomic model of the actin filament. *Nature*. 347:44-49.

Hu, P., S. Wu, and N. Hernandez. 2004. A role for beta-actin in RNA polymerase III transcription. *Genes Dev*. 18:3010-3015.

Ishizaki, T., Y. Morishima, M. Okamoto, T. Furuyashiki, T. Kato, and S. Narumiya. 2001. Coordination of microtubules and the actin cytoskeleton by the Rho effector mDia1. *Nat Cell Biol*. 3:8-14.

Iskratsch, T., S. Lange, J. Dwyer, A.L. Kho, C. dos Remedios, and E. Ehler. 2010. Formin follows function: a muscle-specific isoform of FHOD3 is regulated by CK2 phosphorylation and promotes myofibril maintenance. *J Cell Biol*. 191:1159-1172.

Iskratsch, T., S. Reijntjes, J. Dwyer, P. Toselli, I.R. Dégano, I. Dominguez, and E. Ehler. 2013. Two distinct phosphorylation events govern the function of muscle FHOD3. *Cell Mol Life Sci*. 70:893-908.

Jaffe, A.B., and A. Hall. 2005. Rho GTPases: biochemistry and biology. *Annu Rev Cell Dev Biol*. 21:247-269.

Ji, P., S.R. Jayapal, and H.F. Lodish. 2008. Enucleation of cultured mouse fetal erythroblasts requires Rac GTPases and mDia2. *Nat Cell Biol*. 10:314-321.

Kapoor, P., M. Chen, D.D. Winkler, K. Luger, and X. Shen. 2013. Evidence for monomeric actin function in INO80 chromatin remodeling. *Nat Struct Mol Biol*. 20:426-432.

Kim, T., J.A. Cooper, and D. Sept. 2010. The interaction of capping protein with the barbed end of the actin filament. *J Mol Biol*. 404:794-802.

Kitzing, T.M., A.S. Sahadevan, D.T. Brandt, H. Knieling, S. Hannemann, O.T. Fackler, J. Grosshans, and R. Grosse. 2007. Positive feedback between Dia1, LARG, and RhoA regulates cell morphology and invasion. *Genes Dev*. 21:1478-1483.

Kitzing, T.M., Y. Wang, O. Pertz, J.W. Copeland, and R. Grosse. 2010. Formin-like 2 drives amoeboid invasive cell motility downstream of RhoC. *Oncogene*. 29:2441-2448.

Korobova, F., V. Ramabhadran, and H.N. Higgs. 2013. An actin-dependent step in mitochondrial fission mediated by the ER-associated formin INF2. *Science*. 339:464-467.

Kosugi, S., M. Hasebe, M. Tomita, and H. Yanagawa. 2009. Systematic identification of cell cycle-dependent yeast nucleocytoplasmic shuttling proteins by prediction of composite motifs. *Proc Natl Acad Sci U S A*. 106:10171-10176.

Kovar, D.R. 2006. Molecular details of formin-mediated actin assembly. *Curr Opin Cell Biol*. 18:11-17.

Kovar, D.R., E.S. Harris, R. Mahaffy, H.N. Higgs, and T.D. Pollard. 2006. Control of the assembly of ATP- and ADP-actin by formins and profilin. *Cell*. 124:423-435.

Kovar, D.R., and T.D. Pollard. 2004. Insertional assembly of actin filament barbed ends in association with formins produces piconewton forces. *Proc Natl Acad Sci U S A*. 101:14725-14730.

la Cour, T., L. Kiemer, A. Mølgaard, R. Gupta, K. Skriver, and S. Brunak. 2004. Analysis and prediction of leucine-rich nuclear export signals. *Protein Eng Des Sel*. 17:527-536.

Lammers, M., R. Rose, A. Scrima, and A. Wittinghofer. 2005. The regulation of mDia1 by autoinhibition and its release by Rho*GTP. *EMBO J*. 24:4176-4187.

Le Clainche, C., and M.F. Carlier. 2008. Regulation of actin assembly associated with protrusion and adhesion in cell migration. *Physiol Rev*. 88:489-513.

Leader, B., H. Lim, M.J. Carabatsos, A. Harrington, J. Ecsedy, D. Pellman, R. Maas, and P. Leder. 2002. Formin-2, polyploidy, hypofertility and positioning of the meiotic spindle in mouse oocytes. *Nat Cell Biol*. 4:921-928.

Lederer, M., B.M. Jockusch, and M. Rothkegel. 2005. Profilin regulates the activity of p42POP, a novel Myb-related transcription factor. *J Cell Sci*. 118:331-341.

Lee, K., M.J. Kang, S.J. Kwon, Y.K. Kwon, K.W. Kim, J.H. Lim, and H. Kwon. 2007. Expansion of chromosome territories with chromatin decompaction in BAF53-depleted interphase cells. *Mol Biol Cell*. 18:4013-4023.

Li, F., and H.N. Higgs. 2005. Dissecting requirements for auto-inhibition of actin nucleation by the formin, mDia1. *J Biol Chem*. 280:6986-6992.

Liu, W., A. Sato, D. Khadka, R. Bharti, H. Diaz, L.W. Runnels, and R. Habas. 2008. Mechanism of activation of the Formin protein Daam1. *Proc Natl Acad Sci U S A*. 105:210-215.

Louvet, E., and P. Percipalle. 2009. Transcriptional control of gene expression by actin and myosin. *Int Rev Cell Mol Biol*. 272:107-147.

Machesky, L.M., S.J. Atkinson, C. Ampe, J. Vandekerckhove, and T.D. Pollard. 1994. Purification of a cortical complex containing two unconventional actins from Acanthamoeba by affinity chromatography on profilin-agarose. *J Cell Biol*. 127:107-115.

Madrid, R., J.F. Aranda, A.E. Rodríguez-Fraticelli, L. Ventimiglia, L. Andrés-Delgado, M. Shehata, S. Fanayan, H. Shahheydari, S. Gómez, A. Jiménez, F. Martín-Belmonte, J.A. Byrne, and M.A. Alonso. 2010. The formin INF2 regulates basolateral-to-apical transcytosis and lumen formation in association with Cdc42 and MAL2. *Dev Cell*. 18:814-827.

Mattila, P.K., and P. Lappalainen. 2008. Filopodia: molecular architecture and cellular functions. *Nat Rev Mol Cell Biol*. 9:446-454.

Matusek, T., A. Djiane, F. Jankovics, D. Brunner, M. Mlodzik, and J. Mihály. 2006. The Drosophila formin DAAM regulates the tracheal cuticle pattern through organizing the actin cytoskeleton. *Development*. 133:957-966.

McDonald, D., G. Carrero, C. Andrin, G. de Vries, and M.J. Hendzel. 2006. Nucleoplasmic beta-actin exists in a dynamic equilibrium between low-mobility polymeric species and rapidly diffusing populations. *J Cell Biol*. 172:541-552.

Medjkane, S., C. Perez-Sanchez, C. Gaggioli, E. Sahai, and R. Treisman. 2009. Myocardin-related transcription factors and SRF are required for cytoskeletal dynamics and experimental metastasis. *Nat Cell Biol*. 11:257-268.

Melak, M., M. Plessner, and R. Grosse. 2017. Actin visualization at a glance. *J Cell Sci*.

Miki, T., K. Okawa, T. Sekimoto, Y. Yoneda, S. Watanabe, T. Ishizaki, and S. Narumiya. 2009. mDia2 shuttles between the nucleus and the cytoplasm through the importin-{alpha}/{beta}- and CRM1-mediated nuclear transport mechanism. *J Biol Chem*. 284:5753-5762.

Miralles, F., G. Posern, A.I. Zaromytidou, and R. Treisman. 2003. Actin dynamics control SRF activity by regulation of its coactivator MAL. *Cell*. 113:329-342.

Miyagi, Y., T. Yamashita, M. Fukaya, T. Sonoda, T. Okuno, K. Yamada, M. Watanabe, Y. Nagashima, I. Aoki, K. Okuda, M. Mishina, and S. Kawamoto. 2002. Delphilin: a novel PDZ and formin homology domain-containing protein that synaptically colocalizes and interacts with glutamate receptor delta 2 subunit. *J Neurosci*. 22:803-814.

Mouilleron, S., C.A. Langer, S. Guettler, N.Q. McDonald, and R. Treisman. 2011. Structure of a pentavalent G-actin*MRTF-A complex reveals how G-actin controls nucleocytoplasmic shuttling of a transcriptional coactivator. *Sci Signal*. 4:ra40.

Mullins, R.D., J.A. Heuser, and T.D. Pollard. 1998. The interaction of Arp2/3 complex with actin: nucleation, high affinity pointed end capping, and formation of branching networks of filaments. *Proc Natl Acad Sci U S A*. 95:6181-6186.

Ménard, I., F.G. Gervais, D.W. Nicholson, and S. Roy. 2006. Caspase-3 cleaves the formin-homology-domain-containing protein FHOD1 during apoptosis to generate a C-terminal fragment that is targeted to the nucleolus. *Apoptosis*. 11:1863-1876.

Neidt, E.M., B.J. Scott, and D.R. Kovar. 2009. Formin differentially utilizes profilin isoforms to rapidly assemble actin filaments. *J Biol Chem*. 284:673-684.

Neidt, E.M., C.T. Skau, and D.R. Kovar. 2008. The cytokinesis formins from the nematode worm and fission yeast differentially mediate actin filament assembly. *J Biol Chem*. 283:23872-23883.

Nezami, A., F. Poy, A. Toms, W. Zheng, and M.J. Eck. 2010. Crystal structure of a complex between amino and carboxy terminal fragments of mDia1: insights into autoinhibition of diaphanous-related formins. *PLoS One*. 5.

Nezami, A.G., F. Poy, and M.J. Eck. 2006. Structure of the autoinhibitory switch in formin mDia1. *Structure*. 14:257-263.

Norman, C., M. Runswick, R. Pollock, and R. Treisman. 1988. Isolation and properties of cDNA clones encoding SRF, a transcription factor that binds to the c-fos serum response element. *Cell*. 55:989-1003.

Obrdlik, A., and P. Percipalle. 2011. The F-actin severing protein cofilin-1 is required for RNA polymerase II transcription elongation. *Nucleus*. 2:72-79.

Olson, E.N., and A. Nordheim. 2010. Linking actin dynamics and gene transcription to drive cellular motile functions. *Nat Rev Mol Cell Biol*. 11:353-365.

Olson, M.F., and E. Sahai. 2009. The actin cytoskeleton in cancer cell motility. *Clin Exp Metastasis*. 26:273-287.

Ostlund, C., E.S. Folker, J.C. Choi, E.R. Gomes, G.G. Gundersen, and H.J. Worman. 2009. Dynamics and molecular interactions of linker of nucleoskeleton and cytoskeleton (LINC) complex proteins. *J Cell Sci*. 122:4099-4108.

Otomo, T., C. Otomo, D.R. Tomchick, M. Machius, and M.K. Rosen. 2005a. Structural basis of Rho GTPase-mediated activation of the formin mDia1. *Mol Cell*. 18:273-281.

Otomo, T., D.R. Tomchick, C. Otomo, M. Machius, and M.K. Rosen. 2010. Crystal structure of the Formin mDia1 in autoinhibited conformation. *PLoS One*. 5.

Otomo, T., D.R. Tomchick, C. Otomo, S.C. Panchal, M. Machius, and M.K. Rosen. 2005b. Structural basis of actin filament nucleation and processive capping by a formin homology 2 domain. *Nature*. 433:488-494.

Otterbein, L.R., P. Graceffa, and R. Dominguez. 2001. The crystal structure of uncomplexed actin in the ADP state. *Science*. 293:708-711.

Panayiotou, R., F. Miralles, R. Pawlowski, J. Diring, H.R. Flynn, M. Skehel, and R. Treisman. 2016. Phosphorylation acts positively and negatively to regulate MRTF-A subcellular localisation and activity. *Elife*. 5.

Paul, A.S., A. Paul, T.D. Pollard, and T. Pollard. 2008. The role of the FH1 domain and profilin in formin-mediated actin-filament elongation and nucleation. *Curr Biol*. 18:9-19.

Paul, A.S., and T.D. Pollard. 2009. Review of the mechanism of processive actin filament elongation by formins. *Cell Motil Cytoskeleton*. 66:606-617.

Pawłowski, R., E.K. Rajakylä, M.K. Vartiainen, and R. Treisman. 2010. An actin-regulated importin α/β-dependent extended bipartite NLS directs nuclear import of MRTF-A. *EMBO J*. 29:3448-3458.

Pederson, T. 2008. As functional nuclear actin comes into view, is it globular, filamentous, or both? *J Cell Biol*. 180:1061-1064.

Pederson, T., and U. Aebi. 2002. Actin in the nucleus: what form and what for? *J Struct Biol*. 140:3-9.

Pellegrin, S., and H. Mellor. 2005. The Rho family GTPase Rif induces filopodia through mDia2. *Curr Biol*. 15:129-133.

Peng, J., B.J. Wallar, A. Flanders, P.J. Swiatek, and A.S. Alberts. 2003. Disruption of the Diaphanous-related formin Drf1 gene encoding mDia1 reveals a role for Drf3 as an effector for Cdc42. *Curr Biol*. 13:534-545.

Percipalle, P. 2013. Co-transcriptional nuclear actin dynamics. *Nucleus*. 4:43-52.

Perrin, B.J., and J.M. Ervasti. 2010. The actin gene family: function follows isoform. *Cytoskeleton (Hoboken)*. 67:630-634.

Philimonenko, V.V., J. Zhao, S. Iben, H. Dingová, K. Kyselá, M. Kahle, H. Zentgraf, W.A. Hofmann, P. de Lanerolle, P. Hozák, and I. Grummt. 2004. Nuclear actin and myosin I are required for RNA polymerase I transcription. *Nat Cell Biol*. 6:1165-1172.

Pipes, G.C., E.E. Creemers, and E.N. Olson. 2006. The myocardin family of transcriptional coactivators: versatile regulators of cell growth, migration, and myogenesis. *Genes Dev*. 20:1545-1556.

Plessner, M., and R. Grosse. 2015. Extracellular signaling cues for nuclear actin polymerization. *Eur J Cell Biol*. 94:359-362.

Plessner, M., M. Melak, P. Chinchilla, C. Baarlink, and R. Grosse. 2015. Nuclear F-actin formation and reorganization upon cell spreading. *J Biol Chem*. 290:11209-11216.

Pollard, T.D., L. Blanchoin, and R.D. Mullins. 2000. Molecular mechanisms controlling actin filament dynamics in nonmuscle cells. *Annu Rev Biophys Biomol Struct*. 29:545-576.

Pollard, T.D., and J.A. Cooper. 2009. Actin, a central player in cell shape and movement. *Science*. 326:1208-1212.

Posern, G., A. Sotiropoulos, and R. Treisman. 2002. Mutant actins demonstrate a role for unpolymerized actin in control of transcription by serum response factor. *Mol Biol Cell*. 13:4167-4178.

Prehoda, K.E., J.A. Scott, R.D. Mullins, and W.A. Lim. 2000. Integration of multiple signals through cooperative regulation of the N-WASP-Arp2/3 complex. *Science*. 290:801-806.

Pring, M., M. Evangelista, C. Boone, C. Yang, and S.H. Zigmond. 2003. Mechanism of formin-induced nucleation of actin filaments. *Biochemistry*. 42:486-496.

Pring, M., A. Weber, and M.R. Bubb. 1992. Profilin-actin complexes directly elongate actin filaments at the barbed end. *Biochemistry*. 31:1827-1836.

Pruyne, D., M. Evangelista, C. Yang, E. Bi, S. Zigmond, A. Bretscher, and C. Boone. 2002. Role of formins in actin assembly: nucleation and barbed-end association. *Science*. 297:612-615.

Quinlan, M.E., J.E. Heuser, E. Kerkhoff, and R.D. Mullins. 2005. Drosophila Spire is an actin nucleation factor. *Nature*. 433:382-388.

Ramabhadran, V., P.S. Gurel, and H.N. Higgs. 2012. Mutations to the formin homology 2 domain of INF2 protein have unexpected effects on actin polymerization and severing. *J Biol Chem*. 287:34234-34245.

Ramabhadran, V., A.L. Hatch, and H.N. Higgs. 2013. Actin monomers activate inverted formin 2 by competing with its autoinhibitory interaction. *J Biol Chem*. 288:26847-26855.

Ramabhadran, V., F. Korobova, G.J. Rahme, and H.N. Higgs. 2011. Splice variant-specific cellular function of the formin INF2 in maintenance of Golgi architecture. *Mol Biol Cell*. 22:4822-4833.

Ramalingam, N., H. Zhao, D. Breitsprecher, P. Lappalainen, J. Faix, and M. Schleicher. 2010. Phospholipids regulate localization and activity of mDia1 formin. *Eur J Cell Biol*. 89:723-732.

Ran, F.A., P.D. Hsu, J. Wright, V. Agarwala, D.A. Scott, and F. Zhang. 2013. Genome engineering using the CRISPR-Cas9 system. *Nat Protoc*. 8:2281-2308.

Rao, M.V., P.H. Chu, K.M. Hahn, and R. Zaidel-Bar. 2013. An optogenetic tool for the activation of endogenous diaphanous-related formins induces thickening of stress fibers without an increase in contractility. *Cytoskeleton (Hoboken)*. 70:394-407.

Riedl, J., A.H. Crevenna, K. Kessenbrock, J.H. Yu, D. Neukirchen, M. Bista, F. Bradke, D. Jenne, T.A. Holak, Z. Werb, M. Sixt, and R. Wedlich-Soldner. 2008. Lifeact: a versatile marker to visualize F-actin. *Nat Methods*. 5:605-607.

Robinson, R.C., K. Turbedsky, D.A. Kaiser, J.B. Marchand, H.N. Higgs, S. Choe, and T.D. Pollard. 2001. Crystal structure of Arp2/3 complex. *Science*. 294:1679-1684.

Rollason, R., M. Wherlock, J.A. Heath, K.J. Heesom, M.A. Saleem, and G.I. Welsh. 2016. Disease causing mutations in inverted formin 2 regulate its binding to G-actin, F-actin capping protein (CapZ α-1) and profilin 2. *Biosci Rep*. 36:e00302.

Romero, S., C. Le Clainche, D. Didry, C. Egile, D. Pantaloni, and M.F. Carlier. 2004. Formin is a processive motor that requires profilin to accelerate actin assembly and associated ATP hydrolysis. *Cell*. 119:419-429.

Rose, R., M. Weyand, M. Lammers, T. Ishizaki, M.R. Ahmadian, and A. Wittinghofer. 2005. Structural and mechanistic insights into the interaction between Rho and mammalian Dia. *Nature*. 435:513-518.

Rotty, J.D., C. Wu, and J.E. Bear. 2013. New insights into the regulation and cellular functions of the ARP2/3 complex. *Nat Rev Mol Cell Biol*. 14:7-12.

Sakuma, T., A. Nishikawa, S. Kume, K. Chayama, and T. Yamamoto. 2014. Multiplex genome engineering in human cells using all-in-one CRISPR/Cas9 vector system. *Sci Rep*. 4:5400.

Schratt, G., U. Philippar, J. Berger, H. Schwarz, O. Heidenreich, and A. Nordheim. 2002. Serum response factor is crucial for actin cytoskeletal organization and focal adhesion assembly in embryonic stem cells. *J Cell Biol*. 156:737-750.

Sept, D., and J.A. McCammon. 2001. Thermodynamics and kinetics of actin filament nucleation. *Biophys J*. 81:667-674.

Seth, A., C. Otomo, and M.K. Rosen. 2006. Autoinhibition regulates cellular localization and actin assembly activity of the diaphanous-related formins FRLalpha and mDia1. *J Cell Biol*. 174:701-713.

Shao, X., Q. Li, A. Mogilner, A.D. Bershadsky, and G.V. Shivashankar. 2015. Mechanical stimulation induces formin-dependent assembly of a perinuclear actin rim. *Proc Natl Acad Sci U S A*. 112:E2595-2601.

Shikama, N., C.W. Lee, S. France, L. Delavaine, J. Lyon, M. Krstic-Demonacos, and N.B. La Thangue. 1999. A novel cofactor for p300 that regulates the p53 response. *Mol Cell*. 4:365-376.

Shimada, A., M. Nyitrai, I.R. Vetter, D. Kühlmann, B. Bugyi, S. Narumiya, M.A. Geeves, and A. Wittinghofer. 2004. The core FH2 domain of diaphanous-related formins is an elongated actin binding protein that inhibits polymerization. *Mol Cell*. 13:511-522.

Shore, P., and A.D. Sharrocks. 1995. The MADS-box family of transcription factors. *Eur J Biochem*. 229:1-13.

Simon, D.N., and K.L. Wilson. 2011. The nucleoskeleton as a genome-associated dynamic 'network of networks'. *Nat Rev Mol Cell Biol*. 12:695-708.

Skau, C.T., S.V. Plotnikov, A.D. Doyle, and C.M. Waterman. 2015. Inverted formin 2 in focal adhesions promotes dorsal stress fiber and fibrillar adhesion formation to drive extracellular matrix assembly. *Proc Natl Acad Sci U S A*. 112:E2447-2456.

Small, J.V., T. Stradal, E. Vignal, and K. Rottner. 2002. The lamellipodium: where motility begins. *Trends Cell Biol*. 12:112-120.

Spracklen, A.J., T.N. Fagan, K.E. Lovander, and T.L. Tootle. 2014. The pros and cons of common actin labeling tools for visualizing actin dynamics during Drosophila oogenesis. *Dev Biol*. 393:209-226.

Stradal, T.E., and G. Scita. 2006. Protein complexes regulating Arp2/3-mediated actin assembly. *Curr Opin Cell Biol*. 18:4-10.

Stüven, T., E. Hartmann, and D. Görlich. 2003. Exportin 6: a novel nuclear export receptor that is specific for profilin.actin complexes. *EMBO J*. 22:5928-5940.

Subramanian, B., H. Sun, P. Yan, V.T. Charoonratana, H.N. Higgs, F. Wang, K.M. Lai, D.M. Valenzuela, E.J. Brown, J.S. Schlöndorff, and M.R. Pollak. 2016. Mice with mutant Inf2 show impaired podocyte and slit diaphragm integrity in response to protamine-induced kidney injury. *Kidney Int*. 90:363-372.

Suetsugu, S., and T. Takenawa. 2003. Translocation of N-WASP by nuclear localization and export signals into the nucleus modulates expression of HSP90. *J Biol Chem*. 278:42515-42523.

Sun, H., K.I. Al-Romaih, C.A. MacRae, and M.R. Pollak. 2014. Human Kidney Disease-causing INF2 Mutations Perturb Rho/Dia Signaling in the Glomerulus. *EBioMedicine*. 1:107-115.

Sun, H., J. Schlondorff, H.N. Higgs, and M.R. Pollak. 2013. Inverted formin 2 regulates actin dynamics by antagonizing Rho/diaphanous-related formin signaling. *J Am Soc Nephrol*. 24:917-929.

Sun, H., J.S. Schlondorff, E.J. Brown, H.N. Higgs, and M.R. Pollak. 2011. Rho activation of mDia formins is modulated by an interaction with inverted formin 2 (INF2). *Proc Natl Acad Sci U S A*. 108:2933-2938.

Sun, H.Q., M. Yamamoto, M. Mejillano, and H.L. Yin. 1999. Gelsolin, a multifunctional actin regulatory protein. *J Biol Chem*. 274:33179-33182.

Szerlong, H., K. Hinata, R. Viswanathan, H. Erdjument-Bromage, P. Tempst, and B.R. Cairns. 2008. The HSA domain binds nuclear actin-related proteins to regulate chromatin-remodeling ATPases. *Nat Struct Mol Biol*. 15:469-476.

Söderberg, E., V. Hessle, A. von Euler, and N. Visa. 2012. Profilin is associated with transcriptionally active genes. *Nucleus*. 3:290-299.

Takeya, R., K. Taniguchi, S. Narumiya, and H. Sumimoto. 2008. The mammalian formin FHOD1 is activated through phosphorylation by ROCK and mediates thrombin-induced stress fibre formation in endothelial cells. *EMBO J*. 27:618-628.

Theriot, J.A. 1997. Accelerating on a treadmill: ADF/cofilin promotes rapid actin filament turnover in the dynamic cytoskeleton. *J Cell Biol*. 136:1165-1168.

Thompson, M.E., E.G. Heimsath, T.J. Gauvin, H.N. Higgs, and F.J. Kull. 2013. FMNL3 FH2-actin structure gives insight into formin-mediated actin nucleation and elongation. *Nat Struct Mol Biol*. 20:111-118.

Treisman, R. 1986. Identification of a protein-binding site that mediates transcriptional response of the c-fos gene to serum factors. *Cell*. 46:567-574.

Tseng, Y., T.P. Kole, J.S. Lee, E. Fedorov, S.C. Almo, B.W. Schafer, and D. Wirtz. 2005. How actin crosslinking and bundling proteins cooperate to generate an enhanced cell mechanical response. *Biochem Biophys Res Commun*. 334:183-192.

Tseng, Y., B.W. Schafer, S.C. Almo, and D. Wirtz. 2002. Functional synergy of actin filament cross-linking proteins. *J Biol Chem*. 277:25609-25616.

Vaillant, D.C., S.J. Copeland, C. Davis, S.F. Thurston, N. Abdennur, and J.W. Copeland. 2008. Interaction of the N- and C-terminal autoregulatory domains of FRL2 does not inhibit FRL2 activity. *J Biol Chem*. 283:33750-33762.

Vandekerckhove, J., A. Deboben, M. Nassal, and T. Wieland. 1985. The phalloidin binding site of F-actin. *EMBO J*. 4:2815-2818.

Vartiainen, M.K., S. Guettler, B. Larijani, and R. Treisman. 2007. Nuclear actin regulates dynamic subcellular localization and activity of the SRF cofactor MAL. *Science*. 316:1749-1752.

Vavylonis, D., D.R. Kovar, B. O'Shaughnessy, and T.D. Pollard. 2006. Model of formin-associated actin filament elongation. *Mol Cell*. 21:455-466.

Vizcarra, C.L., B. Kreutz, A.A. Rodal, A.V. Toms, J. Lu, W. Zheng, M.E. Quinlan, and M.J. Eck. 2011. Structure and function of the interacting domains of Spire and Fmn-family formins. *Proc Natl Acad Sci U S A*. 108:11884-11889.

Volkmann, N., K.J. Amann, S. Stoilova-McPhie, C. Egile, D.C. Winter, L. Hazelwood, J.E. Heuser, R. Li, T.D. Pollard, and D. Hanein. 2001. Structure of Arp2/3 complex in its activated state and in actin filament branch junctions. *Science*. 293:2456-2459.

Wada, A., M. Fukuda, M. Mishima, and E. Nishida. 1998. Nuclear export of actin: a novel mechanism regulating the subcellular localization of a major cytoskeletal protein. *EMBO J*. 17:1635-1641.

Wales, P., C.E. Schuberth, R. Aufschnaiter, J. Fels, I. García-Aguilar, A. Janning, C.P. Dlugos, M. Schäfer-Herte, C. Klingner, M. Wälte, J. Kuhlmann, E. Menis, L. Hockaday Kang, K.C. Maier, W. Hou, A. Russo, H.N. Higgs, H. Pavenstädt, T. Vogl, J. Roth, B. Qualmann, M.M. Kessels, D.E. Martin, B. Mulder, and R. Wedlich-Söldner. 2016. Calcium-mediated actin reset (CaAR) mediates acute cell adaptations. *Elife*. 5.

Wallar, B.J., and A.S. Alberts. 2003. The formins: active scaffolds that remodel the cytoskeleton. *Trends Cell Biol*. 13:435-446.

Wallar, B.J., A.D. Deward, J.H. Resau, and A.S. Alberts. 2007. RhoB and the mammalian Diaphanous-related formin mDia2 in endosome trafficking. *Exp Cell Res*. 313:560-571.

Wang, D., P.S. Chang, Z. Wang, L. Sutherland, J.A. Richardson, E. Small, P.A. Krieg, and E.N. Olson. 2001. Activation of cardiac gene expression by myocardin, a transcriptional cofactor for serum response factor. *Cell*. 105:851-862.

Wang, D.Z., S. Li, D. Hockemeyer, L. Sutherland, Z. Wang, G. Schratt, J.A. Richardson, A. Nordheim, and E.N. Olson. 2002. Potentiation of serum response factor activity by a family of myocardin-related transcription factors. *Proc Natl Acad Sci U S A*. 99:14855-14860.

Wang, Y., A. Arjonen, J. Pouwels, H. Ta, P. Pausch, G. Bange, U. Engel, X. Pan, O.T. Fackler, J. Ivaska, and R. Grosse. 2015. Formin-like 2 Promotes β1-Integrin Trafficking and Invasive Motility Downstream of PKCα. *Dev Cell*. 34:475-483.

Watanabe, S., Y. Ando, S. Yasuda, H. Hosoya, N. Watanabe, T. Ishizaki, and S. Narumiya. 2008. mDia2 induces the actin scaffold for the contractile ring and stabilizes its position during cytokinesis in NIH 3T3 cells. *Mol Biol Cell*. 19:2328-2338.

Weber, A., C.R. Pennise, G.G. Babcock, and V.M. Fowler. 1994. Tropomodulin caps the pointed ends of actin filaments. *J Cell Biol*. 127:1627-1635.

Wegner, A., and G. Isenberg. 1983. 12-fold difference between the critical monomer concentrations of the two ends of actin filaments in physiological salt conditions. *Proc Natl Acad Sci U S A*. 80:4922-4925.

Weissbach, J., F. Schikora, A. Weber, M. Kessels, and G. Posern. 2016. Myocardin-Related Transcription Factor A Activation by Competition with WH2 Domain Proteins for Actin Binding. *Mol Cell Biol*. 36:1526-1539.

Welch, M.D., and R.D. Mullins. 2002. Cellular control of actin nucleation. *Annu Rev Cell Dev Biol*. 18:247-288.

Weston, L., A.S. Coutts, and N.B. La Thangue. 2012. Actin nucleators in the nucleus: an emerging theme. *J Cell Sci*. 125:3519-3527.

Wickstead, B., and K. Gull. 2011. The evolution of the cytoskeleton. *J Cell Biol*. 194:513-525.

Wu, X., Y. Yoo, N.N. Okuhama, P.W. Tucker, G. Liu, and J.L. Guan. 2006. Regulation of RNA-polymerase-II-dependent transcription by N-WASP and its nuclear-binding partners. *Nat Cell Biol*. 8:756-763.

Wulf, E., A. Deboben, F.A. Bautz, H. Faulstich, and T. Wieland. 1979. Fluorescent phallotoxin, a tool for the visualization of cellular actin. *Proc Natl Acad Sci U S A*. 76:4498-4502.

Xu, Y., J.B. Moseley, I. Sagot, F. Poy, D. Pellman, B.L. Goode, and M.J. Eck. 2004. Crystal structures of a Formin Homology-2 domain reveal a tethered dimer architecture. *Cell*. 116:711-723.

Yasuda, S., F. Oceguera-Yanez, T. Kato, M. Okamoto, S. Yonemura, Y. Terada, T. Ishizaki, and S. Narumiya. 2004. Cdc42 and mDia3 regulate microtubule attachment to kinetochores. *Nature*. 428:767-771.

Ye, J., J. Zhao, U. Hoffmann-Rohrer, and I. Grummt. 2008. Nuclear myosin I acts in concert with polymeric actin to drive RNA polymerase I transcription. *Genes Dev*. 22:322-330.

Yoo, Y., X. Wu, and J.L. Guan. 2007. A novel role of the actin-nucleating Arp2/3 complex in the regulation of RNA polymerase II-dependent transcription. *J Biol Chem*. 282:7616-7623.

Young, K.G., and J.W. Copeland. 2010. Formins in cell signaling. *Biochim Biophys Acta*. 1803:183-190.

Zaromytidou, A.I., F. Miralles, and R. Treisman. 2006. MAL and ternary complex factor use different mechanisms to contact a common surface on the serum response factor DNA-binding domain. *Mol Cell Biol*. 26:4134-4148.

Zhao, K., W. Wang, O.J. Rando, Y. Xue, K. Swiderek, A. Kuo, and G.R. Crabtree. 1998. Rapid and phosphoinositol-dependent binding of the SWI/SNF-like BAF complex to chromatin after T lymphocyte receptor signaling. *Cell*. 95:625-636.

Zigmond, S.H., M. Evangelista, C. Boone, C. Yang, A.C. Dar, F. Sicheri, J. Forkey, and M. Pring. 2003. Formin leaky cap allows elongation in the presence of tight capping proteins. *Curr Biol*. 13:1820-1823.

Zuchero, J.B., B. Belin, and R.D. Mullins. 2012. Actin binding to WH2 domains regulates nuclear import of the multifunctional actin regulator JMY. *Mol Biol Cell*. 23:853-863.

Zuchero, J.B., A.S. Coutts, M.E. Quinlan, N.B. Thangue, and R.D. Mullins. 2009. p53-cofactor JMY is a multifunctional actin nucleation factor. *Nat Cell Biol*. 11:451-459.

Appendix

List of academic teachers

My academic teachers at the University of Vienna were Prof. Dr. Manuela Baccarini, Prof. Dr. Friedrich Barth, Prof. Dr. Johannes Berger, Prof. Dr. Udo Bläsi, Prof. Dr. Thomas Decker, Prof. Dr. Roland Foisner, Prof. Dr. Urs Peter Fringeli, Prof. Dr. Friedrich Hammerschmidt, Prof. Dr. Andreas Hartig, Prof. Dr. Erwin Heberle-Bors, Prof. Dr. Ernst Kenndler, Prof. Dr. Franz Klein, Prof. Dr. Robert Konrat, Prof. Dr. Pavel Kovarik, Prof. Dr. Andrea Leodolter-Barta, Prof. Dr. Johannes Nimpf, Prof. Dr. Josef Penninger, Prof. Dr. Marianne Popp, Prof. Dr. Friedrich Probst, Prof. Dr. Andreas Rizzi, Prof. Dr. Renée Schroeder, Prof. Dr. Peter Schuster, Prof. Dr. Dieter Schweizer, Prof. Dr. Rudolf Schweyen, Prof. Dr. Horst Seidler, Prof. Dr. Gerhard Sontag, Prof. Dr. Graham Warren, Prof. Dr. Gerhard Wiche, Prof. Dr. Erhard Wintersberger, Prof. Dr. Ulrike Wintersberger, Prof. Dr. Angela Witte.

Acknowledgment

First of all, I would like to thank my supervisor Prof. Dr. Robert Grosse for making it possible to work in his lab on such an interesting project and for guiding me through my PhD work as well as for his support and scientific discussions.

I also would like to thank all current and former colleagues for sharing their scientific knowledge and experience, excellent advice, the inspiring working atmosphere and of course for common activities outside the lab (BBQ, football, climbing, etc.). My special thanks go to Marga Losekam, Andrea Wüstenhagen and Christiane Kleber for their technical support as well as to Tanja Pfeffer-Eckel for her help with administrative questions.

Thanks a lot to Prof. Dr. Henry N. Higgs from Dartmouth Medical School, Hanover, US for sharing the hINF2 Plasmids.

I would like to thank particularly my entire family in Austria for their unconditional support and for providing enjoyable stays in my home country.

Last but not least, I would like to take the opportunity to express my deep gratitude to my beloved wife Thea for always being there for me and for encouraging and supporting me during tough and stressful times. And thanks to you, Kilian, Atreo and Jaron for sharing with me the most beautiful moments of my life.